CHALMERS

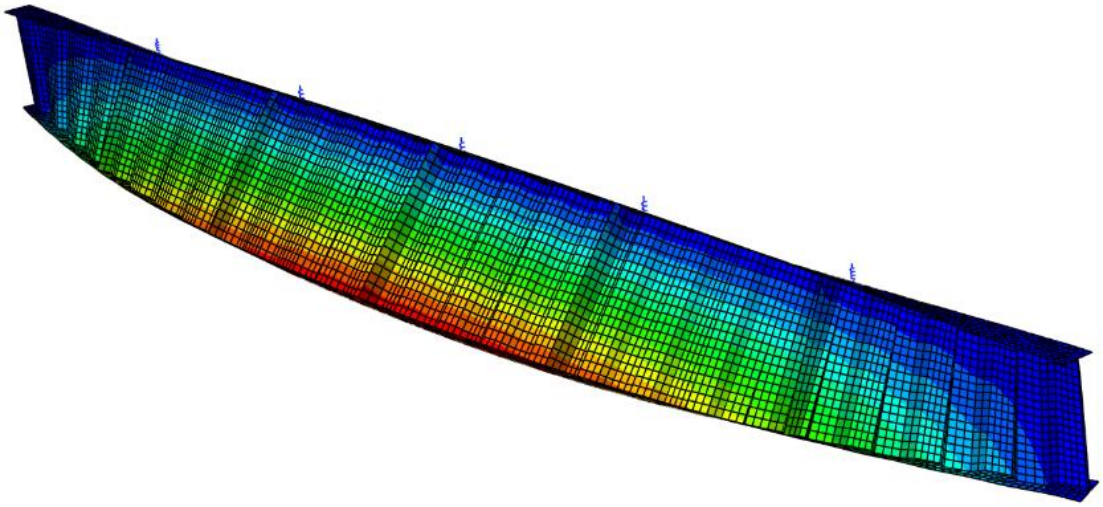

Influence of Purlins on Lateral-Torsional Buckling of Steel Girders with Corrugated Web

Master of Science Thesis in the Master's Programme Structural Engineering and Building Technology

GUÐNI ELLERT EDVARDSSON
BENGT LUNDQUIST
Department of Civil and Environmental Engineering
Division of Structural Engineering
Steel and Timber Structures
CHALMERS UNIVERSITY OF TECHNOLOGY
Göteborg, Sweden 2014
Master's Thesis 2014:100

MASTER'S THESIS 2014:100

Influence of Purlins on Lateral-Torsional Buckling of Steel Girders with Corrugated Web

Master of Science Thesis in the Master's Programme Structural Engineering and Building Technology

GUÐNI ELLERT EDVARDSSON

BENGT LUNDQUIST

Department of Civil and Environmental Engineering
Division of Structural Engineering
Steel and Timber Structures
CHALMERS UNIVERSITY OF TECHNOLOGY
Göteborg, Sweden 2014

Influence of Purlins on Lateral-Torsional Buckling of Steel Girders with Corrugated Web

Master of Science Thesis in the Master's Programme Structural Engineering and Building Technology

GUÐNI ELLERT EDVARDSSON
BENGT LUNDQUIST

Examensarbete / Institutionen för bygg- och miljöteknik,
Chalmers tekniska högskola 2014:100

Department of Civil and Environmental Engineering
Division of Structural Engineering
Steel and Timber Structures
Chalmers University of Technology
SE-412 96 Göteborg
Sweden
Telephone: + 46 (0)31-772 1000

Cover:
Finite element model showing lateral-torsional buckling of a girder with trapezoidally corrugated web with five restraints along its length.

Chalmers Reproservice / Department of Civil and Environmental Engineering
Göteborg, Sweden 2014

Influence of Purlins on Lateral-Torsional Buckling of Steel Girders with Corrugated Web

Master of Science Thesis in the Master's Programme Structural Engineering and Building Technology

GUÐNI ELLERT EDVARDSSON
BENGT LUNDQUIST
Department of Civil and Environmental Engineering
Division of Structural Engineering
Steel and Timber Structures
Chalmers University of Technology

ABSTRACT

Lateral-torsional buckling is a well-known stability problem in slender unrestrained steel girders with doubly symmetric I-section. A rather recent method to increase the stability of girders is to have a corrugated shape of the web instead of a flat web. Purlins connected to girders improve the stability due to their restraining effects. The purlins will restrain lateral movements of the girder at their connection point. In addition, rotation of the cross-section can be restrained by attaching the purlins rigidly to the girder. In that way, the rotation is controlled by the stiffness of the purlins. This increment in stability is of great interest from the designers' point of view due to economic reasons.

The aim of the thesis is to investigate the lateral-torsional buckling behaviour of steel girders with corrugated web of trapezoidal shape, restrained by purlins. The increased stability due to the torsional stiffness provided by rigidly attached purlins is of special interest. The thesis comprises a literature study and finite element analyses of restrained girders.

In this thesis, the method stated by Horne & Ajmani (1968) to obtain the critical moment due to lateral-torsional buckling of restrained girders is investigated. In addition, the method presented by Lindner & Aschinger (1990) to include the effects from a corrugated shape of the web is studied. The applicability of these expressions is evaluated for restrained girders with corrugated web. This evaluation is carried out by comparing the critical buckling moment from these expressions with the results from linear buckling analyses using elastic material response. In addition, non-linear buckling analyses are carried out in order to evaluate how restrained girders with corrugated web fit with the design approach, for lateral-torsional buckling, suggested in Eurocode 3.

The thesis concludes that the critical buckling moment can accurately be calculated with Horne & Ajmani's expression. This expression can be used with comparable accuracy both for girders with flat web and girders with corrugated web, using Lindner's method. In addition, it is concluded that the design approach for lateral-torsional buckling suggested in Eurocode 3 is applicable for restrained girders with corrugated web in a conservative way.

Key words: Lateral-torsional buckling, corrugated web, steel girder, purlins, discrete restraints, torsional stiffness

Takåsars inverkan på vippning av stålbalkar med korrugerade liv

Examensarbete inom Masterprogrammet *Structural Engineering and Building Technology*

GUÐNI ELLERT EDVARDSSON
BENGT LUNDQUIST
Institutionen för bygg- och miljöteknik
Avdelningen för konstruktionsteknik
Stål- och träbyggnad
Chalmers tekniska högskola

SAMMANFATTNING

Vippning är ett välkänt stabilitetsproblem i slanka ostagade stålbalkar med dubbelsymmetriskt I-tvärsnitt. En ny metod att öka stabiliteten i balkar är att ha ett korrugerat liv istället för ett plant liv. Takåsar anslutna till balkar förbättrar stabiliteten på grund av deras återhållande verkan. Takåsar hindrar rörelser i sidled i deras anslutningspunkter. Utöver detta, kan rotation av tvärsnittet hindras genom att fästa takåsarna styvt på balken. Då är tvärsnittets rotation styrd av takåsarnas styvhet. Denna ökning av stabilitet är, ur designers synpunkt, intressant på grund av ekonomiska skäl.

Syftet med denna rapport är att undersöka det kritiska vippningsmomentet av stålbalkar, med trapetskorrugerade liv, stagade av takåsar. Den ökade stabiliteten på grund av vridstyvhet försedd av styvt anslutna takåsar är av särskilt intresse. Rapporten består av en litteraturstudie och finita element-analyser av stagade balkar.

I denna rapport undersöks metoden föreslagen av Horne & Ajmani (1968) för att erhålla det kritiska vippningsmomentet av stagade balkar. Utöver detta, undersöks metoden föreslagen av Lindner och Aschinger (1990) för att inkludera effekterna av att ha ett korrugerat liv. Utvärderingen av dessa metoder utförs för stagade balkar med korrugerat liv. Utvärderingen utförs genom att jämföra det kritiska vippningsmomentet från dessa uttryck med resultat från linjära bucklingsanalyser med elastisk materialrespons. Dessutom utförs icke-linjära bucklingsanalyser för att utvärdera hur stagade balkar med korrugarade liv passar in i designmetoden för vippning föreslagen i Eurocode 3.

Rapporten fastslår att det kritiska vippningsmomentet med hög noggrannhet kan beräknas med Horne & Ajmanis metod. Uttrycket kan användas med jämförbar noggrannhet både för balkar med plana liv och balkar med korrugerade liv, användandes Lindners metod. Utöver detta dras slutsatsen att designmetoden för vippning föreslagen i Eurocode 3 kan användas för stagade balkar med korrugerade liv med konservativa resultat.

Nyckelord: Vippning, korrugerat liv, stålbalk, takåsar, stagning, vridstyvhet

Contents

Preface

This thesis was carried out at the Division of Structural Engineering, Department of Civil and Environmental Engineering, of Chalmers University of Technology during the spring of 2014.

In the thesis, the influence of purlins on the behaviour of steel girders, with corrugated web of trapezoidal shape, is investigated. Borga Steel Building produces steel portal frames with corrugated webs and they are interested in the possible advantages of taking the torsional stiffness, provided by rigidly attached purlins, into account when sizing the frames. This thesis was initiated by Chalmers University of Technology and Borga Steel Buildings.

We would like to thank our supervisor, Professor Emeritus Bo Edlund, and our examiner, Associate Professor Mohammad Al-Emrani, for their guidance throughout the project. We would also like to thank our opponent group, Hermann Þór Hauksson and Jón Björn Vilhjálmsson, for their feedback on the thesis. At last, we would like to thank the other students carrying out their theses at the department for making the work environment enjoyable.

Guðni Ellert Edvardsson

Bengt Lundquist

Notations

Roman upper case letters

A	Cross-sectional area
E	Modulus of elasticity
E_t	Tangent modulus
F	Force
G	Shear modulus
I	Second moment of area
I_t	Torsion constant
I_t^*	Equivalent torsion constant from Lindner's approach
I_t'	Equivalent torsion constant from modified Lindner's approach
I_w	Warping constant
I_w^*	Equivalent warping constant from Lindner's approach
I_w'	Equivalent warping constant from modified Lindner's approach
I_y	Second moment of area around the y-axis
I_x	Second moment of area around the x-axis
I_{y1}	Second moment of area around the y-axis for the top flange of an I-beam
I_{y2}	Second moment of area around the y-axis for the bottom flange of an I-beam
I_η	Second moment of area around the η-axis
I_ξ	Second moment of area around the ξ-axis
M	Bending moment
$M_{b,Rd}$	Design buckling resistance moment according to Eurocode 3
M_{cr}	Critical buckling moment
$M_{cr,1}$	Critical buckling moment caused by torsion along a restrained beam
$M_{cr,2}$	Critical buckling moment caused by lateral-torsional buckling between restraints
M_{Ed}	Design moment according to Eurocode 3
M_u	Ultimate moment
M_{yield}	Yield moment
M_0	External bending moment applied at end supports of a beam
M_ζ	Bending moment around the ζ-axis
M_η	Bending moment around the η-axis
M_ξ	Bending moment around the ξ-axis
P	Axial load
P_{cr}	Critical axial buckling load
T_t	St. Venant torsional moment
T_w	Vlasov torsional moment
U	Strain energy
V	Potential energy
W_y	Sectional modulus

Roman lower case letters

a	Length of the longitudinal panel of a corrugated web
a_r	Distance between the shear centre and the lateral restraint of a restrained cross-section

b	Projected length of the inclined panel of a corrugated web
b_f	Width of the flange of an I-beam
c	Length of the inclined panel of a corrugated web
d	Maximum corrugation eccentricity of a corrugated web
f_y	Yield stress
h_m	Distance between centroids of flanges of an I-beam
h_w	Height of the web of an I-beam
k	Buckling coefficient
k_{LT}	Reduction factor for initial imperfection in Eurocode 3
k_s	Spring stiffness
k_ϕ	Torsional stiffness
l	Total length of a structural element
n	Number of half-sine waves in the longitudinal direction of a member
n_b	Number of restraints along the total length of a girder
r	Radius of gyration
s	Spacing of purlins
t	Wall thickness of a plate or shell
t_f	Thickness of the flange of an I-beam
t_w	Thickness of the web of an I-beam
u	Deflection in the direction of the x-axis
u_L	Lateral component of lateral displacement due to lateral-torsional buckling
u_T	Torsional component of lateral displacement due to lateral-torsional buckling
v	Deflection in the direction of the y-axis
w	Width of a plate
x	Lateral axis of the global coordinate system
y	Vertical axis of the global coordinate system
z	Longitudinal axis of the global coordinate system

Greek lower case letters

α	Angle of the inclined panel in relation to the longitudinal axis
α_{LT}	Imperfection factor in Eurocode 3
γ_{M1}	Partial factor in Eurocode 3
δ	Maximum deflection
δ_s	Deformation of a spring
ε_e	Elastic strain
ε_p	Plastic strain
ζ	Longitudinal axis of the local coordinate system
η	Vertical axis of the local coordinate system
$\overline{\lambda}$	Non-dimensional slenderness ratio of steel members
$\bar{\lambda}_{LT}$	Non-dimensional slenderness ratio of beams
ν	Poisson's ratio
ξ	Lateral axis of the local coordinate system
σ_{cr}	Critical stress
ϕ	Angle of rotation
χ	Reduction factor
χ_{LT}	Reduction factor according to Eurocode 3

Definitions

Beam – Structural element that is capable of withstanding load primarily by resisting bending.

Bifurcation load – The critical load for buckling to occur in a structure.

Bifurcation point – The point on a load-deflection curve where the bifurcation load has been reached.

Bracing – Lateral and/or torsional restraint on a structure.

Critical buckling moment – Used to determine the load-carrying capacity against elastic lateral-torsional buckling.

Elastic strain, ε_e – Strain in which the deformed element returns to its original shape and size when the deforming force is removed.

Girder – Main structural member, often supporting smaller beams i.e. purlins.

Lateral restraint – Full restraint against lateral movement at a specific point. In this report it is caused by purlins.

Linear analysis – Assumes elastic material with no geometrical imperfections nor residual stresses in this study.

Mode shape – Describes the shape of a buckled beam. The mode shape number tells in how many half-sine waves the beam buckles.

Non-dimensional slenderness ratio, $\overline{\lambda}$ – Used to describe the slenderness of steel members in a non-dimensional expression.

Non-linear analysis – Assumes plastic material with strain hardening, geometrical imperfection and residual stresses in this study.

Poisson's ratio, ν – Negative ratio of transverse strain and axial strain.

Plastic strain, ε_p – Strain in which the deformed element does not return to its original size and shape after the deforming force has been removed.

Purlins – Secondary beams connected to girders to support the roof cladding. Provide restraint against lateral movement and torsion.

Radius of gyration – Is used to describe the distribution of cross-sectional area in a column around its centroidal axis, $r = \sqrt{\frac{I}{A}}$.

Reduction factor, χ – Ratio between the critical stress and the yield stress, expressed as: $\chi = \sigma_{cr}/f_y$.

Torsional restraint – Partial restraint against torsion at a specific point. In this report it is caused by purlins.

Ultimate moment, M_u – The maximum moment obtained from non-linear plastic analysis.

Yield moment – Moment that causes the yielding in the cross-section, expressed as: $W \cdot f_y$

1 Introduction

1.1 Background

Steel portal frames are commonly used in construction of industry halls. They are typically low-rise structures that consist of rigidly connected columns and beams. One of the governing failure modes of such structures is often lateral-torsional buckling of the beam. The stability of the frame can be increased by designing a haunch in the beams, by using a corrugated web or by adding stiffeners to the web.

The top flanges of the beams in the steel portal frames are connected to purlins at certain intervals which in turn are connected to the roof cladding. The top flange of each beam is usually in tension close to the eave of the frame and in compression close to the apex. In order to increase the lateral-torsional buckling capacity of the beam, stiffeners are provided at certain intervals to prevent rotation. The connection between the purlins and the frame in-between the stiffeners are usually not rigid, and can be considered to only provide lateral restraint to the frame. If the connection would be made rigid, the torsional stiffness from the purlins could be taken into account and consequently the distance between the stiffeners could be increased.

Important parameters that affect the stability of the frames are the load distribution, the shape of the corrugation and the geometrical parameters of the cross-section. The problem can be simplified by only consider the beam segment in-between two stiffeners. The beam segment is considered to be subjected to pure bending and connected to purlins at evenly spaced intervals.

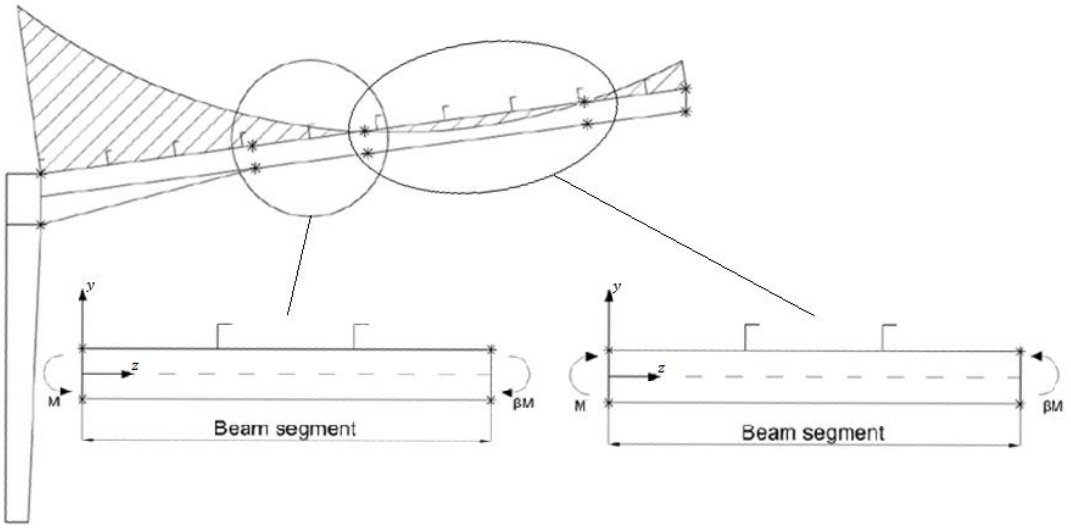

Figure 1.1: Beam segments extracted from a steel portal frame.

1.2 Aim and objective

The aim of this thesis is to investigate the lateral-torsional stability of steel girders with corrugated web of trapezoidal shape loaded in pure bending. The increased strength due to the torsional stiffness provided by rigidly attached purlins is of special interest. The objective of the thesis can be split into different parts:

- To carry out a literature study on how purlins affect the lateral-torsional stability of steel girders and how existing knowledge is treating the problem.
- To investigate how corrugated shape of the web influence the lateral-torsional stability of steel girders and how it is treated in analytical expressions.
- Evaluate the applicability of the analytical expressions for the critical moment due to lateral-torsional buckling of restrained girders with corrugated web.
- Investigate if the existing design approach for lateral-torsional buckling resistance from Eurocode 3 is applicable for laterally and torsionally restrained girders with corrugated web.

1.3 Method

A literature review was performed in order to achieve comprehensive understanding of the behaviour of steel beams undergoing lateral-torsional buckling. The effects from discrete lateral and torsional restraints along the beam were also investigated in order to understand how purlins affect the lateral-torsional buckling phenomenon. A further investigation was also performed in order to find an effective method of taking the increased stiffness, from the corrugated profile of the web, into account when calculating the critical buckling moment of the beam with analytical solutions.

A parametric study was carried out, with linear buckling analysis in ABAQUS CAE, in order to understand how the most influencing parameters affect the lateral-torsional buckling phenomenon of girders with flat and corrugated webs. The critical buckling moment from the parametric study was compared with an analytical solution, derived by Horne & Ajmani (1968), in order to examine its applicability. The difference in behaviour of girders with flat and corrugated webs was also investigated in order to evaluate the applicability of the analytical expression, proposed by Lindner (1990), to take the corrugated shape of the web into account.

In order to evaluate the applicability of the design approach for lateral-torsional buckling resistance in Eurocode 3 for restrained girders, non-linear buckling analyses with plastic material properties, including initial imperfections, were performed in ABAQUS CAE. From the analyses, buckling curves were obtained and compared with equivalent buckling curves in Eurocode 3. This was performed for girders with flat web and girders with corrugated web in order to investigate the difference in behaviour between the two girder types.

1.4 Limitations

In this project, only doubly symmetric, prismatic, I-sections with flat web and equivalent cross-sections with corrugated web will be considered. Fork supports are chosen as boundary conditions in order to imitate a beam segment between torsional stiffeners in steel portal frames. All structural members mentioned in this report will be considered to be of steel unless otherwise stated. Welds between the web and the flanges are not considered in this study.

The study will be limited to:

- Girders with homogeneous, isotropic material properties.

- Lateral-torsional buckling, other failure modes are not of interest.
- Bending moment around the strong axis, applied at the end supports.
- Steel with a yield stress of 355 MPa when non-linear material properties are used.

1.5 Outline of the thesis

Chapter 1 – Introduction of the project including background information, aim and objective, method and limitations.

Chapter 2 – Literature review comprising the theory describing lateral-torsional buckling, effects from restraints, the influence of corrugated shape of the web in girders and design approach suggested in Eurocode 3.

Chapter 3 – Description of the method used to obtain the aim of the project.

Chapter 4 – Procedure of the finite element analyses.

Chapter 5 – The results of the project are presented and discussed.

Chapter 6 – Conclusions of the project.

2 Literature Review

Lateral-torsional buckling is a well-known stability problem in slender unrestrained steel beams with doubly symmetric cross-section. Purlins will provide an increased stability due to their restraining effects. The purlins will restrain lateral movements of the beam at their connection points. In addition, they will restrain rotation of the sections if the connections are rigid. This increment in stability is of great interest from the designers' point of view due to economic reasons. Another alternative to increase lateral-torsional stability in beams is to have a corrugated web instead of a flat web. This chapter will explain the lateral-torsional buckling phenomenon and discuss the restraining effects from purlins as well as the effects from having corrugated web instead of flat web.

2.1 Stability of steel members

The structural stability of steel members is controlled by different failure modes, such as yielding, fatigue and buckling. Elastic buckling of steel members can only occur in the parts of members which are in compression when instability conditions are reached before yielding of the steel. In order to understand lateral-torsional buckling of beams, it is good to have some understanding of different kinds of buckling behaviour in simple steel members.

Columns are the simplest structural element for the study of buckling. According to Timoshenko & Gere (1961), the Euler theory suggests an expression for the critical buckling load of axially loaded columns. It assumes the column to be perfectly straight with ideally elastic material response and centrally applied load. After the bifurcation point is reached, the column becomes unstable and the magnitude of the deflection becomes indeterminate. The column will require the same amount of energy to buckle in any direction and is therefore symmetric around the bifurcation point. For a column hinged at both ends the critical load can be expressed by the following equation:

$$P_{cr} = \frac{\pi^2 n^2 EI}{l^2} \qquad 2.1$$

where E is the modulus of elasticity, I is the second moment of area, l is the length of the column and n is mode shape number. The first mode shape (for $n = 1$) requires the lowest critical load. Mode shapes with higher number are only of interest in very slender bars or when lateral restraints are applied at the inflection points.

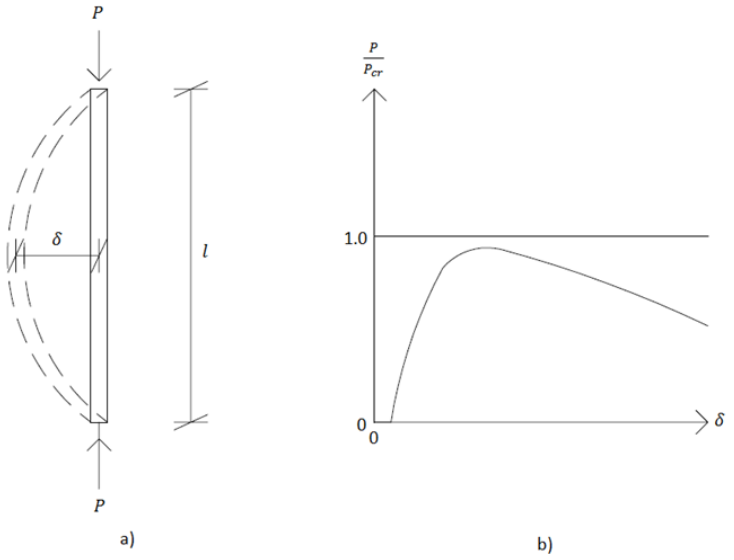

Figure 2.1: Column buckling; a) an axially loaded column of length $\boldsymbol{l}$ *with deflection* $\boldsymbol{\delta}$*;*
b) a normalized axial load as a function of deflection for a perfectly straight column and a column with an initial bow imperfection.

Figure 2.1b shows a graph of the applied load on the column, normalised with the critical buckling load, as a function of the deflection for perfectly straight column and a column with an initial bow imperfection. As can be seen, the perfectly straight column remains straight until the critical load is reached and it becomes unstable If an initial bow imperfection is present, further deflection increases with increasing load until it becomes unstable. The maximum load for the column to remain stable becomes lower as the initial imperfection is higher.

The buckling phenomenon can be described with the Euler buckling curve in terms of the non-dimensional slenderness ratio, $\bar{\lambda}$, and the reduction factor, χ, according to Al-Emrani & Åkesson (2013), which can be seen in figure 2.2. From the slenderness of the column, the reduction factor can be obtained and the critical buckling load calculated according to the following expression:

$$P_{max} = \chi \cdot f_y \cdot A \qquad 2.2$$

where f_y is the yield stress of the steel and A is the cross-sectional area of the column. By assuming elastic material response, the reduction factor increases to infinity as the slenderness ratio approaches zero. Since columns will undergo failure due to yielding when the yield stress is reached, the Euler curve is fixed to not exceed $\chi = 1$. It can be seen from figure 2.2 that the critical buckling load gets lower as the columns get more slender. Due to initial imperfections, which are inevitable in steel members, the critical buckling load from the Euler theory is an upper bound solution. In order to take this into account when designing steel structures, design curves have been implemented to reflect the actual behaviour of the column and to avoid unconservative design approaches.

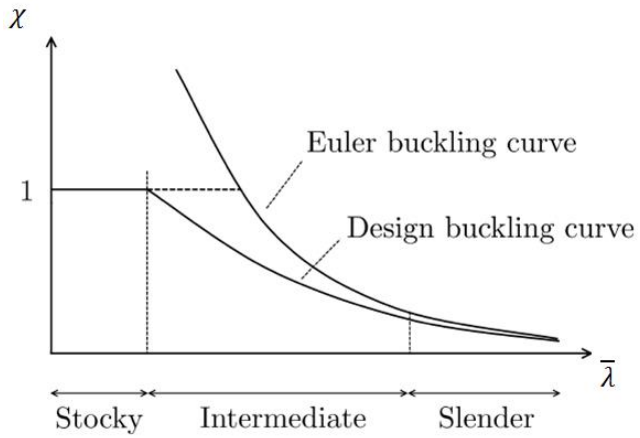

Figure 2.2: The Euler buckling curve and a design curve for columns, presented with the reduction factor,χ , as a function of the non-dimensional slenderness ratio,$\bar{\lambda}$, (Larsson & Persson, 2013).

The Euler theory can be extended to derive the critical buckling stress for axially loaded plates, simply supported on the loaded edges, according to figure 2.3a. The lowest critical axial load for such plates can be expressed by taking the Poisson's ratio, ν, into account and is expressed with the following equation:

$$P_{cr} = \frac{\pi^2 n^2 EI}{l^2} \cdot \frac{1}{(1-\nu^2)} \qquad 2.3$$

This can be reformulated as the critical axial stress of plates with equation 2.4, where t is the thickness of the plate.

$$\sigma_{cr} = \frac{\pi^2 n^2 E}{12(1-\nu^2) \cdot \left(\frac{l}{t}\right)^2} \qquad 2.4$$

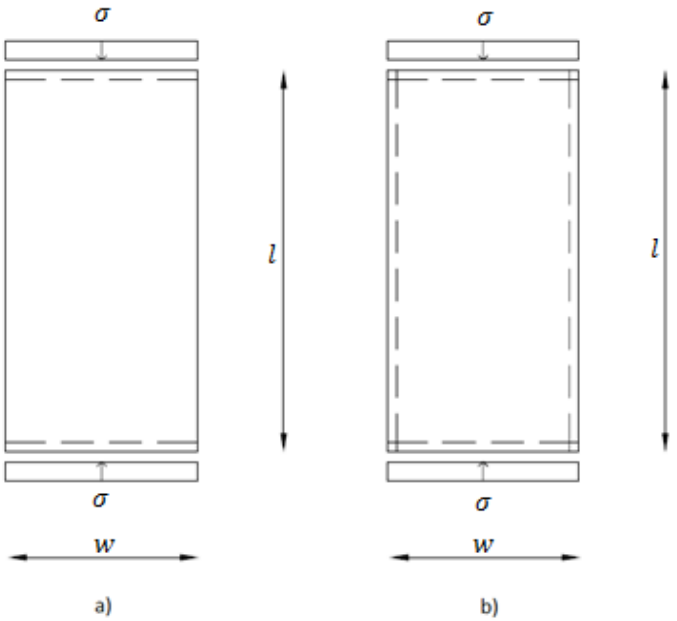

Figure 2.3: a) An axially loaded plate simply supported on its loaded edges; b) An axially loaded plate simply supported on all four edges.

For a plate simply supported on all four edges, as can be seen in figure 2.3b, the critical axial stress can be expressed with the following equation:

$$\sigma_{cr} = k \cdot \frac{\pi^2 E}{12(1-\nu^2) \cdot \left(\frac{w}{t}\right)^2} \quad 2.5$$

where w is the width of the plate and the buckling coefficient, k, is expressed with the following equation:

$$k = \left(\frac{n \cdot w}{l} + \frac{l}{n \cdot w}\right)^2 \quad 2.6$$

where n is the number of half-sine waves in the longitudinal direction of the buckled shape of the plate. The value of n is dependent on the aspect ratio, l/w, and will always be a natural number. The minimum value of the buckling coefficient is $k = 4.0$ when n has the same value as the aspect ratio.

The buckling behaviour of plates is strongly dependent on the boundary conditions. A plate supported only on the loaded edges will behave in a similar way as the column in figure 2.1. On the contrary, if the plate is supported on all four edges it will behave in a different way. When the bifurcation stress is exceeded in a perfectly plane plate, supported on all four edges, it will start to deflect. Due to the boundary conditions, a redistribution of stresses will result in a stable state of the plate, as can be seen in figure 2.4. As the load is increased further, the deflection increases until a maximum stress is reached and failure occurs. This increased strength is often, according to Al-Emrani & Åkesson (2013), referred to as a post-buckling strength. The plate will require the same amount of energy to buckle in both directions. Consequently the post-buckling behaviour can be considered as stable and symmetric around its bifurcation point.

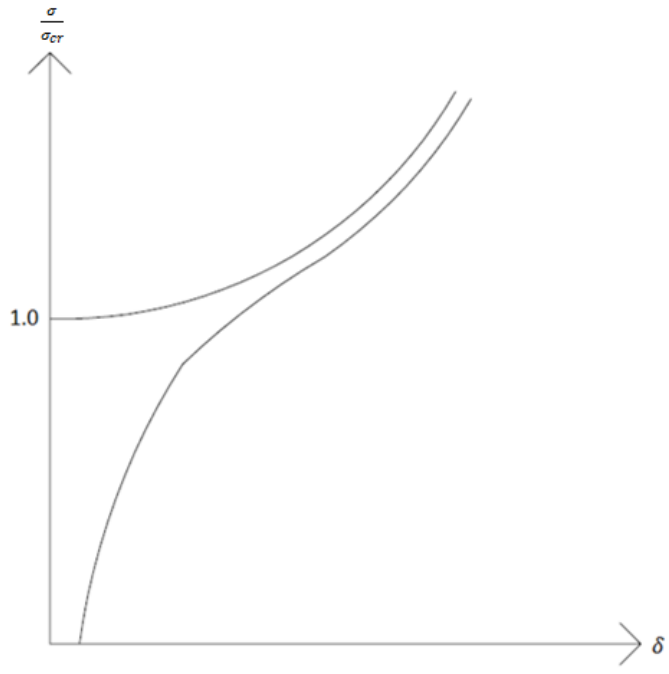

Figure 2.4: Plate buckling; normalized axial stress as a function of deflection for a perfectly plane plate and a plate with an initial bow imperfection.

Buckling in shell elements is of interest when comparing different buckling behaviour. Consider a thin-walled cylindrical shell with length l and radius r loaded in axial compression, as can be seen in figure 2.5a. According to Timoshenko & Gere (1961), the critical buckling stress of a perfect cylinder at the bifurcation point is expressed by the following equation:

$$\sigma_{cr} = \frac{P_{cr}}{t} = \frac{t\sqrt{EE_t}}{r\sqrt{3(1-\nu^2)}} \qquad 2.7$$

where t is the wall thickness of the shell and E_t is the tangent modulus of the cylinder.

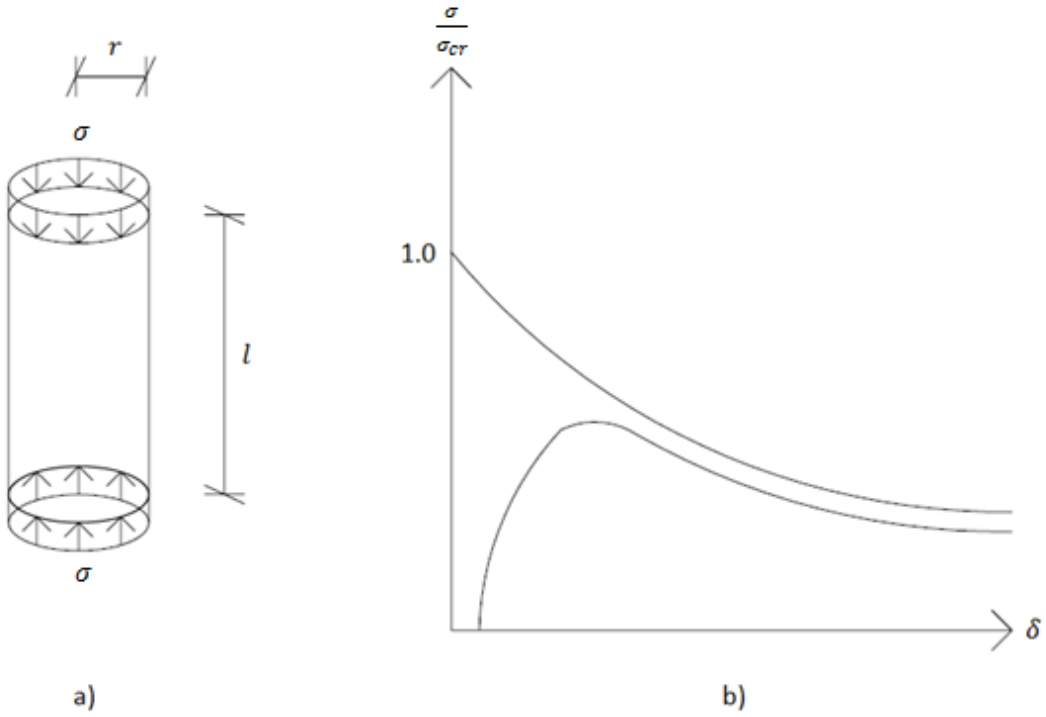

Figure 2.5: Shell buckling; a) An axially loaded shell of length $\boldsymbol{l}$ *with deflection* $\boldsymbol{\delta}$*; b) a normalized axial stress as a function of deflection for perfect shell and a shell with an initial imperfection.*

When the critical stress is reached in the perfect shell it becomes unstable. For a shell with initial imperfection the critical stress reduces very fast with increasing imperfections, which makes shells more sensitive to initial imperfections than columns and plates. A shell requires more energy to buckle outwards than inwards. Consequently the buckling behaviour after the bifurcation stress is exceeded can be considered as unstable and asymmetric around its bifurcation point.

2.1.1 Local and global behaviour

Buckling phenomena of steel members can be subdivided into local and global behaviour. Local behaviour occurs at one specific part of the member. Global buckling, on the other hand, is an overall instability mode of the member.

Local buckling occurs where the in-plane stresses are concentrated in a structural member and is usually described with theory for plates, according to Trahair (1993).

Resistance against local buckling in beams with doubly symmetric I-section can be increased by adding stiffeners to the web or having a corrugated shape of the web.

Flexural buckling occurs when a member buckles around one of its main axes. Buckling around its weak axis is referred to as lateral buckling. For a beam subjected to torsion, the cross-sections twist around its central axis. Lateral-torsional buckling is a combination of a lateral buckling and torsion. Flexural buckling, torsion and lateral-torsional buckling can be referred to as global buckling modes.

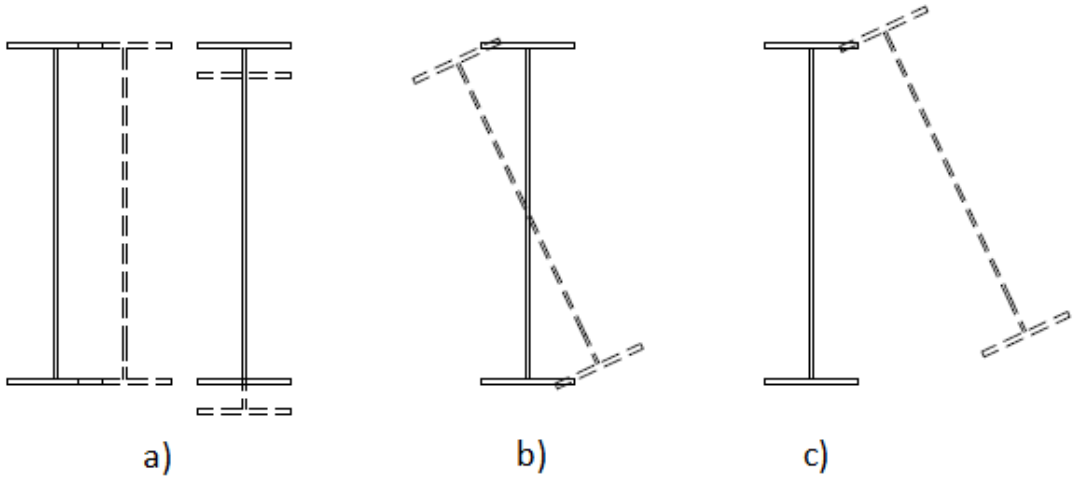

Figure 2.6: a) Flexural buckling; lateral buckling to the left and vertical buckling to the right; b) torsion; c) lateral-torsional buckling.

Distortional buckling is intermediate to local and global behaviour. It involves a deformation of the cross-sectional shape and the mode typically has the shape of a half-wavelength in the web or the flange of a beam.

2.2 Lateral-torsional buckling of I-beams

The structural stability of slender I-beams loaded in bending is often controlled by the lateral-torsional buckling capacity. This section treats topics such as lateral buckling and torsion in order to derive the expression describing lateral-torsional buckling of doubly symmetric I-beams.

2.2.1 Coordinate system

Global and local coordinate systems have to be defined in order to describe the buckling behaviour of an I-beam. The global coordinate system is defined with the fixed axes x, y, z where the x-axis is in the lateral direction, the y-axis is in the vertical direction and the z-axis is in the longitudinal direction of the beam. The x-axis can also be referred to as the major (strong) axis and the y-axis can be referred to as the minor (weak) axis. The local coordinate system is defined with the axes ξ, η, ζwhich are taken at the centre of the cross-section at any section of the beam and is equivalent to the global coordinate system. The definition of both coordinate systems can be seen in figure 2.7.

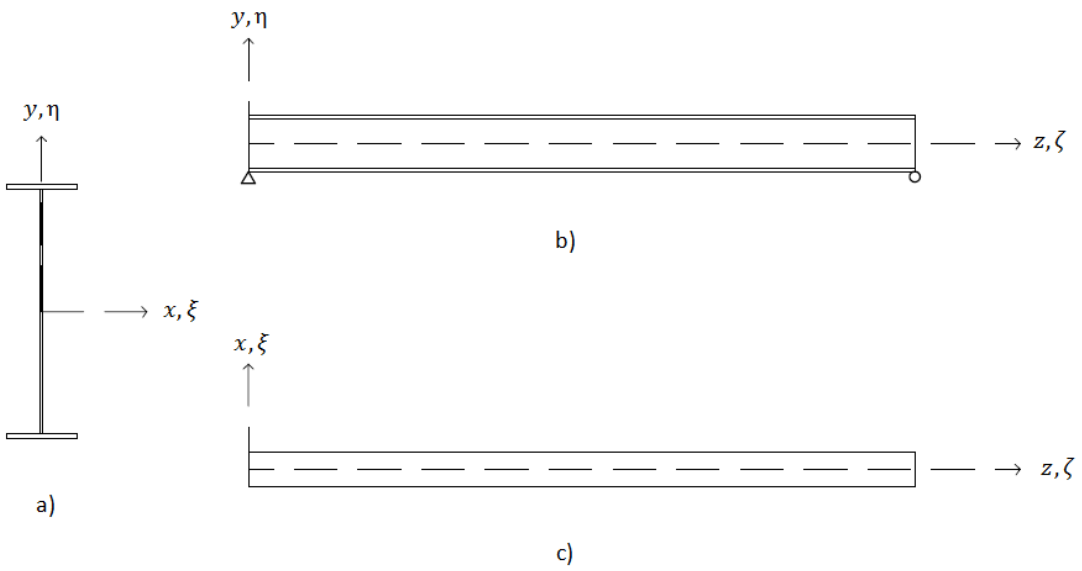

Figure 2.7: Definition of the global and local coordinate systems; a) a cross-sectional view; b) a beam seen from the side; c) a beam seen from above.

2.2.2 Lateral buckling

Flexural buckling causes deformation of the beam around one of the main global axes, which has the lowest stiffness. An I-beam loaded in bending in the plane of the web will buckle laterally when the critical buckling moment has been reached. The deflections of the beam are expressed with the variables u and v in the x- and y-direction respectively. For small deflections, the curvature of the beam can be expressed as $\frac{d^2u}{dz^2}$ for the xz-plane and $\frac{d^2v}{dz^2}$ for the yz-plane. The bending moment around the ξ- and η-axes can then, according to Timoshenko & Gere (1961), be described with the Euler-Bernoulli beam theory:

$$M_\xi = EI_\xi \frac{d^2v}{dz^2} \tag{2.8a}$$

$$M_\eta = EI_\eta \frac{d^2u}{dz^2} \tag{2.8b}$$

where the variables I_ξ and I_η are the second moment of area around ξ- and η-axis respectively.

2.2.3 Torsion

Torsional resistance of structural members can be divided into two distinct mechanisms. These mechanisms are often referred to as St. Venant torsional resistance and Vlasov torsional resistance, according to Estabrooks & Grondin (2008).

St. Venant torsion, or pure torsion, is defined as the rotation of a cross-section through an angle ϕ, according to Seaburg & Carter (2003). For non-circular cross-sections, such as I-sections, pure torsion is usually accompanied by Vlasov torsion. Vlasov

torsion, or warping torsion, occurs when the transverse sections do not remain plane during torsion. These two mechanisms are illustrated by figure 2.8.

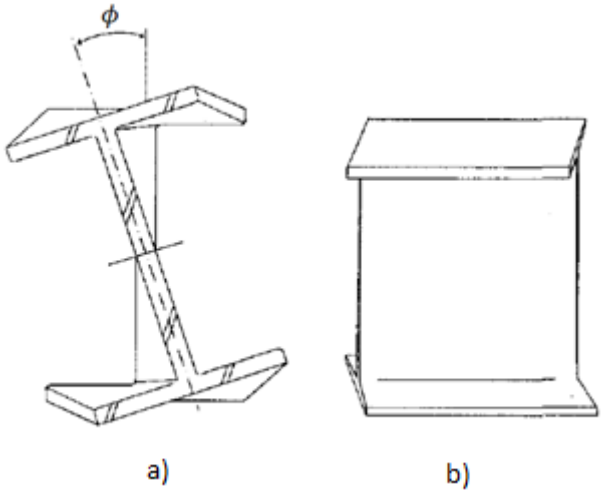

Figure 2.8: a) St. Venant torsion, or pure torsion; b) Vlasov torsion, or warping torsion (Seaburg & Carter, 2003).

An I-beam, loaded with torsional moment at both ends, as shown in figure 2.9, with all sections free to warp will have the same shear stress distribution in all sections of the beam (Timoshenko & Gere, 1961). If these conditions are fulfilled, the total St. Venant torsional resistance is expressed with the following equation:

$$T_t = GI_t\phi' \tag{2.9}$$

where G is the shear modulus for steel, I_t is the torsion constant for the cross-section and ϕ' is the first derivative of the angle of rotation. GI_t can also be referred to the torsional stiffness of the cross-section. The torsion constant for doubly symmetric I-beams with flat web is, according to Lundh (2000), expressed with the following equation:

$$I_t = \frac{2b_f t_f^3 + h_w t_w^3}{3} \tag{2.10}$$

where b_f and t_f are the width and the thickness of the flanges, respectively. h_w and t_w are the height and the thickness of the web, respectively.

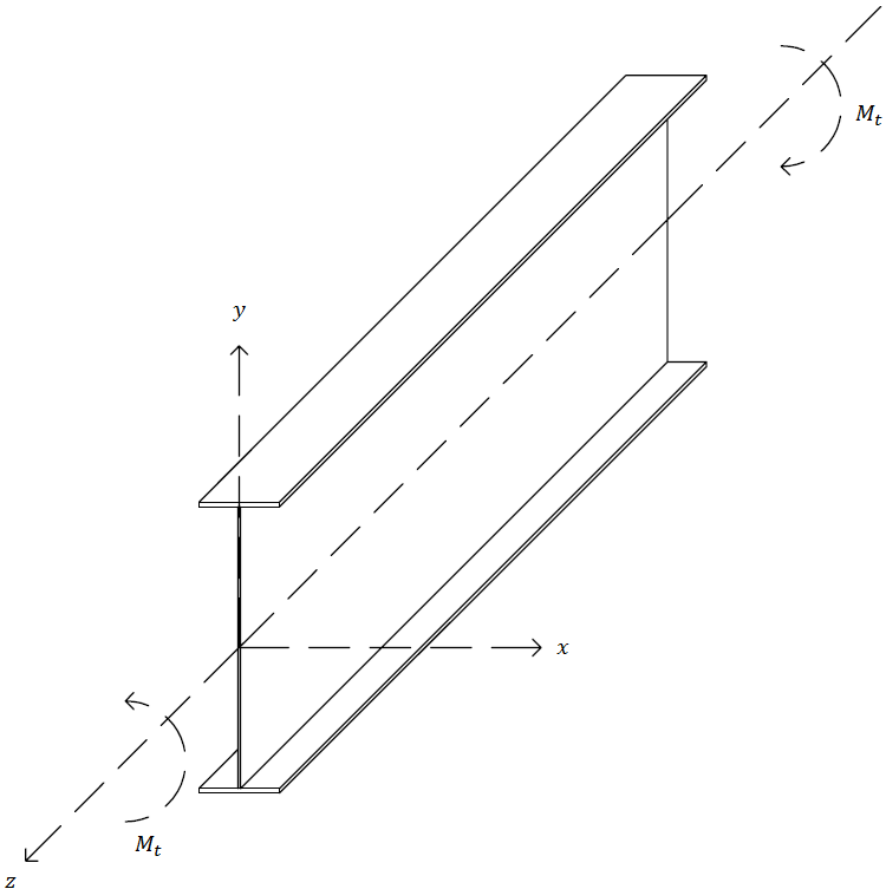

Figure 2.9: An I-beam subjected to torsional moment, $\boldsymbol{M_t}$*, at both ends.*

If any section of the beam is restrained to warp or if the torsional moment, M_t, varies along the length of the beam, there will be tension or compression of the longitudinal fibres and the warping will vary along the length of the beam. The total resisting moment due to restrained warping of the cross-section is, according to Timoshenko & Gere (1961), described with the following equation:

$$T_w = -EI_w\phi''' \tag{2.11}$$

where EI_w is the warping stiffness of the cross-section and ϕ''' is the third derivative of the angular displacement. The warping constant, I_w, for doubly symmetric I-beams with flat web is expressed with equation 2.12 according to Seaburg (2003).

$$I_w = \frac{I_y h_m^2}{4} \tag{2.12}$$

where I_y is the second moment of area around the y-axis and h_m is the distance between the centroids of the flanges. The total torsional resistance of the beam can now be expressed as the sum of the St. Venant and Vlasov components:

$$T = GI_t\phi' - EI_w\phi''' \tag{2.13}$$

2.2.4 Lateral-torsional buckling

Regard a simply supported I-beam which is subjected to bending moment M_o around the x-axis at each support as indicated in figure 2.10.

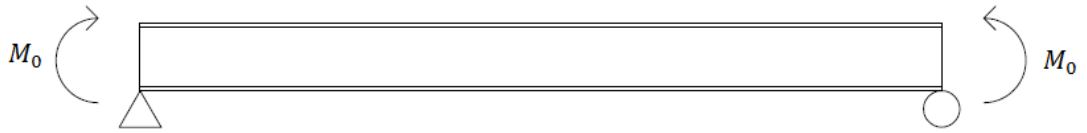

Figure 2.10: A beam with bending moment applied at both ends.

If the applied moment, M_0, is smaller than the critical buckling moment, M_{cr}, it will cause vertical deflection without any out-of-plane movement. If the moment is increased until it exceeds the critical buckling moment, M_{cr}, the beam will buckle laterally along with an angle of twist, according to Galambos & Surovek (2008). This is due to redistribution of the applied moment to the main axes of the local coordinate system as indicated in figure 2.11. The moments contributing to the deflection in the vertical and lateral directions are expressed with the variables M_ξ and M_η. The moment contributing to the rotation of the cross-section is expressed with M_ζ. For a small angle of deflection, this can be stated in terms of the applied moment M_0 in the following way:

$$M_\xi = M_0 \tag{2.14a}$$

$$M_\eta = \phi M_0 \tag{2.14b}$$

$$M_\zeta = -\frac{du}{dz} M_0 \tag{2.14c}$$

where $\frac{du}{dz}$ is the angle between the local ζ-axis and the global x-axis. The moment around the ζ-axis is negative considering the positive direction of the moments.

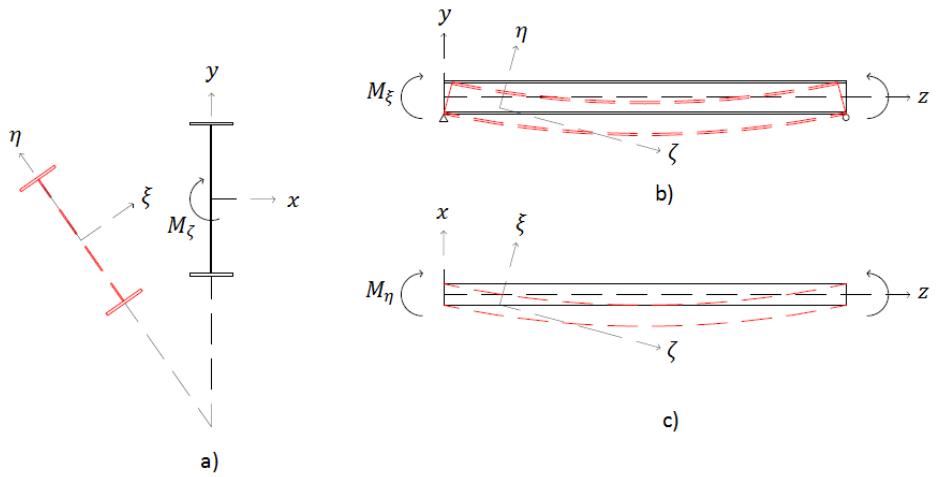

*Figure 2.11: a) Rotation of the cross-section caused by the moment $\boldsymbol{M_\zeta}$ around the **ζ**-axis; b) vertical deflection of the beam caused by the moment $\boldsymbol{M_\xi}$ around the **ξ**-axis; c) lateral deflection caused by the moment $\boldsymbol{M_\eta}$ around the **η**-axis.*

In order to derive a formulation to describe lateral-torsional buckling, the moment from equation 2.14b is set equal to equation 2.8b, describing lateral deflection. In addition, the moment from equation 2.14c is set equal to the total torsional resistance in equation 2.13. These equations can now be combined to obtain the following expression:

$$GI_t \frac{d^2\phi}{dz^2} - EI_w \frac{d^4\phi}{dz^4} + \frac{M_0^2}{EI_\eta}\phi = 0 \qquad 2.15$$

This can be solved mathematically by finding a general solution for the differential equation and use the boundary conditions of a simply supported beam. This will, according to Timoshenko & Gere (1961), lead to the following expression for the critical buckling moment:

$$M_{cr} = \frac{\pi^2 EI_y}{l^2}\sqrt{\frac{I_w}{I_y} + \frac{l^2 GI_t}{\pi^2 EI_y}} \qquad 2.16$$

2.3 Restrained buckling

Structural members are often influenced by different types of restraints that can affect the stability. A beam is considered to be continuously restrained if all sections of the beam are restrained. Continuous restraints are typically provided by slabs or metal decks, which are connected to the flange of beams. Continuous stiffeners can also be added to the web or the flanges of a beam. Discrete restraints, on the other hand, consist of a finite number of restraints on the beam. One type of discrete restraints is purlins attached to the top flange of an I-beam.

Stabilisation of beams can be divided into two types, lateral and torsional restraints. The following sections describe important factors that affect the lateral and torsional restraints, focusing on the effects of purlins.

2.3.1 Lateral restraints

There are several factors that influence the performance of laterally restrained girders. According to Yura (2001), the most important factors are how the member is loaded, where at the cross-section the restraint is applied, the number of restraints along the girder and the stiffness of the restraints.

Since the location of the restraint at the cross-section is an important parameter, the behaviour of a laterally restrained girder during lateral-torsional buckling will be different if the compression flange or the tension flange of an I-beam is restrained. An I-beam undergoing lateral-torsional buckling will have the maximum lateral deflection at the compression flange. A lateral restraint connected to this flange will effectively eliminate lateral movements of the restrained section. Consequently, there will be no rotation of the restrained section.

Lateral restraints on the tension flange of an I-beam will lower the centre of rotation during lateral-torsional buckling at the restrained section, as can be seen in figure 2.12. The lateral displacement can be split up into two components, deflection due to

lateral movement, u_L, and deflection due to torsion of the cross section, u_T. Lateral restraints will cause reduction of u_L but u_T will not be affected, unless torsional stiffness of the restraint is present.

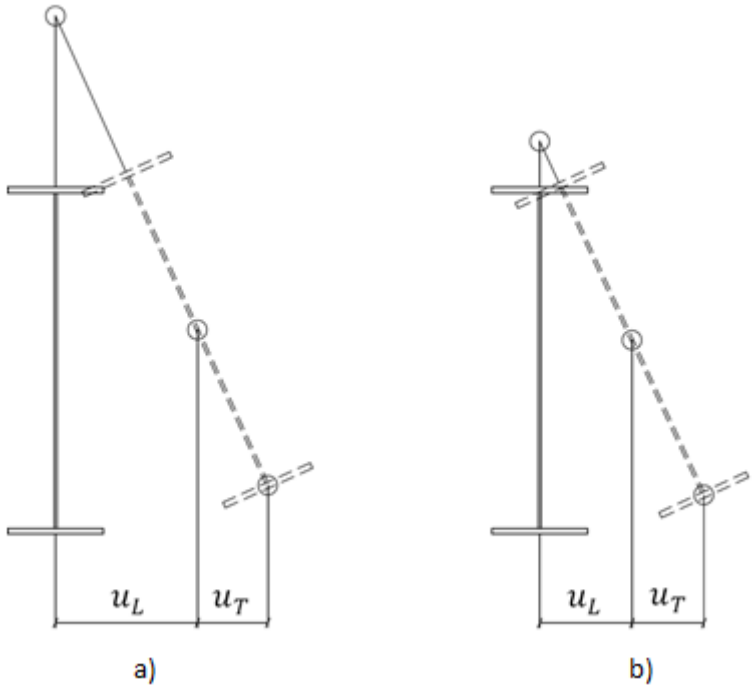

Figure 2.12: a) Rotation of an unrestrained I-section undergoing lateral-torsional buckling; b) rotation of a laterally restrained I-section undergoing lateral-torsional buckling, resulting in lower centre of rotation and smaller $\boldsymbol{u_L}$.

2.3.2 Torsional restraints

The number of stiffeners and the location of the load on the cross-section are, according to Galambos (2008), not as important for torsional restraints as for lateral restraints. Torsional restraints are equally effective if they are applied at the compression flange or at the tension flange of girders.

A combination of lateral and torsional restraints is of interest when regarding the effects from rigidly attached purlins on a girder. As mentioned in section 2.3.1, lateral restraints at the compression flange effectively eliminate rotation of the restrained section. The torsional stiffness, provided by rigidly attached purlins, is therefore only of interest when the purlins are connected to the flange subjected to tension. As can be seen in figure 2.13, both the lateral and the torsional components of the lateral displacement are affected by torsional restraints. The torsional stiffness provided by the purlins is greatly dependent on the rigidity of the connection of the purlins to the girder and is therefore often disregarded in design due to lack of rigidity. However, this torsional stiffness can be of interest for design purposes due to economic reasons.

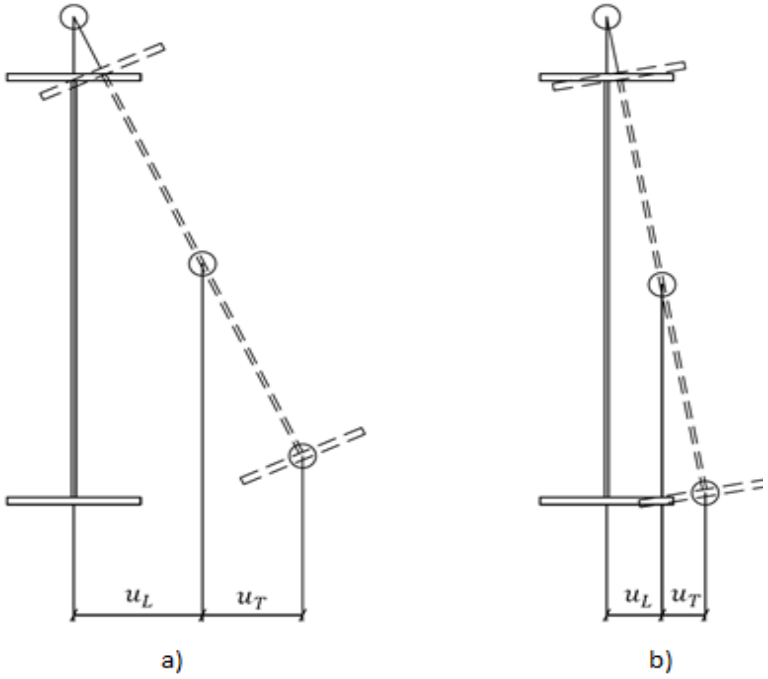

Figure 2.13: a) Rotation of a cross-section of a torsionally unrestrained girder; b) rotation of a cross-section of a torsionally restrained girder, resulting in smaller $\boldsymbol{u_L}$ *and* $\boldsymbol{u_T}$.

The torsional stiffness that rigidly attached purlins would provide to a girder at the connection points is dependent on the properties of the purlins. The torsional stiffness can be estimated from the angle of rotation due to the moment M_ζ around the ζ-axis caused by lateral-torsional buckling of the girder. The expression for the torsional stiffness, k_ϕ, is presented in equation 2.17 and the derivation of it can be seen in appendix A.

$$k_\phi = \frac{3E_p I_p}{l_p} \tag{2.17}$$

The parameter l_p is the span of the purlin, i.e. length between adjacent girders, E_p and I_p are the modulus of elasticity and the second moment of area of the purlin, respectively.

2.4 Critical moment for girders restrained by purlins

The following sections describe how the critical buckling moment for girders, loaded in pure bending and discretely restrained by purlins, can be approximated with analytical expressions. The critical buckling moment will be regarded for girders restrained either at its compression flange or its tension flange.

2.4.1 Girders restrained at the compression flange

When a girder is connected to purlins at its compression flange, the restraining effect from the purlins will prevent lateral movement and rotation of the entire restrained section of the girder as described in section 2.3.1. The girder will therefore not be able

to undergo lateral-torsional buckling along its total length and will instead buckle along the length between the purlins. The critical buckling moment can therefore be approximated to be equal to the critical buckling moment for an unrestrained girder, from equation 2.16, where the length of the girder, l, is reduced to the spacing between the purlins, s. The critical buckling moment for girders connected to purlins at the compression flange can now be expressed with the following equation:

$$M_{cr} = \frac{\pi^2 E I_y}{s^2}\sqrt{\frac{I_w}{I_y} + \frac{s^2 G I_t}{\pi^2 E I_y}} \qquad 2.18$$

Reducing the buckling length will increase the critical buckling moment. For short spacing between purlins, the critical buckling moment will be high and it is likely that other failure mode than lateral-torsional buckling will be critical for the total load bearing capacity.

2.4.2 Girders restrained at the tension flange

An approach to determine the critical buckling load of axially loaded columns supported with discrete lateral and torsional restraints was developed by Dooley (1966). This was further developed by Horne & Ajmani (1968) by taking bending moment into account. Both approaches start off similarly where the strain energy U caused by the buckling process is put equal to the change in potential energy V. Both articles derive expressions for two different cases. The first case is when the number of half-sine waves of the buckled girder, n, is not equal to the number of intervals between the discrete restraints, l/s. The second case is when n is equal to the number of intervals. Horne & Ajmani derived the critical buckling moment for these two cases for pure bending moment, which can be expressed in the following way:

Case 1: $\boldsymbol{n \neq \frac{l}{s}}$

This case occurs when the girder buckles by twisting around the restrained longitudinal axis of the girder. The critical buckling moment is described with the following equation:

$$M_{cr,1} = \frac{1}{2a_r}\left(GI_t + \frac{\pi^2 n^2 E}{l^2}(I_w + a_r^2 I_y) + \frac{k_\phi}{s}\frac{l^2}{n^2\pi^2}\right) \qquad 2.19$$

where a_r is the distance between the shear centre of the girder and the centre of the rotation of the restraint. k_ϕ is the torsional stiffness provided by each restraint and s is the spacing between the restraints. The critical buckling moment is the minimum value of $M_{cr,1}$ for $n = 1,2,\dots,n_b$ where n_b is the number of purlins attached to the girder.

Case 2: $\boldsymbol{n = \frac{l}{s}}$

When this requirement is fulfilled, the torsional stiffness is high enough to assume full torsional restraint. The critical buckling moment is therefore independent of the torsional stiffness and represents the critical buckling moment caused by lateral-torsional buckling along the length between restraints. This can be expressed with the following equation:

$$M_{cr,2} = \frac{\pi^2 E I_y}{s^2}\sqrt{\frac{I_w}{I_y} + \frac{s^2 G I_t}{\pi^2 E I_y}} \qquad 2.20$$

These equations will hereafter be referred to as Horne & Ajmani's expression. They are derived under the assumption that the tension flange is continuously restrained. Consequently, they only apply when the restraints are equally spaced.

The critical buckling moment of a restrained girder, calculated with equation 2.19, increases linearly with increasing torsional stiffness for each mode shape. As the mode shape number gets higher, the increment of the critical buckling moment becomes less steep for increasing torsional stiffness of the restraint. When the mode shape has the same number as the number of spans between restraints, i.e $n = l/s$, the requirement for case 2 is reached and the critical buckling moment is calculated according to equation 2.20.

Consider a girder with three evenly spaced purlins connected to its tension flange, as can be seen in figure 2.14. The critical buckling moment can be plotted as a function of the torsional stiffness of the restraints as can be seen in figure 2.15, for all possible mode shapes. For each value of the torsional stiffness, the critical buckling moment is given with the minimum value from each mode shape.

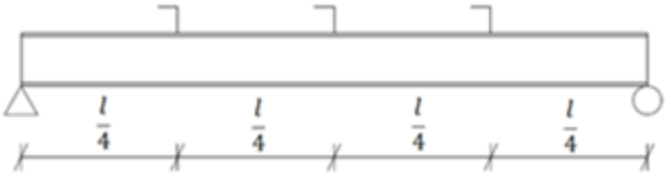

Figure 2.14: A side view of a girder attached to three purlins at its tension flange.

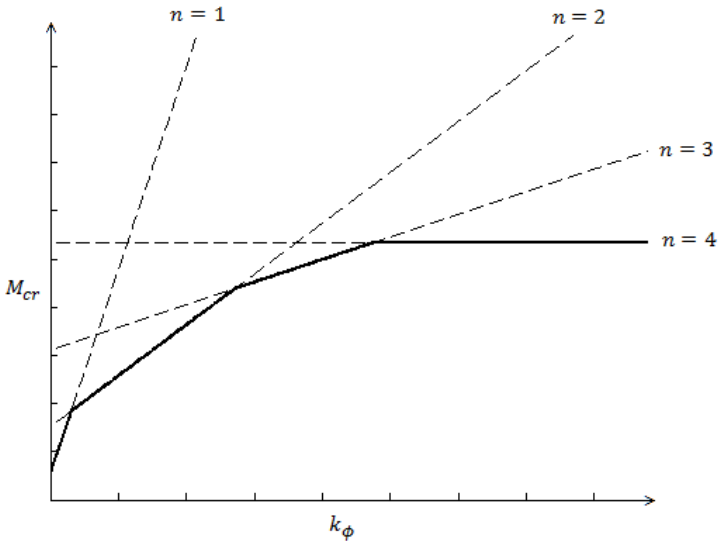

Figure 2.15: The critical buckling moment from Horne & Ajmani's expression, $\boldsymbol{M_{cr}}$,plotted as a function of the torsional stiffness, $\boldsymbol{k_\phi}$, for every mode shape for a girder with three purlins along its length. The critical buckling moment of the girder is obtained from the minimum value of $\boldsymbol{M_{cr}}$ for each mode shape, indicated with the thick solid line.

2.5 Girders with corrugated web

A common way of increasing the buckling strength in steel girders is to add stiffeners to the web. The most common way of adding those stiffeners to the girder is to weld them manually, which is both time consuming and expensive. A more recent alternative is to use corrugated web in order to obtain increased stiffness and delay fatigue failure. The corrugated web and the flanges can be machine-welded together which will save time and cost, according to Sayed-Ahmed (2007). A commonly used shape of the corrugated profile is trapezoidal, which can be seen in figure 2.16.

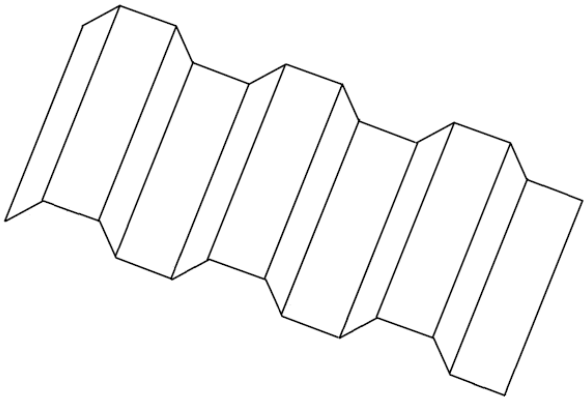

Figure 2.16: Trapezoidal profile of a corrugated web.

Some research has been carried out to investigate the effects from the corrugated web on the structural stability, but the knowledge is still limited. From a theoretical point of view, the corrugated shape of the web makes the derivation of load bearing formulations more complicated. The shear strength of corrugated webs can be calculated with relatively good accuracy, according to Galambos (1998). When the shape of the web has course corrugation, the shear strength of the web is controlled by local buckling in the web. As the corrugation gets denser, global buckling of the whole beam is more likely to become the critical failure mode.

Unlike girders with flat web, girders with corrugated web are considered to resist bending only by their flanges and the shear force is resisted by the web. The web is therefore not taken into account in the second moment of area around the major axis.

One of the main design aspects, for thin-walled I-beams, is lateral-torsional buckling. One way of taking the effects from the corrugated shape of the web into account is a method suggested by Lindner & Aschinger (1990) which hereafter will be referred to as Lindner's approach.

2.5.1 Lindner's approach

A beam with corrugated web has an increased critical buckling moment, M_{cr}, compared to a beam with flat web. The eccentricity of the web gives an increased strength against warping and torsion. One way of taking this increment into account is suggested by Lindner & Aschinger (1990). This method proposes that the critical buckling moment of unrestrained and simply supported beams with corrugated web can be calculated using the same formula for M_{cr} as for beams with flat web but inserting new warping and torsion constants in order to take the effects from the corrugated web into account. These constants are expressed with the following equations:

$$I_t^* = I_t \tag{2.21a}$$

$$I_w^* = I_w + c_w \frac{l^2}{\pi^2 E} \tag{2.21b}$$

By this approach, the torsion constant is approximated to be the same as for an equivalent beam with flat web and the increased stiffness due to the corrugated shape is included in the warping constant. The variable c_w is expressed in the following way:

$$c_w = \frac{(2d)^2 \cdot h_m^2}{8 \cdot u_x \cdot (a+b)} \tag{2.22a}$$

$$u_x = \frac{h_m}{2Gat_w} + \frac{h_m^2 (a+b)^3}{600a^2 E} \frac{I_{y1} + I_{y2}}{I_{y1} I_{y2}} \tag{2.22b}$$

where h_m is the distance between the centroids of the flanges and t_w is the thickness of the web. I_{y1} and I_{y2} are the second moment of area around the strong axis for the top and bottom flanges respectively. The parameters a, b and d are defined in figure 2.17.

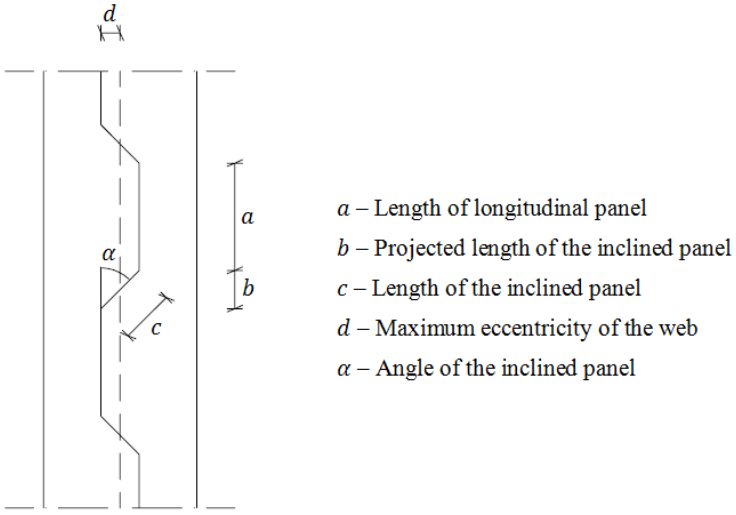

Figure 2.17: Shape of a trapezoidally corrugated web.

Lindner's approach was carried out by assuming unrestrained beams and therefore assumes the beam to buckle in the first mode shape. Restrained girders have the possibility to buckle in higher order mode shape, which needs to be taken into account. The warping constant in equation 2.12b should therefore be rewritten in a more general form by exchanging the length of the beam to the length of each half-sine wave of the buckled shape. This can be expressed with the following equations:

$$I_t^* = I_t \tag{2.23a}$$

$$I_w^* = I_w + c_w \frac{l^2}{\pi^2 n^2 E} \tag{2.23b}$$

These equations apply for both restrained and unrestrained beams. For unrestrained beams, which buckle with the first mode shape, the warping constant from equation 2.23b will become the same as in equation 2.21b, since $n = 1$. This approach of taking the corrugation into account is dependent on the length of the beam and the mode shape. This is not the usual case for sectional constants, which normally only depend on sectional properties. A modification of this approach has been suggested by Larsson & Persson (2013) and is explained in the following section.

2.5.2 Modified Lindner's approach

Lindner's approach suggests that the increased stiffness from the corrugation should be added to the warping constant, while the torsion constant is the same as for an equivalent beam with flat web. In order to make these sectional constants only dependent on sectional properties, Larsson & Persson (2013) suggested a modification of Lindner's approach, which is expressed in equation 2.24. This reformulation adds the effects from the corrugation to the torsion constant instead of the warping constant.

$$I_t' = I_t + \frac{c_w}{G} \tag{2.24a}$$

$$I_w' = I_w \tag{2.24b}$$

The modified Lindner's approach takes higher order mode shapes into account, as can be seen in the derivation in appendix A. Since the modified Lindner's approach is a reformulation of the original Lindner's approach, it will give exactly the same result when calculating the critical buckling moment.

2.6 Lateral-torsional buckling in Eurocode 3

Design suggestions for buckling resistance of steel members are treated in Eurocode 3. It suggests a verification against lateral-torsional buckling for laterally unrestrained steel members, subjected to major axis bending, with the following condition:

$$\frac{M_{Ed}}{M_{b,Rd}} \leq 1.0 \tag{2.25}$$

where M_{Ed} is the design value of the moment and $M_{b,Rd}$ is the design buckling resistance moment. $M_{b,Rd}$ is calculated for laterally unrestrained beams according to the following equation:

$$M_{b,Rd} = \chi_{LT} \cdot W_y \frac{f_y}{\gamma_{M1}} \tag{2.26}$$

where W_y is the appropriate section modulus, dependent on the classification of the cross-section, and χ_{LT} is the reduction factor for lateral-torsional buckling. Eurocode 3 suggests two different ways of calculating the reduction factor, which will be described hereafter.

1. Lateral-torsional buckling curves - General case

The reduction factor is given for the general case for members in bending with constant cross-section with the following equations:

$$\chi_{LT} = \frac{1}{\Phi_{LT} + \sqrt{\Phi_{\mathrm{LT}}^2 - \overline{\lambda}_{LT}^2}} \leq 1.0 \qquad 2.27$$

$$\Phi_{LT} = 0.5\left[1 + \alpha_{LT}\left(\overline{\lambda}_{LT} - 0.2\right) + \overline{\lambda}_{LT}^2\right] \qquad 2.28$$

$$\overline{\lambda}_{LT} = \sqrt{\frac{W f_y}{M_{cr}}} \qquad 2.29$$

M_{cr} is the elastic critical moment due to lateral-torsional buckling and α_{LT} is an imperfection factor, which is determined from the corresponding buckling curve. The buckling curves in Eurocode 3 are presented as the reduction factor, χ_{LT}, as a function of the non-dimensional slenderness, $\bar{\lambda}_{LT}$, and can be seen in figure 2.18. The recommended value of the imperfection factor, corresponding to the appropriate buckling curve, can be seen in table 2.1. Furthermore, table 2.2 shows the recommendations for the choice of buckling curve with regard to the cross-sectional dimensions.

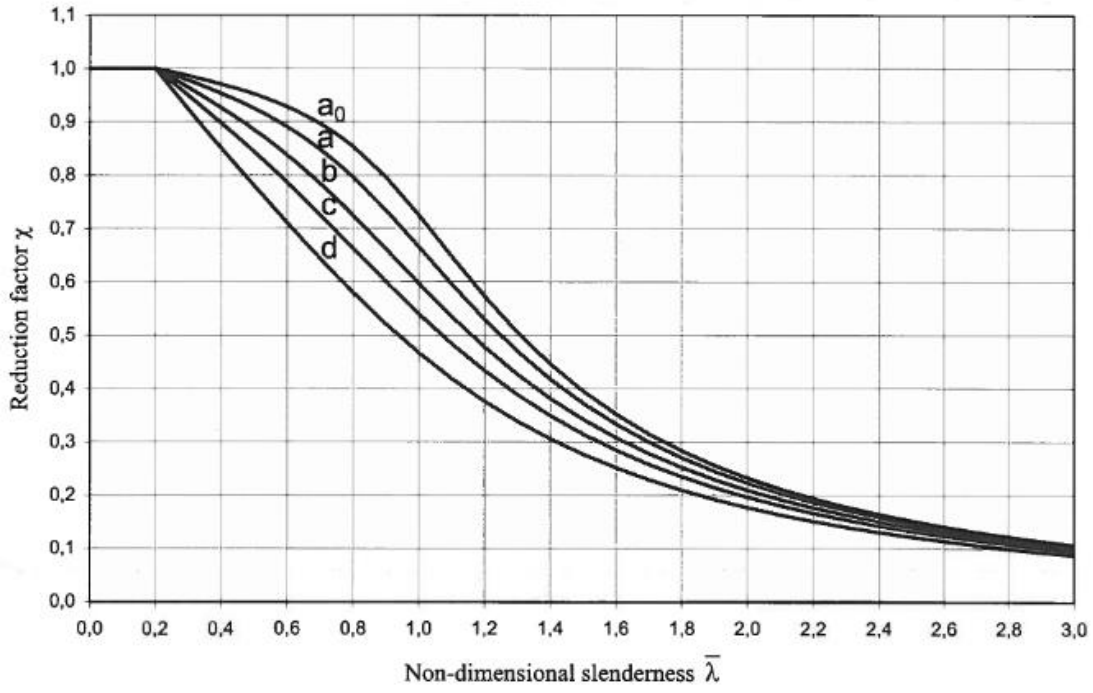

Figure 2.18: Buckling curves according to Eurocode 3.

Table 2.1: Imperfection factor,α_{LT}, corresponding to the appropriate buckling curve in Eurocode 3.

Buckling curve	a_0	a	b	c	d
Imperfection factor, α_{LT}	0.13	0.21	0.34	0.49	0.76

Table 2.2: Recommended values for lateral-torsional buckling curves for cross-sections using equation 2.27. h and b are the total height and the width of the cross-section, respectively.

Cross-section	Limits	Buckling curve
Rolled I-sections	$h/b \leq 2$ $h/b > 2$	a b
Welded I-sections	$h/b \leq 2$ $h/b > 2$	c d
Other cross-sections	-	d

2. Lateral-torsional buckling curves for rolled sections or equivalent welded sections

The reduction factor for rolled sections or equivalent welded sections is calculated in similar way as in the general case, with the exception of the variables $\overline{\lambda}_{LT,0}$ and β, which have the recommended values 0.4 and 0.75, respectively. Table 2.3 shows the recommended choice of buckling curve with regard to the cross-sectional dimensions. The reduction factor is given with the following equations:

$$\chi_{LT} = \frac{1}{\Phi_{LT} + \sqrt{\Phi_{\mathrm{LT}}^2 - \beta\overline{\lambda}_{LT}^2}} \leq \begin{cases} 1.0 \\ \frac{1}{\overline{\lambda}_{LT}^2} \end{cases} \qquad 2.30$$

$$\Phi_{LT} = 0.5\left[1 + \alpha_{LT}\left(\overline{\lambda}_{LT} - \overline{\lambda}_{LT,0}\right) + \beta\overline{\lambda}_{LT}^2\right] \qquad 2.31$$

Table 2.3: Recommended values for lateral-torsional buckling curves for cross-sections using equation 2.30. h and b are the total height and the width of the cross-section, respectively.

Cross-section	Limits	Buckling curve
Rolled I-sections	$h/b \leq 2$ $h/b > 2$	b c
Welded I-sections	$h/b \leq 2$ $h/b > 2$	c d

3 Method

The torsional stiffness provided by purlins is of special interest considering the aim of the project. As explained in section 2.3.1, lateral fixation at the compression flange will effectively eliminate lateral-torsional buckling of the restrained section. Consequently, torsional stiffness is only of interest when girders are restrained at their tension flange.

A parametric study is carried out in order to evaluate analytical expressions for the critical buckling moment of restrained girders. The results from the analytical solutions and the linear buckling analyses are compared. In addition, non-linear analyses are carried out in order to evaluate the approach suggested in Eurocode 3 to treat lateral-torsional buckling. The following sections explain the methodology more thoroughly.

3.1 Geometry of the studied girders

There are two main types of girders studied in this project. One has a doubly symmetric I-section with flat web and the other has equivalent cross-section with corrugated web. Both girder types are considered to be welded, but the influence from the welds are neglected in calculations. The sectional view of the girder with flat web can be seen in figure 3.1. The cross-sectional dimensions of the studied girders, along with their total length can be seen in table 3.1. The only difference between the dimensions of the girders is the thickness of the web. The girder with flat web has a thicker web in order to prevent local behaviour in the web, since only global buckling behaviour is of interest in this study. The shape of the corrugated profile can be seen in figure 3.2. The dimensions of the corrugation used in this report are commonly used by the steel product manufacturer Borga Steel Buildings and can be seen in table 3.2.

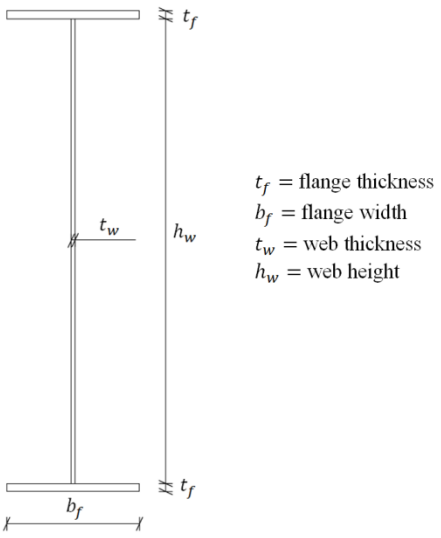

Figure 3.1: Geometry of the cross-section of the studied girder with flat web.

Table 3.1: Dimensions of the studied girders with flat web and with corrugated web. All values are in meters.

	L	b_f	t_f	h_w	t_w
Flat web	9.5	0.2	0.012	0.7	0.006
Corrugated web	9.5	0.2	0.012	0.7	0.002

Table 3.2: Dimensions of the corrugated profile. All values are in meters unless otherwise stated.

a	b	c	d	α [°]
0.140	0.05	0.071	0.025	45

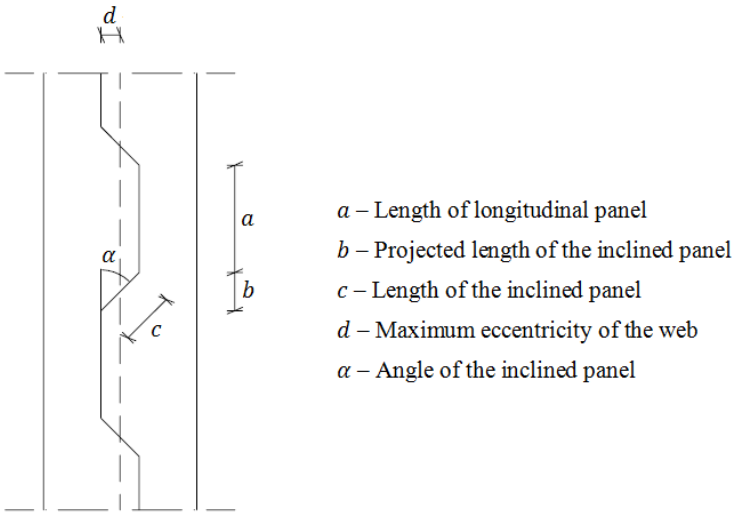

Figure 3.2: Shape of a trapezoidally corrugated web.

3.2 Parametric study

Girders with lateral and torsional restraints connected to the tension flange are modelled in order to verify the applicability of the Horne & Ajmani's expression, equations 2.19 and 2.20. Both girders with flat web and girders with corrugated web are modelled in order to evaluate the applicability of Lindner´s approach, equation 2.23, for restrained girders. In addition to the Lindner's approach, the difference between the analytical expressions of the critical buckling moment for the two girders is the second moment of area. For the girder with flat web it is determined by the whole cross-section and for the girder with the corrugated web, it is determined only by the flanges, excluding the influence from the web. The range of the studied parameters can be viewed in table 3.3.

Table 3.3: Range of the studied parameters for girders restrained at the tension flange.

Parameter	Range
Number of restraints	$1 - 6$
Torsional stiffness	$0 - 2 \cdot 10^5$ Nm/rad
Web thickness	$2 - 10$ mm
Web height	$500 - 1000$ mm
Flange thickness	$8 - 17$ mm
Flange width	$125 - 250$ mm

When the number of restraints and the torsional stiffness of the restraints are studied, the cross-sectional dimensions are set to the values stated in section 3.1. For a girder with fixed cross-sectional dimensions, the torsional stiffness of the restraints decides which mode shape requires the lowest amount of energy to occur and consequently is the governing mode shape. Altering cross-sectional dimensions, while the torsional stiffness of the restraints is fixed, will affect the behaviour of a girder in a similar way. It is of interest to study if the behaviour when changing cross-sectional dimensions differs when different modes shapes are decisive. It is decided to study the first and the second mode shape. Consequently, geometrical parameters are studied for two different values of the torsional stiffness, resulting in the first and the second mode shape. These two values differ between the different geometrical parameter studies, in order to obtain the same mode shape throughout the whole range of each studied parameter. All geometrical parameters are studied for girders with five restraints along its length. When cross-sectional dimensions are studied, the remaining dimensions are set to the values stated in section 3.1.

3.3 Evaluation of the design approach in Eurocode 3

Non-linear buckling analyses are carried out using ABAQUS CAE, in order to produce buckling curves for restrained girders. These buckling curves are compared with the buckling curves provided by Eurocode 3, described in section 2.6, in order to evaluate their applicability for laterally and torsionally restrained girders. This procedure is performed for the two girders described in section 3.1. The girders have six lateral and torsional restraints applied at the tension flange.

The buckling curves are obtained by plotting the reduction factor, χ_{LT}, as a function of the non-dimensional slenderness, $\bar{\lambda}_{LT}$, which is calculated with equation 2.29. The reduction factor, χ_{LT} is acquired with the following equation:

$$\chi_{LT} = \frac{M_u}{W f_y} \tag{3.1}$$

where the denominator, Wf_y, is the yield moment. The yield moment is obtained only from the flanges for the girder with corrugated web and the whole cross-section for the girder with the flat web. M_u is the ultimate moment retrieved from non-linear buckling analyses, including appropriate initial imperfection. Geometrical imperfections and residual stresses can be taken into account by adding an initial bow imperfection. Values of the initial imperfection for columns in compression, $e_{0,k}$, are given in Eurocode 3 and can be seen in table 3.4. These values can be converted, to take the lateral-torsional buckling of beams in bending into account, by multiplying $e_{0,k}$ by a factor k_{LT}. Eurocode suggests that the value of k_{LT} is taken as 0.5. The initial bow imperfection for the studied girders is expressed with equation 3.2. This procedure eliminates the need of taking additional torsional imperfection into account. Table 3.4 shows the recommended initial bow imperfections for columns for each buckling curve. For the studied girders, with welded I-sections, buckling curves c and d are of interest.

$$e_0 = k_{LT} \cdot e_{0,k} \tag{3.2}$$

Table 3.4: Values of initial bow imperfections for columns in compression according to Eurocode 3

Buckling Curve	Initial bow imperfection, $e_{0,k}$
a_0	$l/350$
a	$l/300$
b	$l/250$
c	$l/200$
d	$l/150$

Each buckling curve is obtained for torsional stiffness on the range of $0 - 0.5 \cdot 10^5$ Nm/rad, in order to vary the slenderness of the girder by altering M_{cr}. These values of the torsional stiffness are chosen since they result in the first mode shape in linear buckling analyses of the studied girders.

The buckling curves from the FEM analyses are compared with the two approaches suggested in Eurocode 3 and the Euler buckling curve, $\chi = 1/\bar{\lambda}_{\mathrm{LT}}^{-2}$, in order to evaluate the applicability of them for restrained girders. The approach for welded sections is more appropriate than the general case for the studied girders, since they have welded section. The buckling curves suggested in Eurocode 3 are described in section 2.6.

4 Finite Element Modelling

All finite element analyses in this project are carried out in the commercial software ABAQUS CAE version 6.12-1. This chapter contains description of how the modelling of the studied girders is performed. In addition, it includes a convergence study, in order to obtain reasonable element size of the mesh, as well as a verification of the behaviour of the models.

4.1 Modelling procedure

Eight node shell elements with quadratic base function and reduced integration, [S8R] are chosen to be used in all analyses, which are carried out with the Simpson integration rule with five integration points over the thickness. The thickness of the geometry is defined as an extension from the centre of each part. This causes an overlap where two perpendicular parts meet, as can be seen in Figure 4.1. The influence of the overlap on the results is considered to be negligible.

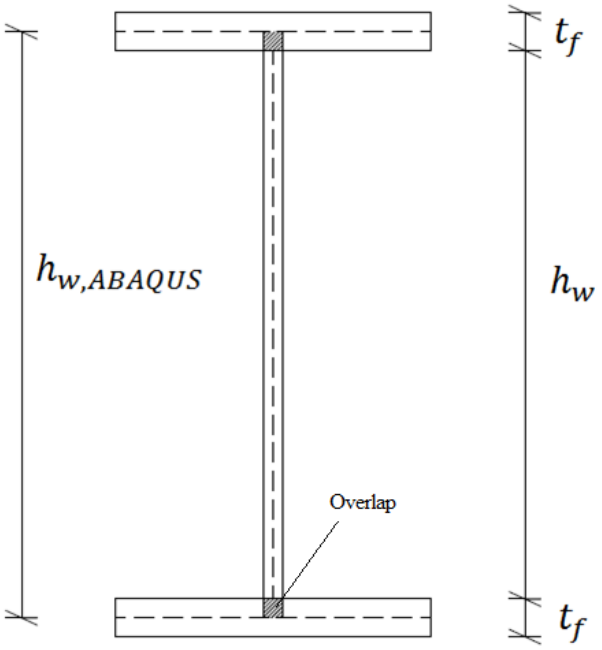

Figure 4.1: Overlap in the cross-section between the web and the flanges.

4.1.1 Linear buckling analysis

Linear buckling analyses are carried out in order to obtain the elastic critical buckling moment of restrained steel girders and compare it with analytical solutions. The material response is elastic with the modulus of elasticity, E, set to 210 GPa and the Poisson's ratio, ν, is 0.3. For these analyses, the procedure type *Linear perturbation - Buckle* is chosen.

The critical buckling moment is acquired in terms of the eigenvalues from the analyses, λ, that are directly proportional to the applied moment, M_{ref} , according to equation 4.1. The eigenvalues are extracted using the Lanczos algorithm.

$$M_{cr} = \lambda \cdot M_{ref} \qquad 4.1$$

4.1.2 Non-linear buckling analysis

Non-linear buckling analyses are carried out in order to obtain the ultimate moment, M_u, where initial imperfection, material plasticity and residual stresses are taken into account. The procedure type is *General – Static, Riks*. An elastic-plastic material response with plastic hardening is chosen for the analyses. The modulus of elasticity and the Poisson's ratio are the same as in the linear buckling analyses and the yield stress of the steel is chosen as 355 MPa. The plastic material properties can be viewed in the table below.

Table 4.1: Material properties for the non-linear analyses.

Yield stress [Mpa]	Plastic strain ($\varepsilon_p - \varepsilon_e$)
355	0
600	0.1167

In order to carry out non-linear analyses with initial imperfections, linear analyses have to be performed first for the same girder. The buckled shape of the girder in the linear buckling analysis is recorded. Thereafter, the initial imperfection is introduced in the non-linear analysis. The software will interpret the imperfection as a portion of the buckled shape from the linear buckling analysis. The initial lateral displacements are calculated with equation 3.2. The load proportionality factor, LPF, and the equivalent moment can be obtained for every iteration of the analyses. The ultimate moment, M_u, is the maximum moment of all iterations.

4.2 Load application

All buckling analyses are performed with a bending moment applied at the end supports of the girders. The moment is applied by adding forces along the edges of the flanges, where the top flange is in tension and the bottom flange is in compression, as shown in Figure 4.2. The edge loads are obtained according to equation 4.2.

$$F = \frac{M_{ref}}{b_f \cdot h_m} \qquad 4.2$$

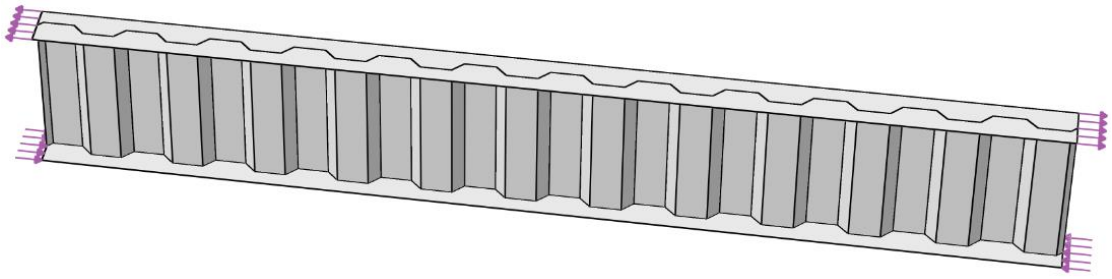

Figure 4.2: Load applied at the edges of the flanges.

4.3 End supports

The applied boundary conditions strongly influence the results of the buckling analyses. The analytical expressions that are evaluated are derived for simply supported girders. The boundary conditions are thereby chosen to simulate these conditions. The end supports are chosen to restrain lateral movement and torsion, but allow warping deformation. This is commonly referred to as fork supports and is modelled in the following way:

- Point A, at the mid-height of the web, is restrained for movement in all three main directions and rotation about the longitudinal axis.
- Point B, at the mid-height of the web, is restrained for movement in the lateral and vertical direction and for rotation about the longitudinal axis.
- Lines a and b, along the edges of the web, are restrained for movement in the lateral direction.

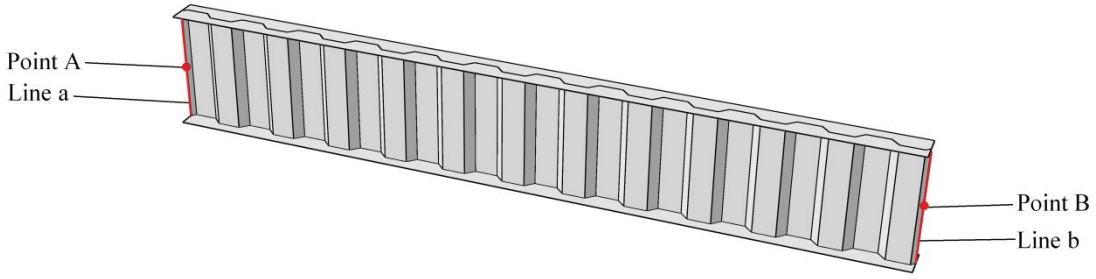

Figure 4.3: Boundary conditions for a simply supported girder is applied at points A and B, and lines a and b.

4.4 Restraints

When the torsional stiffness of the purlins is neglected, the purlins are modelled by restraining the movement in the lateral direction at evenly spaced points on the top flange of the girder, as can be seen in figure 4.4.

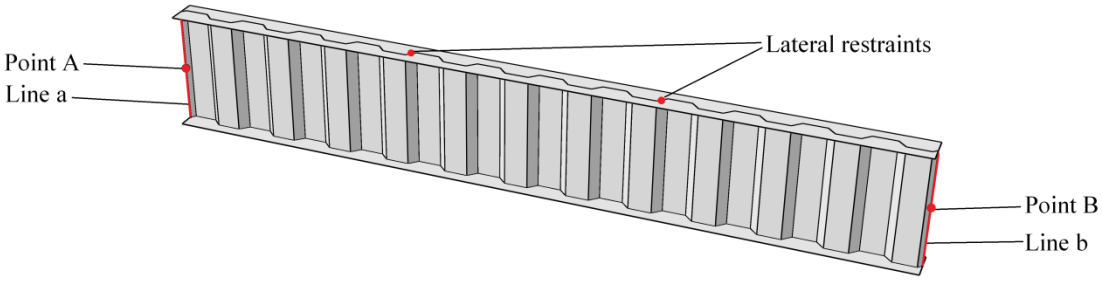

Figure 4.4: A girder with evenly spaced lateral restraints at its top flange.

The torsional stiffness, provided by the purlins when the connection is rigid, is modelled with springs. The springs are connected between points at the edges of the top flange of the girder and reference points defined above them, as can be seen in figure 4.5. The reference points in each restrained section should be constrained to

have the same vertical displacement and be free to move in the other directions. The height of the reference points is arbitrary and the springs should only add stiffness in the vertical direction. Purlins can be modelled in the following way for the studied girders:

- Point B is fully restrained in the lateral direction.
- Reference points are defined at an arbitrary height above points A and C.
- A coupling constraint is defined between the reference points.
- The reference points are restrained to rotate about the longitudinal axis in order to make the vertical displacement of the points to be equal.
- Springs are created between points A and C and their corresponding reference points.

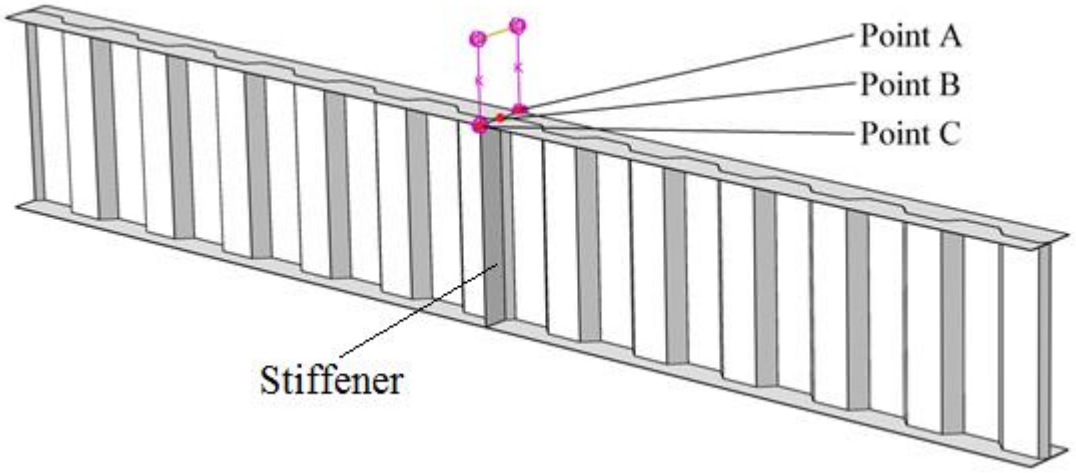

Figure 4.5: Point B is fully restrained in lateral direction and springs are connected between the top flange, points A and C, and reference points above the two points.

The stiffness of the springs should be equivalent to the torsional stiffness provided by each purlin, from equation 2.17. The spring stiffness is expressed with equation 4.3 and the derivation can be seen in appendix A.

$$k_s = \frac{2 \cdot k_\phi}{b_f^2} \tag{4.3}$$

As the torsional stiffness increases, local buckling in the flanges and distortion in the web at the restrained sections can occur. To prevent this, stiffeners are added to the restrained sections as can be seen in figure 4.5. The width and the thickness of the stiffeners will be the same as in the flanges, and the height will be the same as the height of the web. The stiffeners will restrain the warping of the girder, but the torsion will not be affected by them. The restraining effects from the stiffeners are considered to be insignificant and are therefore neglected.

4.5 Convergence study

A convergence study is performed using linear buckling analyses in order to find appropriate element size of the mesh. Girders with corrugated web are chosen for the

study since they require denser mesh than girders with flat web due to complexity of the geometry of the corrugated shape. There are two girders to be studied, one is unrestrained and the other has six restraints along its length. The girder with six restraints is studied for two different cases; with only lateral restraints and with torsional stiffness of $2 \cdot 10^5$ Nm/rad. For each of the studied cases, two different element types are tested:

- 4-node 1st order shell elements with reduced integration [S4R]
- 8-node 2nd order shell elements with reduced integration [S8R]

The convergence study is carried out by studying the critical buckling moment for the two element types with varying element size. As can be seen from the graphs in appendix B, S8R elements give a better convergence than the S4R elements for all studied cases. S8R elements with side length of 40 mm are chosen to be used throughout the entire study.

4.6 Verification of the model

Static analyses are carried out in order to verify the reliability of the models. The results are obtained in terms of vertical mid-span deflection and the average stresses in the flanges, which are compared with analytical solution calculated with the following equations:

$$\sigma = \frac{M}{I_x} y \tag{4.4a}$$

$$\delta = \frac{1}{8} \frac{M l^2}{E I_x} \tag{4.4b}$$

The verification is carried out for the studied girders defined in section 3.1. The stress and the vertical deflection from equation 4.4 are not influenced by lateral nor torsional restraints and should therefore be the same for unrestrained and restrained girders. The verification is consequently performed for girders with varying number of lateral restraints in order to verify this behaviour. The results from the verification can be seen in table 4.2 for girders with flat web and in table 4.3 for girders with corrugated web. The vertical deflection and the stress in the flanges are close to the analytical value in all cases. The analytical mid-span deflection and the average stress in the flanges can be seen in appendix C.

Table 4.2: Vertical deflection and stress in the top and bottom flanges in girders with flat web and different number of restraints. The ratio is obtained from the values from the FEM analyses and analytical values as calculated in appendix C.

No. of restraints	δ_{ABAQUS} [mm]	Ratio: $\frac{\delta_{ABAQUS}}{\delta}$	Stress in top flange [MPa]	Ratio: $\frac{\sigma_{ABAQUS}}{\sigma}$	Stress in bottom flange [MPa]	Ratio: $\frac{\sigma_{ABAQUS}}{\sigma}$
0	0.0680	0.987	0.458	1.003	-0.443	0.970
1	0.0680	0.987	0.458	1.003	-0.443	0.970
2	0.0680	0.987	0.458	1.005	-0.443	0.972
3	0.0679	0.986	0.451	0.989	-0.448	0.981
4	0.0679	0.986	0.458	1.005	-0.443	0.972
5	0.0679	0.986	0.451	0.989	-0.449	0.986
6	0.0679	0.986	0.458	1.005	-0.443	0.971

Table 4.3: Vertical deflection and stress in the top and bottom flanges of girders with corrugated web and different number of restraints. The ratio is obtained from the values from the FEM analyses and analytical values as calculated in appendix C.

No. of restraints	δ_{ABAQUS} [mm]	Ratio: $\frac{\delta_{ABAQUS}}{\delta}$	Stress in top flange [MPa]	Ratio: $\frac{\sigma_{ABAQUS}}{\sigma}$	Stress in bottom flange [MPa]	Ratio: $\frac{\sigma_{ABAQUS}}{\sigma}$
0	0.0871	0.986	0.598	1.022	-0.577	0.986
1	0.0871	0.986	0.598	1.022	-0.577	0.986
2	0.0870	0.986	0.578	0.988	-0.577	0.986
3	0.0870	0.986	0.583	0.996	-0.577	0.986
4	0.0870	0.985	0.588	1.005	-0.581	0.993
5	0.0870	0.985	0.598	1.022	-0.578	0.988
6	0.0870	0.985	0.585	1.000	-0.584	0.998

5 Results and Discussion

The most important results, with regard to the aim of this project, are presented and discussed in this chapter. This includes a parametric study, carried out with linear buckling analyses, where the behaviour of the critical buckling moment is studied on a range of the most influencing parameters. In addition, the results from non-linear buckling analyses are used to evaluate the applicability of the design approach for lateral-torsional buckling in Eurocode 3 for restrained girders with corrugated web. The results of this study are listed in more detail in appendix D.

5.1 Parametric study

The following sections list the results from each of the studied parameters from linear buckling analyses. The critical buckling moment of the studied girders is obtained for the range of each studied parameter and compared with the critical buckling moment from the expression from Horne & Ajmani. For girders with corrugated web, the Lindner's method is used. The geometrical parameters are studied for girders with five restraints and two values of the torsional stiffness, which results in the first and the second mode shape, respectively.

5.1.1 Torsional stiffness and spacing between purlins

The torsional stiffness of each restraint is studied on the range from $0 - 2 \cdot 10^5$ Nm/rad for girders with 1-6 evenly spaced restraints along its length. The critical buckling moment from the analyses correlates well to the analytical solution in all cases for both girder types. However, the correlation improves as the spacing between the purlins is denser, which is reasonable since the analytical solution is derived under the assumption that the restraints are continuously applied. It is also noticeable that there is more deviation for higher torsional stiffness. This is due to local deformations around the restraints that the analytical solution does not take into account.

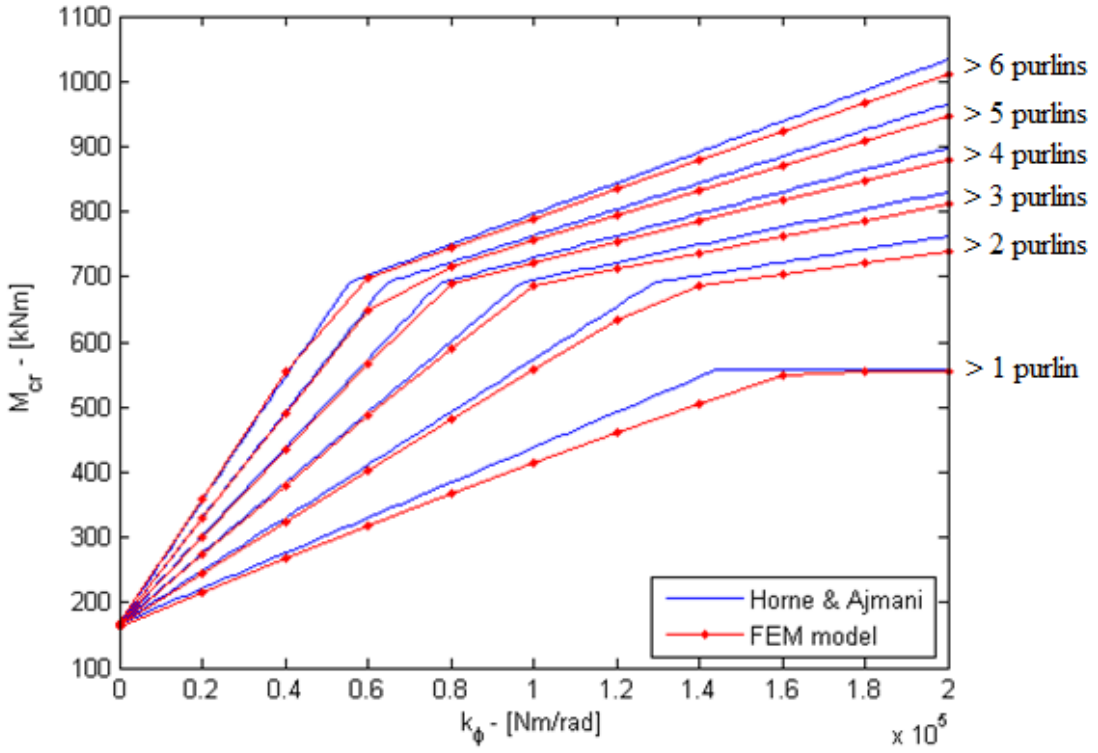

Figure 5.1: Critical buckling moment plotted as a function of the torsional stiffness on the range $\mathbf{0 - 2 \cdot 10^5}$ *Nm/rad for girders with corrugated web and 1-6 restraints along its length. The first and the second mode shape have different slope of* $\boldsymbol{M_{cr}}$ *for each girder.*

Figure 5.1 shows the comparison of the critical buckling moment, from the analyses and the analytical solution, as a function of the torsional stiffness on the studied range, for six different girders with corrugated web. The girders have identical cross-section and length but have different number of restraints, ranging from one to six. The girder with one mid-span restraint shows the maximum variation between the analytical solution and the FEM results, about 7 %, which is considered to be tolerable considering the assumption of continuous restraint in the derivation of the analytical solution.

There is not much difference in the behaviour of the girders with flat and corrugated web on the studied range of the torsional stiffness. However, for further increment of the torsional stiffness, there is a great difference. The girder with flat web is more likely to experience local buckling in the web, which will result in a failure of the girder. The girder with corrugated web will experience increasing local deformation in the flanges, close to the restraints, for increasing torsional stiffness.

When no torsional stiffness of the restraints is present, the girders are affected only by lateral restraints. The critical buckling moment should therefore be constant for varying number of restraints according to Horne & Ajmani's expression. However, the critical buckling moment from the FEM analyses increases slightly for increasing number of restraints. This increment is considered to be so small that it can be neglected and the spacing between the purlins has therefore no influence of the critical buckling moment unless torsional stiffness is taken into account.

5.1.2 Web thickness

The thickness of the web is studied on the range from $2-10$ mm for the studied girders with five evenly spaced restraints. The girders are studied with torsional stiffness of $0.4 \cdot 10^5$ Nm/rad and $1.4 \cdot 10^5$ Nm/rad, which results in the first and the second mode shape, respectively. In all cases, the critical buckling moment is correlating well to the analytical solution and comparison between the girders flat and corrugated web is of more interest.

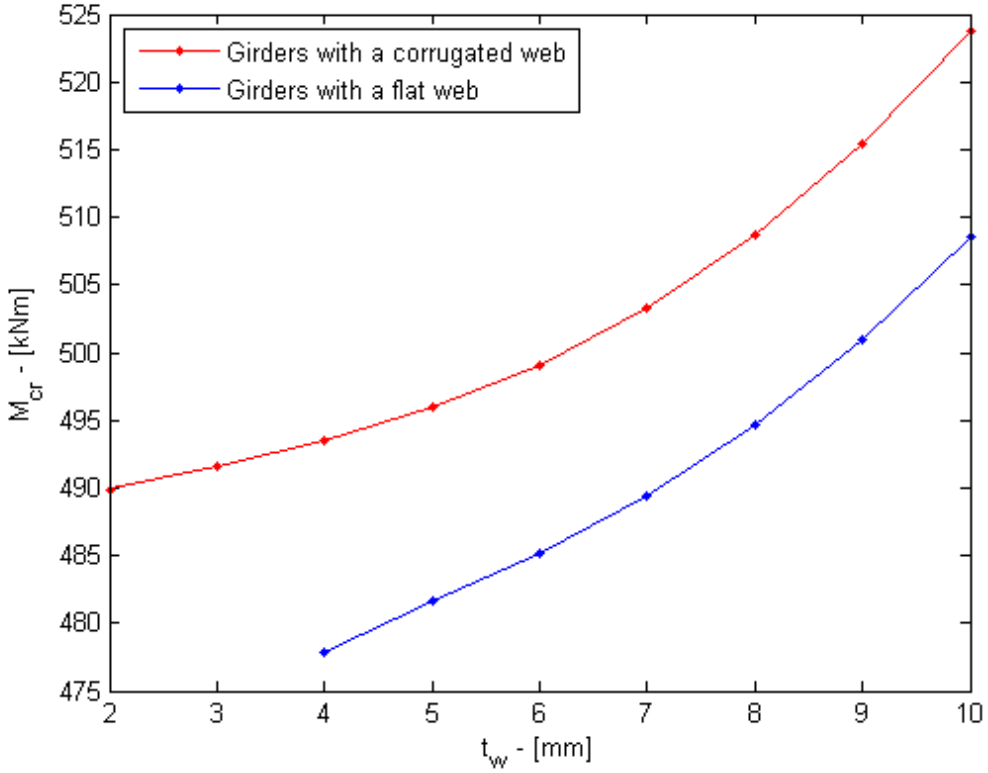

Figure 5.2: Critical buckling moment as a function of the web thickness for girders with flat and corrugated web. Torsional stiffness of the restraint is $\mathbf{0.4 \cdot 10^5}$ *Nm/rad.*

Figure 5.2 shows the comparison of the critical buckling moment, from the analyses, as a function of the web thickness for the studied girders. The torsional stiffness is $0.4 \cdot 10^5$Nm/rad, which results in the first mode shape. Girders with flat web thinner than 4 mm will experience local buckling in the web, which results in failure of the girder. The girder with corrugated web, on the other hand, can have web thickness down to 2 mm without failure.

By increasing the torsional stiffness to $1.4 \cdot 10^5$ Nm/rad, in order to obtain the second mode shape, gives similar behaviour. The difference is that the critical buckling moment increases and the girder with flat web needs to have minimum thickness of 6 mm in order to withstand local buckling of the web, while the girder with corrugated web can still have 2 mm in thickness without failure.

Increased web thickness does not result in large increase of the critical buckling moment on the studied range. Increasing the thickness of the web can therefore not be considered to be an economical way of increasing the buckling strength of the girder since it requires large increase in material use for little improvement in strength. However, this indicates that the advantage of having corrugated shape of the web

instead of a flat web can result in thinner web without reducing the critical buckling moment. The difference in thickness between a flat web and a corrugated web is larger as the web is thinner. The corrugated shape of the web can therefore save material by reducing the web thickness without reducing the buckling strength of the girder.

5.1.3 Web height

The web height is studied on the range of $500 - 1000$ mm for the studied girders with five evenly spaced restraints. The girders are studied with torsional stiffness of $0.3 \cdot 10^5$ Nm/rad and $1.4 \cdot 10^5$ Nm/rad, which results in the first and the second mode shape, respectively. The FEM results show good correlation with the analytical solution in all cases.

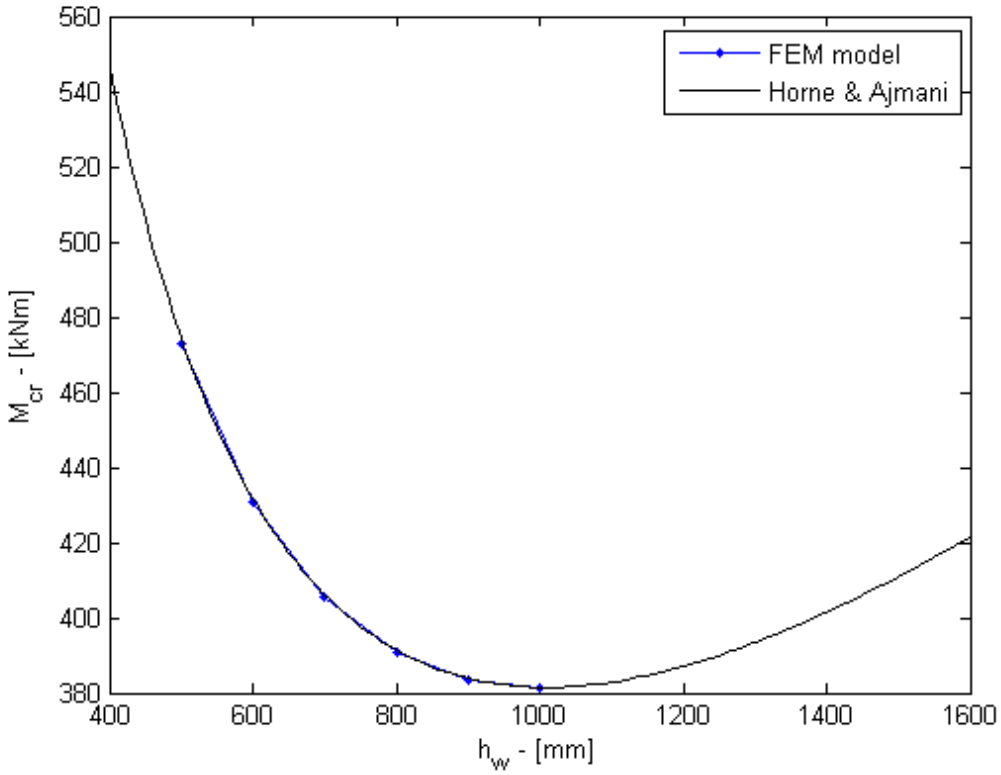

Figure 5.3: The critical buckling moment as a function of the web height. Comparison between the FEM model and the analytical solution of a girder with a corrugated web. Torsional stiffness of each restraint is $\mathbf{0.3 \cdot 10^5}$*Nm/rad.*

Figure 5.3 shows a comparison of the critical buckling moment from the FEM analyses and the analytical solution for girders with corrugated web. The critical buckling moment is plotted as a function of the web height for torsional stiffness of the restraints set to $0.3 \cdot 10^5$ Nm/rad, which results in the first mode shape. The critical buckling moment follows a parabolic shape when varying height of the web.

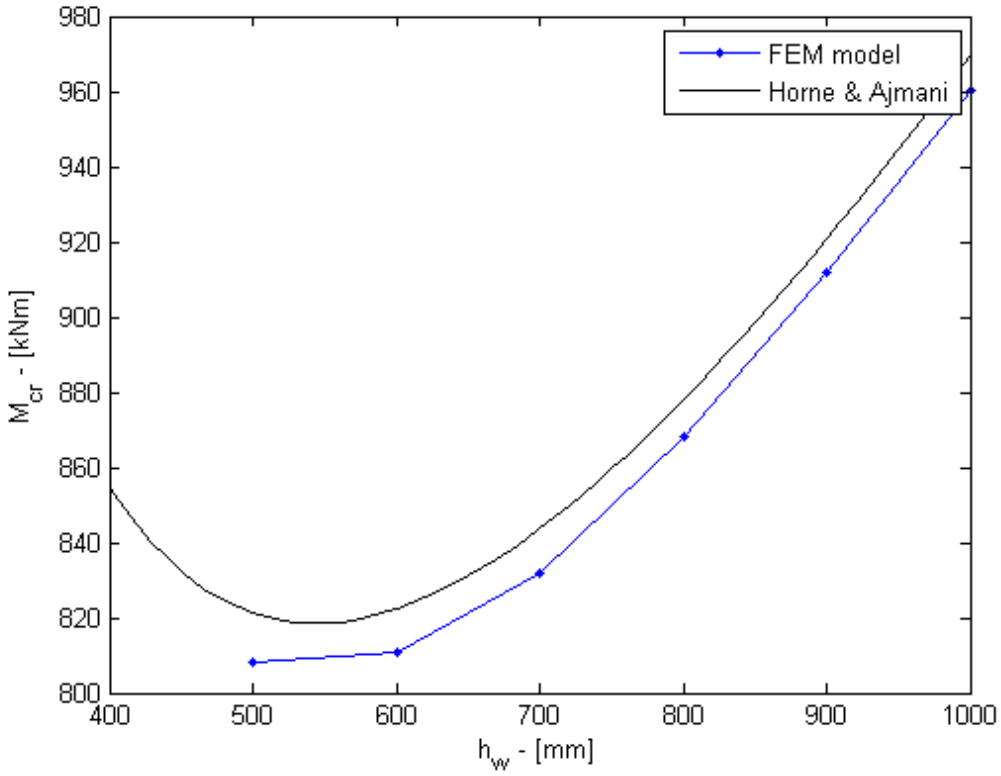

Figure 5.4: The critical buckling moment as a function of the web height. Comparison between the FEM model and the analytical solution of a girder with a corrugated web. Torsional stiffness of each restraint is $\mathbf{1.4 \cdot 10^5}$*Nm/rad.*

Figure 5.4 shows the critical buckling moment as a function of the web height for girders with corrugated web with the torsional stiffness of $1.4 \cdot 10^5$ Nm/rad, which results in the second mode shape. As for the first mode shape, the critical buckling moment has parabolic shape for varying web height. However, the web height, where the minimum value of the parabola is obtained, and the slope of the parabola is not the same compared with the first mode shape.

The parabolic shape of the critical buckling moment can be explained by looking at different influencing factors. By increasing the height of the web of an unrestrained girder, the critical buckling moment increases. However, for restrained girders, the distance between the shear centre of the girder and the centre of the rotation of the restraint, a_r, is also increasing, which affects the critical buckling moment in the opposite way. The proportions of these two factors determine whether the critical buckling moment is increasing or decreasing when the height of the web is changed.

5.1.4 Flange thickness

The thickness of the flanges is studied on the range from $8 - 17$ mm for the studied girders with five evenly spaced restraints. The girders are studied with torsional stiffness of $0.4 \cdot 10^5$ Nm/rad and $1.4 \cdot 10^5$ Nm/rad, which results in the first and the second mode shape, respectively. The results show good correlation with the analytical solution in all cases. However the difference is slightly higher when the torsional stiffness results in the second mode shape.

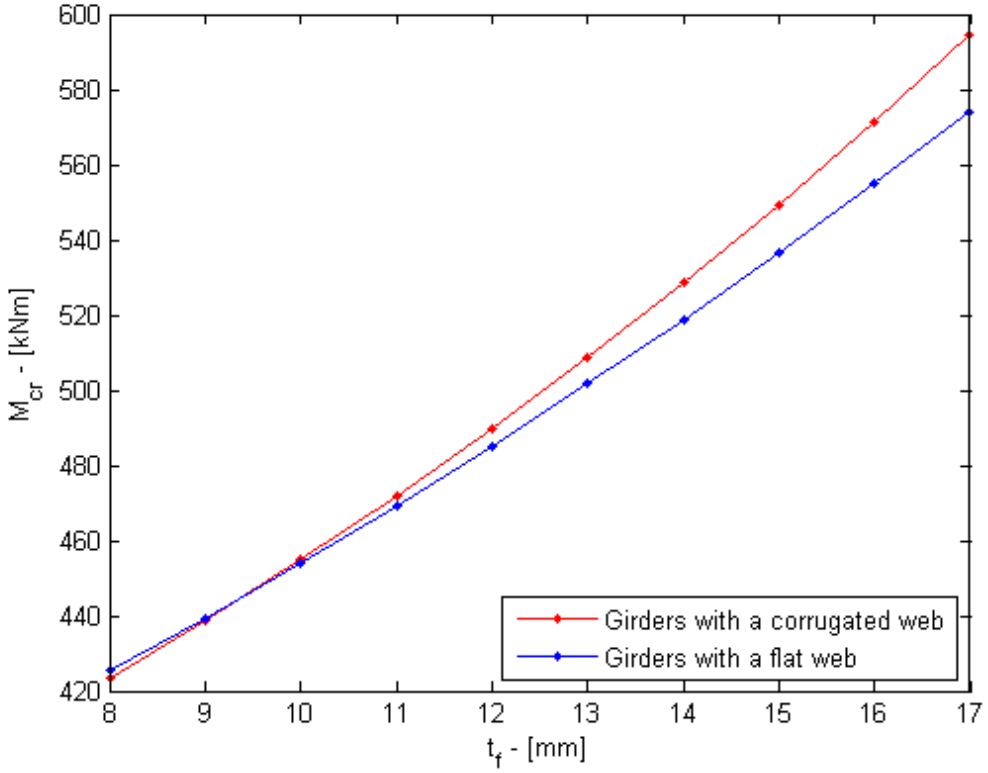

Figure 5.5: The critical buckling moment as a function of flange thickness. Comparison between the FEM models of girders with corrugated web and girders with flat web with 5 restraints and a torsional stiffness of $\mathbf{0.4 \cdot 10^5}$ *Nm/rad.*

Figure 5.5 shows the comparison of the critical buckling moment from the FEM model between the two girder types with a torsional stiffness set to $0.4 \cdot 10^5$ Nm/rad resulting in the first mode shape. As expected, the critical buckling moment increases as the thickness of the flanges increases. It is noteworthy that the critical buckling moment of the girder with corrugated web increases somewhat faster. This occurs both in the FEM analyses and with the analytical expressions as can be seen in table D.7 in appendix D.

The study is also carried out for torsional stiffness of $1.4 \cdot 10^5$ Nm/rad, resulting in the second mode shape. The results show similar behaviour as for the first mode shape.

5.1.5 Flange width

The flange width is studied on the range of $125 - 250$ mm for the studied girders with five evenly spaced restraints. The girders are studied with torsional stiffness of $0.2 \cdot 10^5$ Nm/rad and $1.4 \cdot 10^5$ Nm/rad, which results in the first and the second mode shape, respectively. The results show good correlation with the analytical solution in all cases. However, the second mode shape has slightly higher variation between the critical buckling moment from the FEM analyses and the analytical solution as can be seen in appendix D.

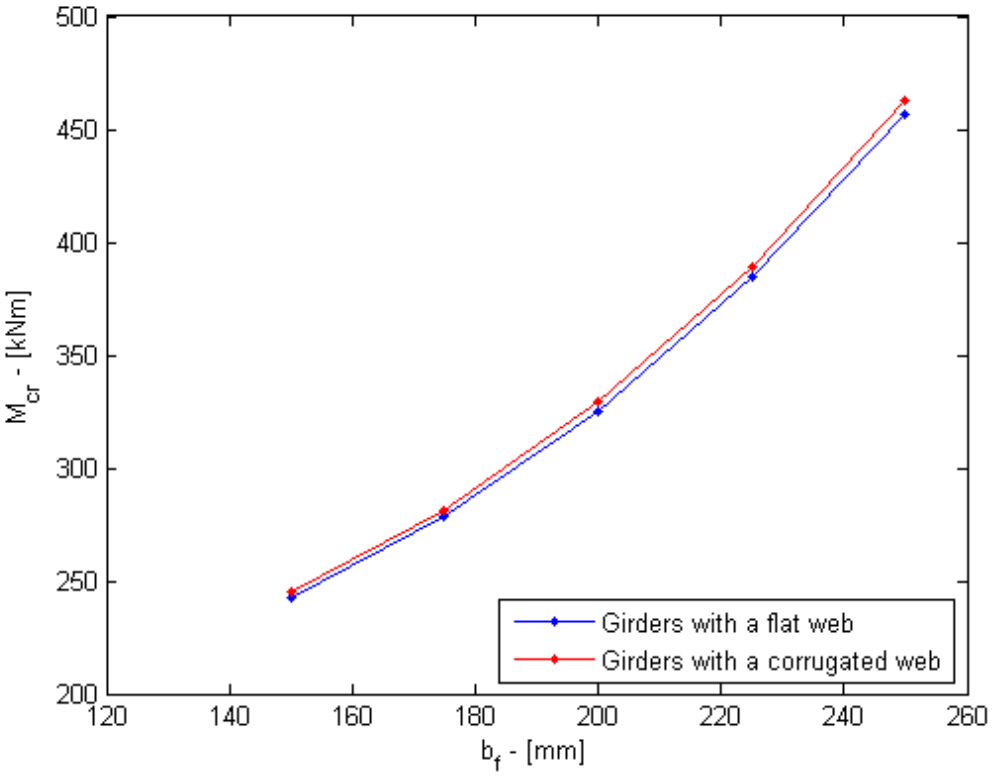

Figure 5.6: The critical buckling moment as a function of flange width. Comparison between the FEM models of girders with corrugated web and girders with flat web with 5 restraints and a torsional stiffness of $\mathbf{0.2 \cdot 10^5}$ *Nm/rad.*

Figure 5.6 shows the comparison of the critical buckling moment, obtained from the FEM analyses, as a function of the flange width for the studied girders when the torsional stiffness of the restraints was set to $0.2 \cdot 10^5$ Nm/rad, resulting in the first mode shape. As expected, increasing flange width results in an increasing critical buckling moment.

By increasing the torsional stiffness to $1.4 \cdot 10^5$ Nm/rad, in order to obtain the second mode shape, the same behaviour is obtained as for the first mode shape.

5.2 Design approach in Eurocode 3

The reduction factor, χ_{LT}, and the non-dimensional slenderness ratio, $\overline{\lambda}_{LT}$, are plotted as a buckling curve. This is done for the studied girders with six restraints with torsional stiffness on the range of $0 - 0.5 \cdot 10^5$ Nm/rad. The procedure of this study is

thoroughly described in section 3.3. The results are compared with the approaches suggested in Eurocode 3; the general case and the case for rolled sections or equivalent welded sections, which are described in section 2.6. The studied girders in this project have welded sections and should be designed for buckling curve d, according to Eurocode 3, based on the cross-sectional properties. In order to see if restrained girders or girders with corrugated web give a reason to lower the requirement of the initial imperfection suggested in Eurocode 3, the studied girders were also compared with buckling curve c.

5.2.1 Buckling curve d

The results from the non-linear buckling analyses, including appropriate value of the initial imperfections as recommended in Eurocode 3 for buckling curve d, are compared with buckling curve d from Eurocode 3 and the Euler buckling curve. Figure 5.7 shows the buckling curves for the girder with flat web. The results from the FEM model give higher reduction factor compared with the design curve for welded sections, which can therefore be considered conservative. Figure 5.8 shows the buckling curves for the girder with corrugated web. This gives very similar results as the girder with flat web, and the design curve for welded section can be considered to give conservative results for girders with corrugated web.

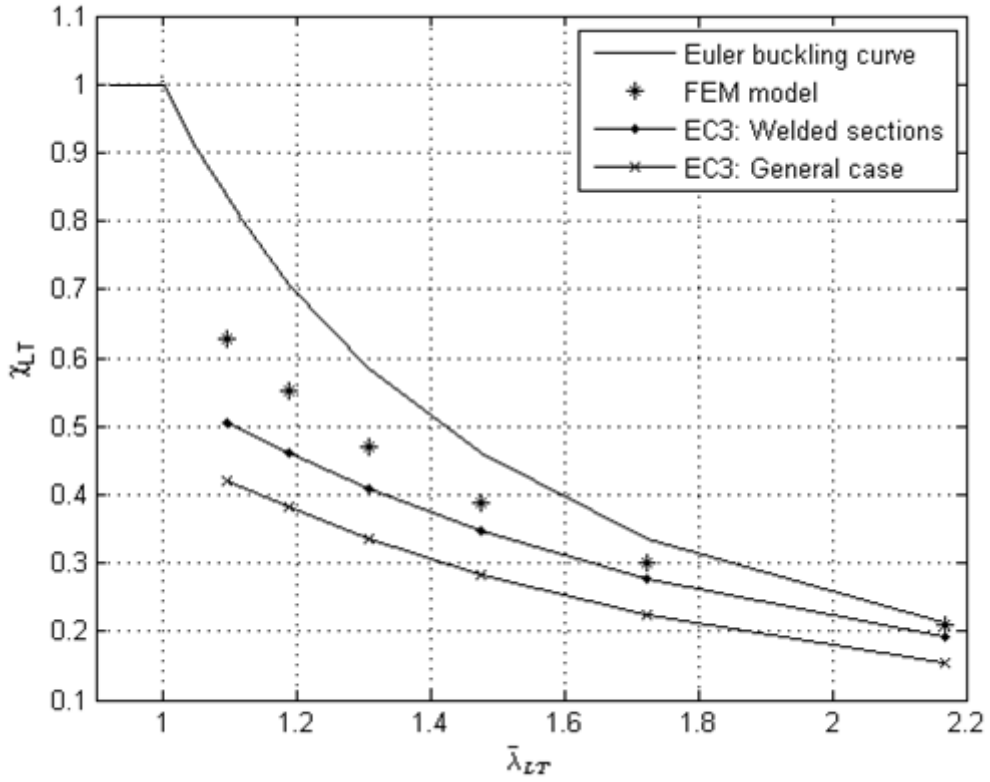

Figure 5.7: Reduction factor,$\boldsymbol{\chi_{LT}}$, as a function of the non-dimensional slenderness,$\boldsymbol{\overline{\lambda}_{LT}}$. Comparison of the results from non-linear analyses to design approach for buckling curve d in Eurocode 3 for a girder with a flat web.

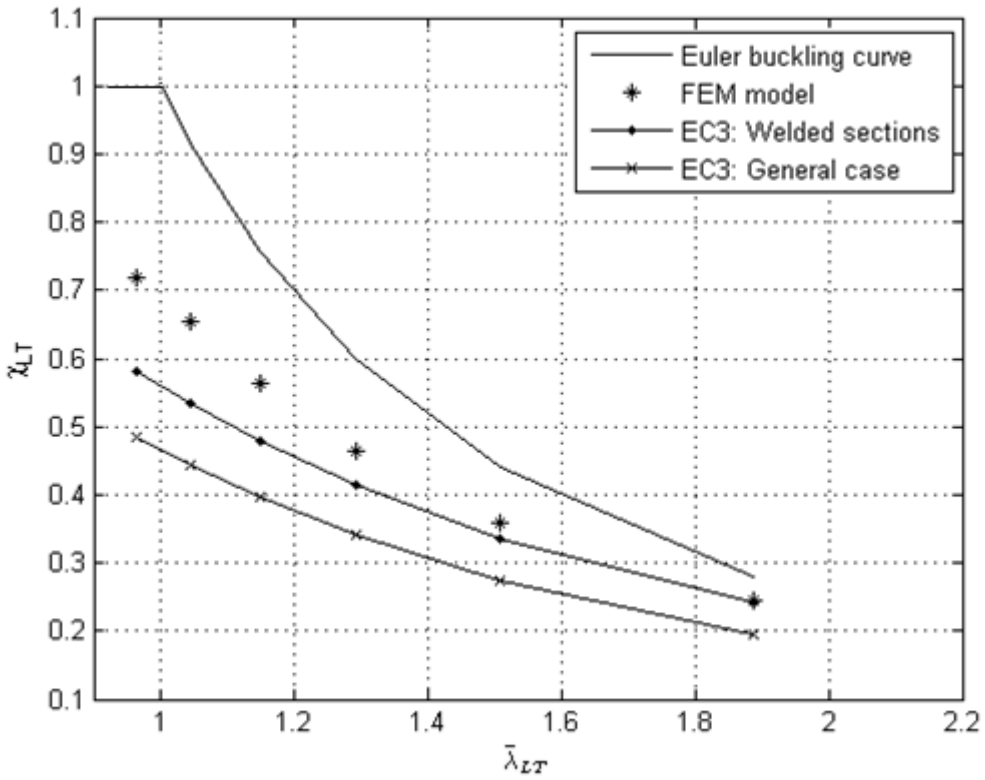

Figure 5.8: Reduction factor,$\boldsymbol{\chi_{LT}}$, as a function of the non-dimensional slenderness,$\boldsymbol{\bar{\lambda}_{LT}}$. Comparison of the results from non-linear analyses to design approach for buckling curve d in Eurocode 3 for a girder with a corrugated web.

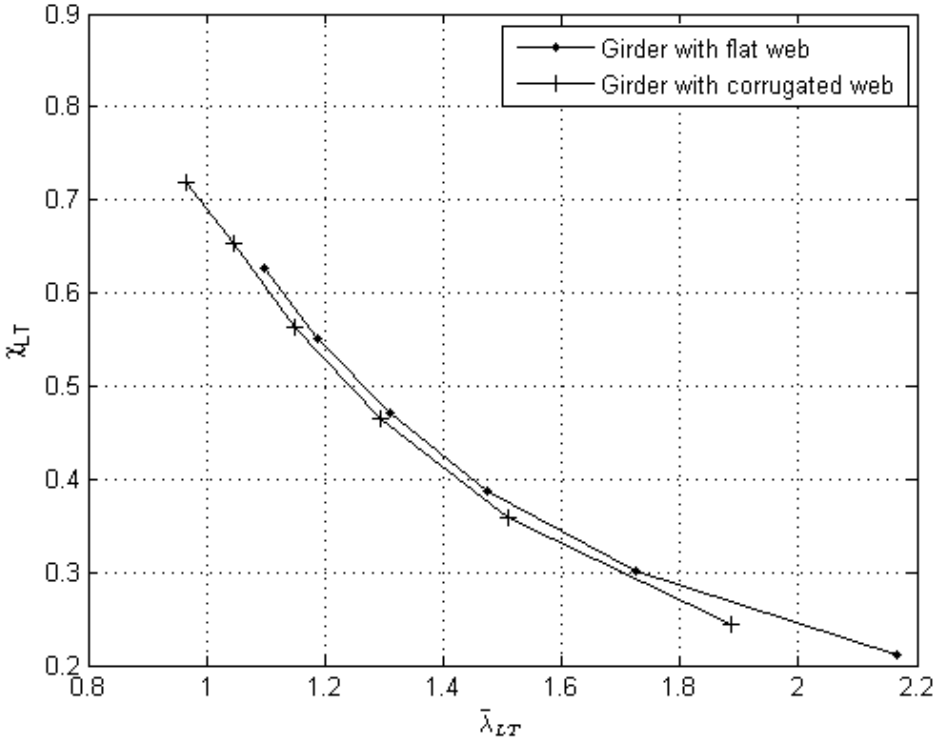

Figure 5.9: Reduction factor,$\boldsymbol{\chi_{LT}}$, as a function of the non-dimensional slenderness,$\boldsymbol{\bar{\lambda}_{LT}}$. Comparison of the results from non-linear analyses between girders with flat- and corrugated web with initial imperfection according to buckling curve d in Eurocode 3.

The buckling curves obtained from the results from the FEM analyses for the two studied girders can be seen in figure 5.9. The girders are equivalent and the range of the torsional stiffness is the same for both girders. The only difference between them is the shape and the thickness of the web. The girder with the flat web has slightly higher reduction factor than the girder with the corrugated web for equivalent value of the non-dimensional slenderness. However, the girder with the corrugated web has lower value of the non-dimensional slenderness than the girder with flat web with equivalent torsional stiffness, resulting in higher reduction factor. This indicates that the corrugated shape of the web reduces the slenderness of the girder.

The difference between the buckling curves for the two girder types can be explained by reviewing the expressions used to obtain the bucking curves:

$$\chi_{LT} = \frac{M_u}{W f_y} \tag{5.1}$$

$$\overline{\lambda}_{LT} = \sqrt{\frac{W f_y}{M_{cr}}} \tag{5.2}$$

When looking at the reduction factor, it can be seen from tables D.10 and D.11 in appendix D that the ultimate moment, M_u, is slightly lower for the girder with corrugated web than the girder with flat web but the difference is not significant. The difference between the yield moment, Wf_y, of the two girder types is relatively large, compared to the difference between the ultimate moments of the two girder types. Consequently, the reduction factor is controlled mainly be the yield moment of the two girders. The yield moment is lower for the girder with corrugated web than the girder with the flat web, since the web is not included in W for the girder with corrugated web. This results in higher reduction factor for the girder with corrugated web than equivalent girder with flat web.

Similar behaviour can be seen in the non-dimensional slenderness. The difference between the critical buckling moments of the two girder types is not significant but the difference between the yield moment is greater in comparison. This results in higher slenderness for girders with flat web than girders with corrugated web. This behaviour can be seen in figure 5.9 by comparing equivalent points on the two curves.

From these results, it can be concluded that girders with corrugated web are considered to be less slender than girders with flat web and are therefore less prone to lateral-torsional buckling due to higher reduction factor. However it is noteworthy to mention that the web is not contributing to the yield strength of girders with corrugated web. This means that even though the lateral-torsional stability has been increased by increasing the reduction factor, the design buckling resistance moment, from equation 2.26, is also controlled by the yield moment, which is lower for girders with corrugated web.

5.2.2 Buckling curve c

The same procedure is performed to obtain buckling curve c as for buckling curve d. Figure 5.10 shows buckling curves c for the girder with flat web. For slender girders, the results from the FEM analyses end up very close to the design curve for welded

sections. This cannot be considered to give conservative design approach and buckling curve c can therefore not be recommended for design purposes. Figure 5.11 shows similar results for the girder with corrugated web. For slender girders, the reduction factor from the FEM analyses is lower than from the design curve for welded sections and is therefore unconservative. Figure 5.12 shows the difference between the buckling curves from the FEM analyses for the two girder types and it behaves in the same way as for buckling curve d, which is discussed in section 5.2.1. From these results, it can be concluded that design curve c is not appropriate for design purposes for the studied girders and the design curve should be chosen according to suggestions from Eurocode 3.

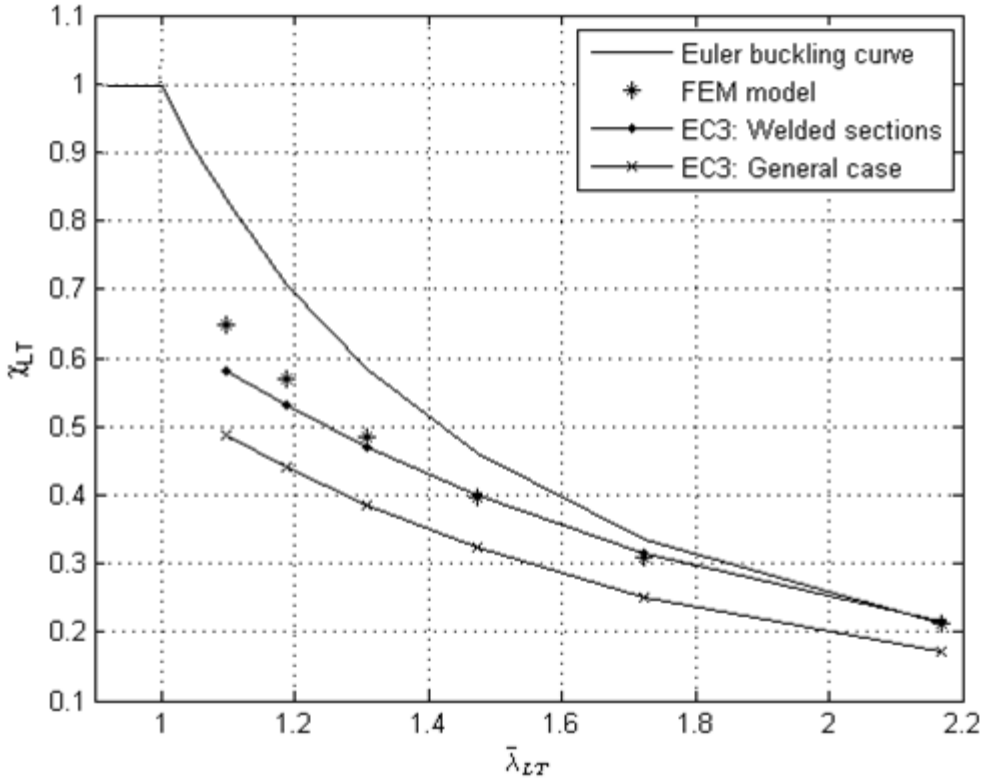

Figure 5.10: Reduction factor,$\boldsymbol{\chi_{LT}}$, as a function of the non-dimensional slenderness,$\boldsymbol{\overline{\lambda}_{LT}}$. Comparison of the results from non-linear analyses to design approach for buckling curve c in Eurocode 3 for a girder with a flat web.

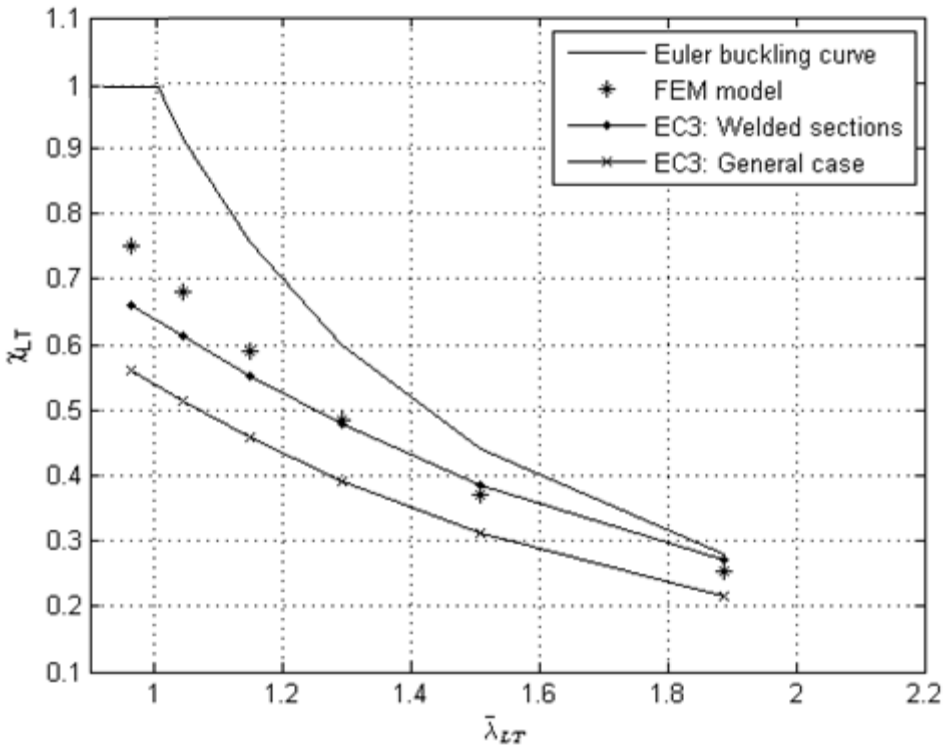

Figure 5.11: Reduction factor,$\boldsymbol{\chi_{LT}}$, as a function of the non-dimensional slenderness,$\boldsymbol{\bar{\lambda}_{LT}}$. Comparison of the results from non-linear analyses to design approach for buckling curve c in Eurocode 3 for a girder with a corrugated web.

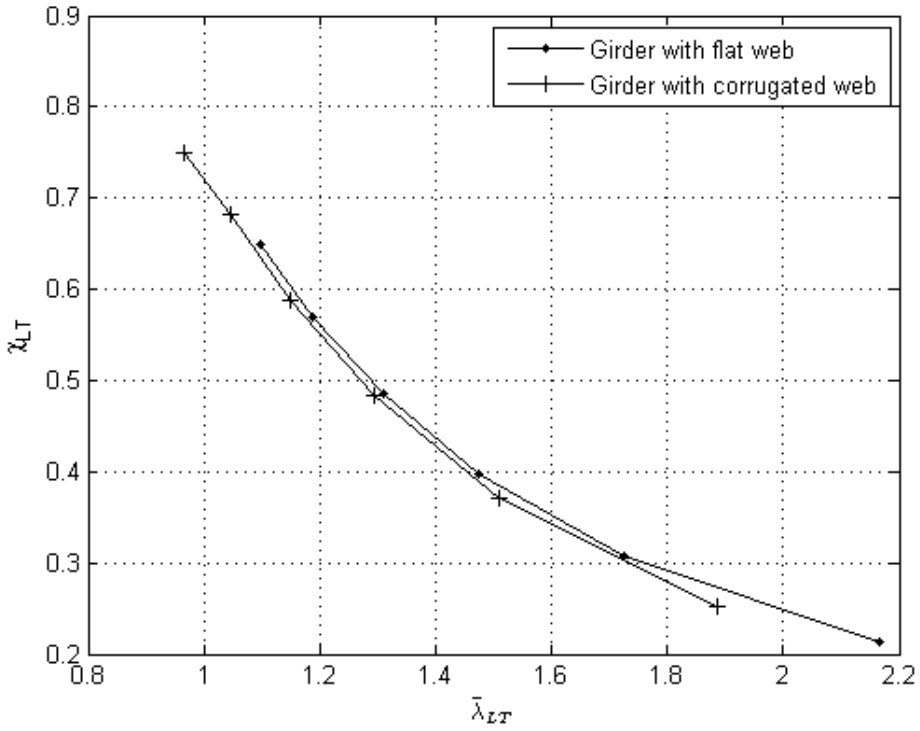

Figure 5.12: Reduction factor,$\boldsymbol{\chi_{LT}}$, as a function of the non-dimensional slenderness,$\boldsymbol{\bar{\lambda}_{LT}}$. Comparison of the results from non-linear analyses between girders with flat- and corrugated web with initial imperfection according to buckling curve c in Eurocode 3.

6 Conclusions

The critical buckling moment of restrained girders, due to lateral-torsional buckling, can be increased significantly by rigidly attaching purlins to the tension flange of girders. This is due to the torsional stiffness provided by rigidly attached purlins. The torsional stiffness is determined from the material- and geometrical properties of the purlins.

Horne & Ajmani's expression of the critical buckling moment for discretely restrained girders correlates well to the results from the FEM analyses performed in this study. This applies to both girders with flat web and corrugated web. The expression correlates well to the results from the FEM analyses for both coarsely and densely spaced restraints. However, the accuracy increases as the spacing of the restraints get denser, due to the assumption of continuous restraint in the derivation of it.

Lindner's approach is applicable to take the influence from the corrugated shape of the web into account for restrained girders and has comparable accuracy as girders with flat web. The main drawback from this approach is that it is dependent on the total length and the buckled shape of the girder. This can be solved by using the modified version of the approach, suggested by Larsson & Persson (2013), which is only dependent on sectional constants of the girder.

The torsional stiffness, provided by rigidly attached purlins, only affects the critical buckling moment when the purlins are attached to the tension flange of the girder. When torsional stiffness is present, the number of purlins is an important influencing factor on the critical buckling moment, which increases with increasing number of purlins. However, if no torsional stiffness is present, and the purlins only provide lateral restraint, the critical buckling moment is close to a constant value for varying spacing of purlins.

Having corrugated shape of the web of the girder instead of a flat web, does not result in large increment in the critical buckling moment. However, the corrugated shape of the web gives the possibility of reducing the thickness of the web without decreasing the critical buckling moment. The girder with corrugated web can therefore have better material efficiency than the girder with flat web. However it should be kept in mind that the shape of the corrugated web requires some increment in material usage, compared to equally thick flat web.

From the non-linear analyses, it can be concluded that the design curves for lateral-torsional buckling in Eurocode 3 can be used in a conservative way for restrained girders when, M_{cr}, is obtained with Horne & Ajmani's expression. Restrained girders with corrugated web can be designed conservatively in a similar way using Lindner's approach. Girders with corrugated web are considered to be less slender than equivalent girders with flat web. By reducing the slenderness, the reduction factor increases and the girder has better resistance against lateral-torsional buckling. However, the yield moment of girders with corrugated web is lower than in equivalent girders with flat web, since the corrugated web is not contributing to the yield strength of the girder.

7 Suggestions for further research

In this thesis it was confirmed that the critical moment of restrained girders can be accurately described with Horne & Ajmani´s method. Furthermore it was concluded that Lindner´s method of taking the increased strength from having a corrugated web into account works well combined with Horne & Ajmani´s method. However, this study was limited to only study uniform bending moment applied at the ends of the girders. The authors of this thesis suggest that load cases such as girders subjected to axial load and girders with non-uniform bending moment are studied. Furthermore, only one shape of the trapezoidal web was investigated. The authors suggest that more corrugation shapes are studied in order to confirm the accuracy of Lindner´s method for other types of corrugated profiles when restrained girders are studied.

The study comprised non-linear analyses in order to produce buckling curves, comparing them with the buckling curves provided by Eurocode 3. This was carried out for a girder with flat web and a girder with corrugated web. However, the number of analyses was limited. Only one set spacing between purlins, and one cross-section for each type of girder was studied. The non-linear buckling analyses could be extended comprising several cross-sections and shapes of the trapezoidal web, extending the $\chi_{LT} - \overline{\lambda}_{LT}$-curves. If this would be done, the curves could be used when designing restrained girders.

References

Al-Emrani, M., Åkesson, B. (2013): *Steel structures: Course literature – VSM 191*. Report. Department of Civil and Environmental Engineering, Chalmers University of Technology, Publication no. 2013:10, Göteborg, Sweden, 2013, 377 pp.

Dooley, J. F. (1966): On the torsional buckling of columns of I-section restrained at finite intervals. *International Journal of Mechanical Sciences*, Vol. 9, 1967, pp. 1-9.

Estabrooks, B. G., Grondin, G. Y. (2008): *Combined bending and torsion of steel I-shaped beams*. Report. Department of Civil & Environmental Engineering, University of Alberta, Report no. 276, Alberta, Canada, 2008, 138 pp.

European Committee for Standardization (2005): *Eurocode 3: Design of steel structures – Part 1-1: general rules for buildings*. Brussels

Galambos, T. V. (1998): *Guide to stability design criteria for metal structures*. 5th edition. John Wiley & Sons, Inc. 911 pp.

Galambos, T. V., Surovek, A. E. (2008): *Structural stability of steel: concepts and application for structural engineering*. John Wiley & Sons, Inc. 373 pp.

Horne, M. R., Ajmani, J. L. (1968): Stability of columns supported laterally by side-rails. *International Journal of Mechanical Sciences*, Vol. 11, 1969, pp. 159-174.

Larsson, M., Persson, J. (2013): *Lateral-torsional buckling of steel girders with trapezoidally corrugated webs*. Master thesis. Department of Civil and Environmental Engineering, Chalmers University of Technology, Publication no. 2013:57, Göteborg, Sweden, 2013, 52 pp.

Lindner, J, Aschinger R. (1990): Zur torsionssteifigkeit von trapezstegträgern (Torsional stiffness of girders with trapezoidal web. In German) *Stahlbau*, Vol. 59, 1990, pp. 113-120.

Lundh, H (2000): *Grundläggande hållfasthetslära* (Fundamental solid mechanics. In Swedish). 3rd edition. Institutionen för hållfasthetslära, KTH, Stockholm, Sweden, 2000, 393 pp.

Sayed-Ahmed, E. Y. (2007): Design aspects of steel I-girders with corrugated steel webs. *Electronic Journal of Structural Engineering*, Volume 7, 2007, pp. 27-40

Seaburg, P. A., Carter, C, J. (2003): *Torsional analysis of structural steel members*. Design guide series, American Institute of Steel Construction, Inc. Publication no. D809 (5M297), Chicago, USA, 2003, 116 pp.

Timoshenko, S. P., Gere, J. M. (1961): *Theory of elastic stability*. 2nd ed. McGraw-Hill Book Company, Inc. New York, USA, 1961, 541 pp.

Trahair, N. S. (1993): *Flexural-torsional buckling of structures*. E & FN Spon. London, UK, 1993, 352 pp.

Yura, J. A. (2001): Fundamentals of beam bracing. *Engineering Journal*, Vol. 38, 2001, first quarter, pp. 11-26.

A – Analytical derivations of equations

This appendix includes derivation of the torsional stiffness provided by the purlins, equation 2.17, and the equivalent spring stiffness used when modelling, equation 4.3 In addition, it contains verification of the applicability of the warping- and torsion constants for girders with corrugated web from modified Lindner's approach for the critical buckling moment for restrained girders.

Appendix A

Spring stiffness from equation 4.3

The spring stiffness in the model in ABAQUS CAE can be calculated in terms of the stiffness of the torsional restraint due to the effects of purlins.

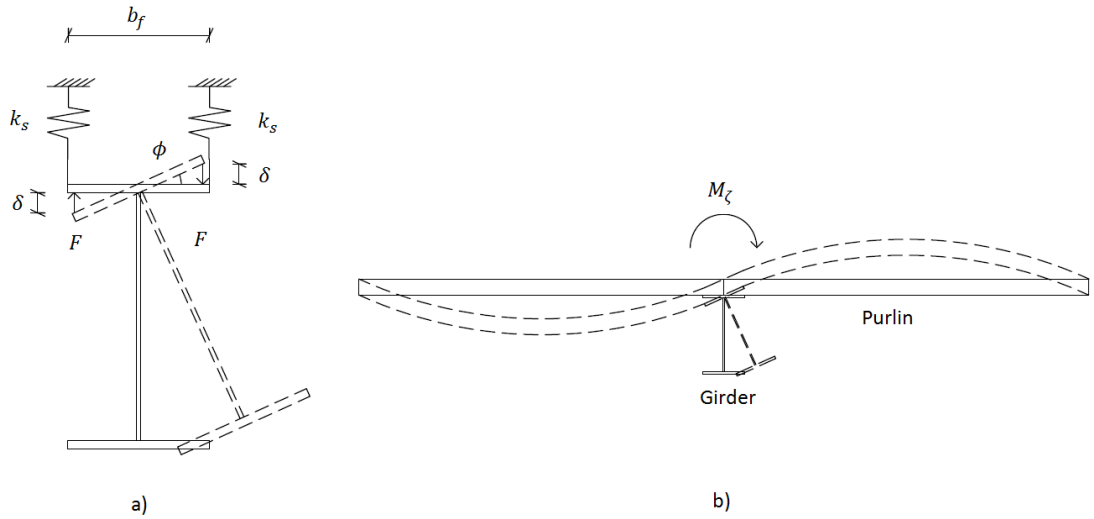

Figure A.1: a) The purlins will give a restraining effect to the girder, which can be simplified as a spring with certain stiffness; b) Deformation of a purlin due to the rotation of a girder caused by LT-buckling.

The stiffness of the torsional restraint of a purlin is expressed according to the definition of torsional stiffness.

$$k_\phi = \frac{M_\zeta}{\phi}$$

where M_ζ is the resulting moment caused by the rotation of the girder and ϕ is the angle of rotation. The moment M_ζ and the angle ϕ can be defined in the following way:

$$M_\zeta = F \cdot b_f$$

$$\phi = \frac{\delta}{b_f/2}$$

where F is the force needed to deform a spring of stiffness k_s of a distance δ and b_f is the width of the flange of the beam. The torsional stiffness can now be rewritten as:

$$k_\phi = \frac{F \cdot b_f^2}{2 \cdot \delta} = \frac{k_s \cdot b_f^2}{2}$$

This can be solved for the spring stiffness as

$$k_s = \frac{2 \cdot k_\phi}{b_f^2}$$

Torsional stiffness from equation 2.17

The angle of rotation at the restrained cross-section of the girder is limited to the angle of rotation of the purlin according to the following equation:

$$\phi_p = \frac{M_\zeta l_p}{3E_p I_p}$$

Where l_p, E_p and I_p are the length, elastic modulus and the second moment of area for the purlin. This can be inserted into the equation for torsional stiffness to obtain the following expression:

$$k_\phi = \frac{3E_p I_p}{l_p}$$

Warping and torsional constants for the modified Lindner's approach

Unrestrained beams

Insert the warping- and torsion constants from the Lindner's approach, equation 2.23 with $n = 1$, into equation 2.16 describing the critical moment due to lateral-torsional buckling for unrestrained beams.

$$M_{cr} = \frac{\pi^2 E I_y}{l^2}\sqrt{\frac{I_w^*}{I_y} + \frac{l^2 G I_t^*}{\pi^2 E I_y}} = \frac{\pi^2 E I_y}{l^2}\sqrt{\frac{I_w + c_w\frac{l^2}{\pi^2 E}}{I_y} + \frac{l^2 G I_t}{\pi^2 E I_y}}$$

$$=> M_{cr} = \frac{\pi^2 E I_y}{l^2}\sqrt{\frac{I_w}{I_y} + c_w\frac{l^2}{\pi^2 E I_y} + \frac{l^2 G I_t}{\pi^2 E I_y}} = \frac{\pi^2 E I_y}{l^2}\sqrt{\frac{I_w}{I_y} + \frac{l^2 G(I_t + \frac{c_w}{G})}{\pi^2 E I_y}}$$

This can now be expressed in terms of the torsion and warping constants from the modified Lindner's approach

$$M_{cr} = \frac{\pi^2 E I_y}{l^2}\sqrt{\frac{I_w'}{I_y} + \frac{l^2 G I_t'}{\pi^2 E I_y}}$$

where $I_t' = I_t + \frac{c_w}{G}$ and $I_w' = I_w$

Beams restrained at its compression flange

Insert the general form of the warping- and torsion constants from the Lindner's approach, equation 2.23, into equation 2.18 describing the critical moment due to lateral-torsional buckling for beams restrained at its compression flange. The spacing between purlins is considered to be $s = l/n$.

$$M_{cr} = \frac{\pi^2 E I_y}{s^2}\sqrt{\frac{I_w^*}{I_y} + \frac{s^2 G I_t^*}{\pi^2 E I_y}} = \frac{\pi^2 n^2 E I_y}{l^2}\sqrt{\frac{I_w + c_w\frac{l^2}{\pi^2 n^2 E}}{I_y} + \frac{l^2 G I_t}{\pi^2 n^2 E I_y}}$$

$$=> M_{cr} = \frac{\pi^2 n^2 E I_y}{l^2}\sqrt{\frac{I_w}{I_y} + c_w\frac{l^2}{\pi^2 n^2 E I_y} + \frac{l^2 G I_t}{\pi^2 n^2 E I_y}} = \frac{\pi^2 n^2 E I_y}{l^2}\sqrt{\frac{I_w}{I_y} + \frac{l^2 G(I_t + \frac{c_w}{G})}{\pi^2 n^2 E I_y}}$$

This can now be expressed in terms of the torsion- and warping constants from the modified Lindner's approach:

$$M_{cr} = \frac{\pi^2 E I_y}{s^2}\sqrt{\frac{I_w'}{I_y} + \frac{s^2 G I_t'}{\pi^2 E I_y}}$$

where $I_t' = I_t + \frac{c_w}{G}$ and $I_w' = I_w$

Appendix A

Beams restrained at its tension flange

Insert the general form of the warping- and torsion constants from the Lindner's approach, equation 2.23, into equation 2.19 describing the critical buckling moment for beams restrained at its tension flange.

$$M_{cr,1} = \frac{1}{2a_r}\left(GI_t^* + \frac{\pi^2 En^2}{l^2}(I_w^* + a_r{}^2 I_y) + \frac{k_\phi}{s}\frac{l^2}{n^2\pi^2}\right)$$

$$=> M_{cr,1} = \frac{1}{2a_r}\left(GI_t + \frac{\pi^2 En^2}{l^2}(I_w + c_w\frac{l^2}{\pi^2 n^2 E} + a_r{}^2 I_y) + \frac{k_\phi}{s}\frac{l^2}{n^2\pi^2}\right)$$

$$=> M_{cr,1} = \frac{1}{2a_r}\left(GI_t + c_w + \frac{\pi^2 En^2}{l^2}(I_w + a_r{}^2 I_y) + \frac{k_\phi}{s}\frac{l^2}{n^2\pi^2}\right)$$

This can now be expressed in terms of the torsion- and warping constants from the modified Lindner's approach

$$M_{cr,1} = \frac{1}{2a_r}\left(GI_t' + \frac{\pi^2 En^2}{l^2}(I_w' + a_r{}^2 I_y) + \frac{k_\phi}{s}\frac{l^2}{n^2\pi^2}\right)$$

where $I_t' = I_t + \frac{c_w}{G}$ and $I_w' = I_w$

B – Convergence study

This appendix contains the results from the convergence study carried out for this project.

Appendix B

Unrestrained beam with a corrugated web:

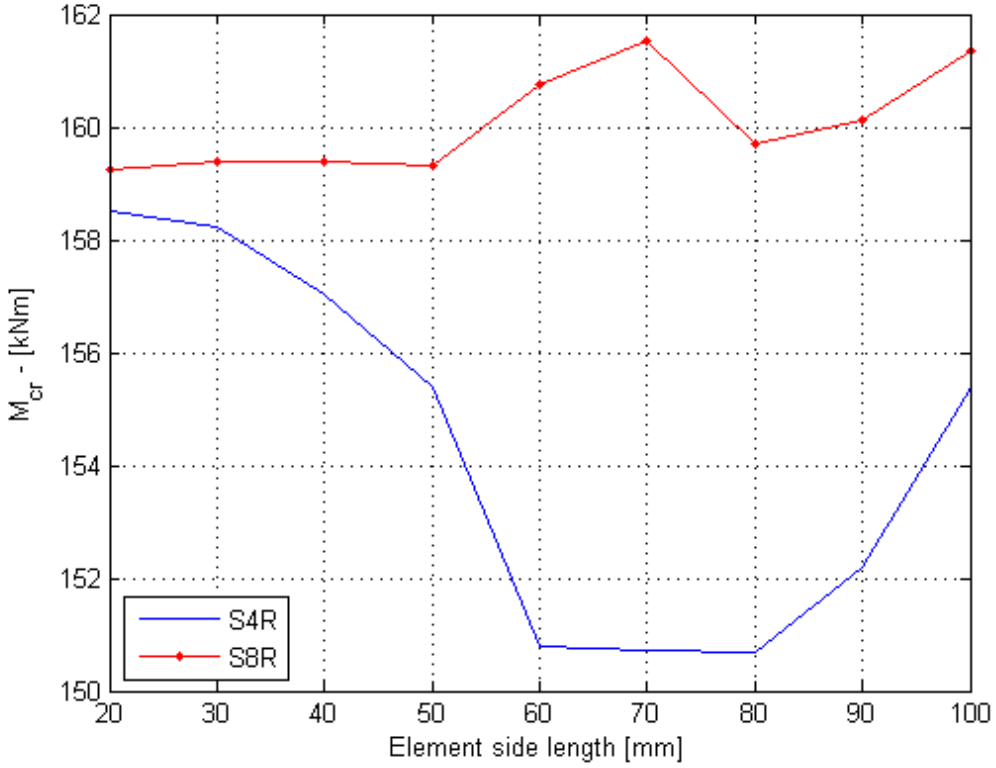

Figure B.1: a) Convergence study for an unrestrained beam with corrugated web.

Girder with corrugated web and six lateral restraints along its length:

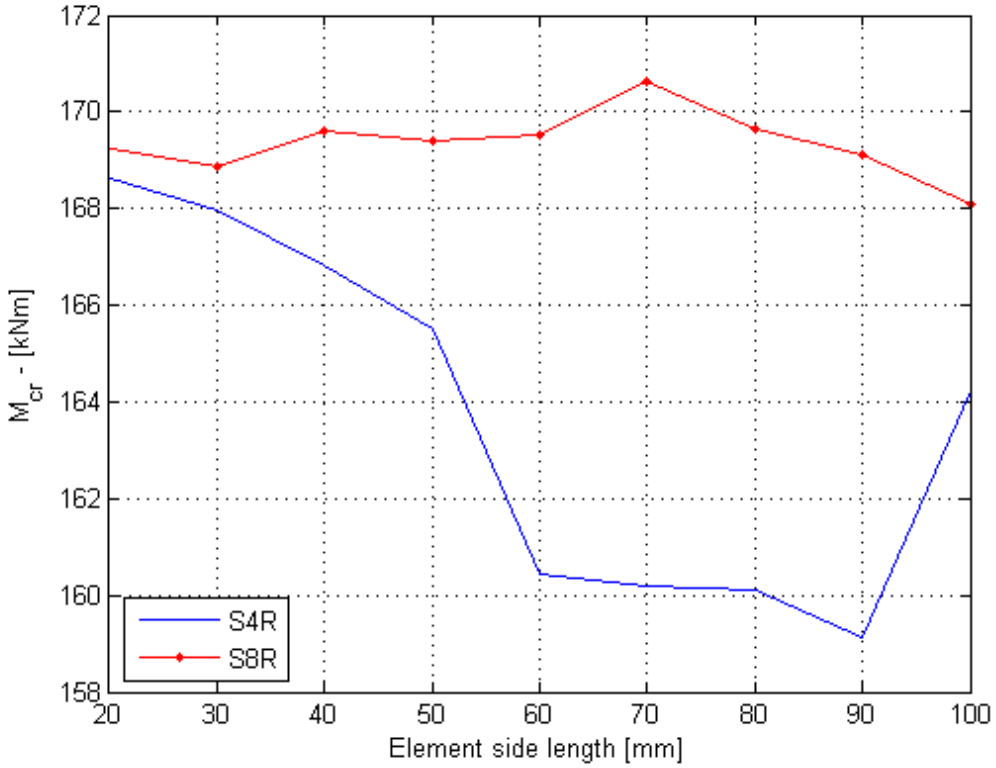

Figure B.2: a) Convergence study for a girder with six evenly spaced lateral restraints.

Girder with a corrugated web and six lateral and torsional restraints along its length. Torsiona stiffness: $k_\phi = 2 \cdot 10^5$ Nm/rad ,

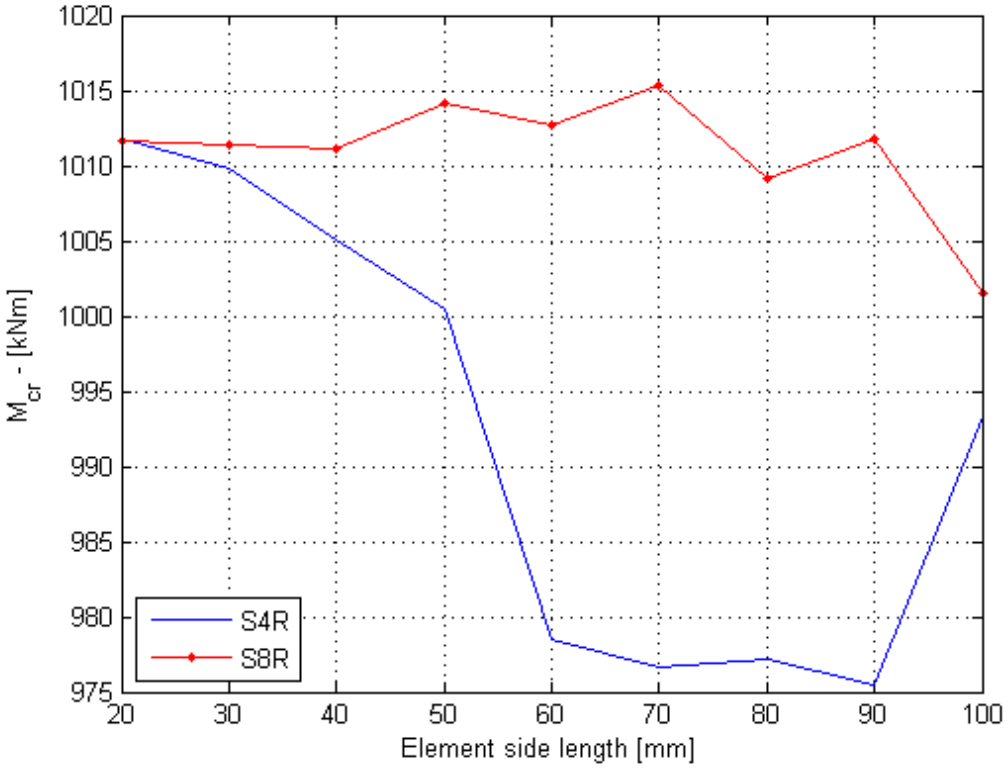

Figure B.3: a) Convergence study for a girder with six evenly spaced restraints with torsional stiffness of $k_\phi = 2 \cdot 10^5$ *Nm/rad.*

Table B.1: Comparison of the critical moment between FEM-model and analytical solution for a girder with flat web

El. size	unrestrained		lateral restraints		$k_\phi = 2 \cdot 10^5$Nm/rad	
[mm]	S4R	S8R	S4R	S8R	S4R	S8R
20	158.5	159.2	168.6	169.2	1011.8	1011.6
30	158.2	159.4	168.0	168.9	1009.8	1011.4
40	157.0	159.4	166.8	169.6	1005.0	1011.1
50	155.4	159.3	165.5	169.4	1000.4	1014.1
60	150.8	160.8	160.4	169.5	978.5	1012.7
70	150.7	161.5	160.2	170.6	976.7	1015.3
80	150.7	159.7	160.1	169.6	977.2	1009.1
90	152.2	160.1	159.1	169.1	975.5	1011.8
100	155.4	161.4	164.2	168.1	993.4	1001.5

Appendix B

C – Verification of the models

This appendix contains comparison of the deflection and stresses in the flanges between the FEM models and the analytical solution in order to verify the reliability of the models.

Appendix C

Verification

Dimensional properties

$t_f := 0.012m$ Thickness of the flanges

$b_f := 0.200m$ Width of the flanges

$t_{wc} := 0.002m$ Thickness of the corrugated web

$t_{w.flat} := 0.006m$ Thickness of the flat web

$h_w := 0.700m$ Height of the web

$l_s := 9.5m$ Length of the beam

Second moment of area

$$I_{flat} := \frac{b_f\left(h_w + 2\cdot t_f\right)^3}{12} - \frac{b_f\cdot h_w^{\,3}}{12} + \frac{t_{w.flat}\cdot h_w^{\,3}}{12} = 7.799\times 10^{-4}\,m^4$$ For beams with flat web

$$I := \frac{b_f\left(h_w + 2\cdot t_f\right)^3}{12} - \frac{b_f\cdot h_w^{\,3}}{12} = 6.084\times 10^{-4}\,m^4$$ For beams with corrugated web

Other

$M := 1kN\cdot m$ Applied moment

$E := 210\cdot GPa$ Elastic modulus

$$y := \frac{\left(h_w + t_f\right)}{2} = 0.356\,m$$ Distance from center of cross-section to center of the flange

Stresses in the flanges according to equation 4.4a

$$\sigma_{flat.top} := \frac{M}{I_{flat}}\cdot y = 4.565\times 10^{5}\,Pa$$ For beams with flat web

$$\sigma_{corr.top} := \frac{M}{I}\cdot y = 5.852\times 10^{5}\,Pa$$ For beams with corrugated web

$$\sigma_{flat.bottom} := \frac{M}{I_{flat}}\cdot -y = -4.565\times 10^{5}\,Pa$$ For beams with flat web

$$\sigma_{corr.bottom} := \frac{M}{I}\cdot -y = -5.852\times 10^{5}\,Pa$$ For beams with corrugated web

Vertical deflection according to equation 4.4b

$$\delta_{flat} := \frac{1}{8}\cdot\frac{M\cdot l_s^{\,2}}{E\cdot I_{flat}} = 6.888\times 10^{-5}\,m$$

$$\delta_{corr} := \frac{1}{8}\cdot\frac{M\cdot l_s^{\,2}}{E\cdot I} = 8.83\times 10^{-5}\,m$$

D – Results

This appendix includes tables and graphs which contain the results from this study. This includes the results for the parametric study, using linear buckling analyses, and buckling curves, using non-linear analyses. The parameter study included the following parameters:

- Torsional stiffness of the restraints
- Spacing between the restraints
- Thickness of the web
- Height of the web
- Thickness of the flanges
- Width of the flanges
- Height of the connection point of the purlins.

Appendix D

Laterally restrained girders
Restrained at the tension flange

Table D.1: Comparison of the critical moment between FEM-model and analytical solution for a girder with flat web

No. of restraints	$M_{cr.ABAQUS}$ [kNm]	M_{cr} [kNm]	Ratio: $\frac{M_{cr,ABAQUS}}{M_{cr}}$
0	156.0	159.6	0.977
1	158.5	162.8	0.974
2	159.9	162.8	0.982
3	161.3	162.8	0.991
4	162.7	162.8	0.999
5	164.1	162.8	1.008
6	165.5	162.8	1.017

Table D.2: Comparison of the critical moment between FEM-model and analytical solution for a girder with a corrugated web

No. of restraints	$M_{cr.ABAQUS}$ [kNm]	M_{cr} [kNm]	Ratio: $\frac{M_{cr,ABAQUS}}{M_{cr}}$
0	159.2	163.4	0.974
1	162.2	167.5	0.968
2	163.8	167.5	0.978
3	165.7	167.5	0.989
4	166.3	167.5	0.993
5	168.2	167.5	1.004
6	169.6	167.5	1.013

Laterally and torsionally restrained girders

Torsional stiffness & Number of purlins

Figure D.1 shows the comparison of the critical buckling moment from the FEM model and the analytical solution from Horne & Ajmani, equations 2.19 and 2.20, for girders with 6 mm thick flat web and with 1-6 purlins along its length. The values for this comparison can be seen in Table D.3.

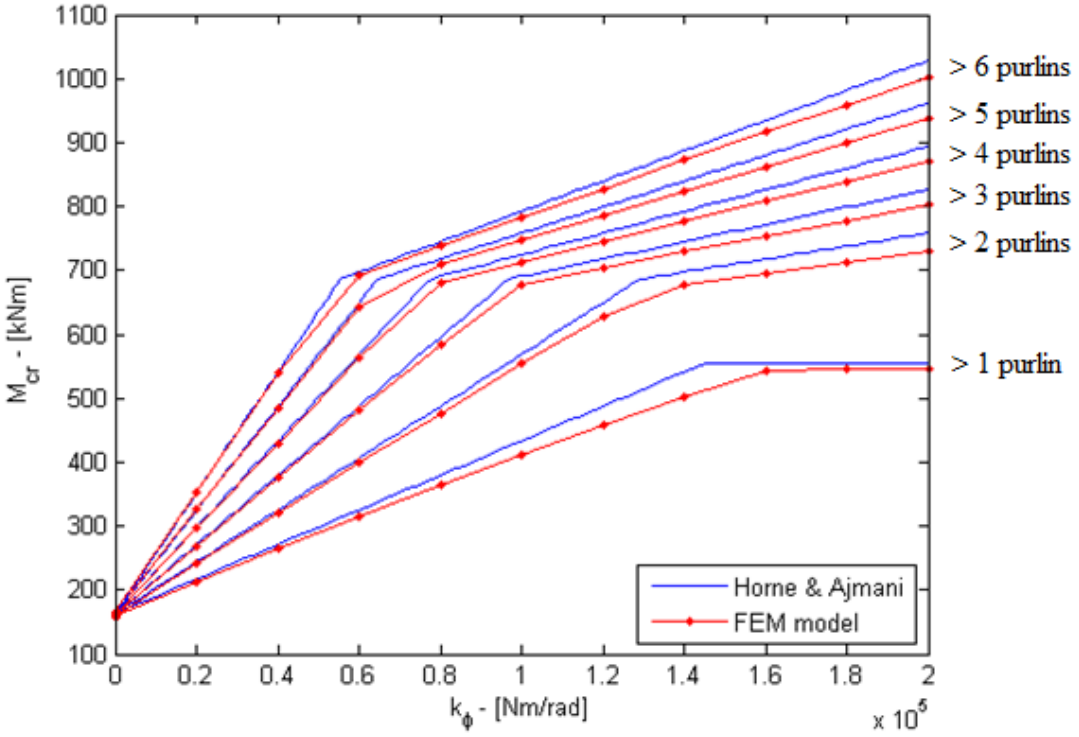

Figure D.1: The critical buckling moment, from the FEM model and the analytical solution, as a function of torsional stiffness provided by each purlin on 6 girders with flat web. The girders have 1-6 purlins along its total length.

Appendix D

Table D.3: Comparison of the critical buckling moment for varying torsional stiffness of the purlins for girders with flat web and number of purlins on the range 1-6.

Torsional Stiffness $\left[\cdot 10^5 \frac{\text{Nm}}{\text{rad}}\right]$	1 purlin			2 purlins		
	$M_{cr,FEM}$ [kNm]	$M_{cr,ana}$ [kNm]	$\frac{M_{cr,FEM}}{M_{cr,ana}}$	$M_{cr,FEM}$ [kNm]	$M_{cr,ana}$ [kNm]	$\frac{M_{cr,FEM}}{M_{cr,ana}}$
0.0	158.5	162.8	0.974	159.9	162.8	0.982
0.2	211.7	216.8	0.976	240.4	243.9	0.986
0.4	263.8	270.9	0.974	320.0	325.0	0.985
0.6	314.4	325.0	0.967	398.7	406.1	0.982
0.8	363.7	379.1	0.959	476.4	487.2	0.978
1.0	411.4	433.1	0.950	553.3	568.3	0.974
1.2	457.4	487.2	0.939	629.2	649.5	0.969
1.4	501.7	541.3	0.927	678.7	697.5	0.973
1.6	544.0	554.6	0.981	696.4	717.7	0.970
1.8	544.8	554.6	0.982	713.9	738.0	0.967
2.0	544.8	554.6	0.982	731.0	758.3	0.964
Torsional Stiffness $\left[\cdot 10^5 \frac{\text{Nm}}{\text{rad}}\right]$	3 purlins			4 purlins		
	$M_{cr,FEM}$ [kNm]	$M_{cr,ana}$ [kNm]	$\frac{M_{cr,FEM}}{M_{cr,ana}}$	$M_{cr,FEM}$ [kNm]	$M_{cr,ana}$ [kNm]	$\frac{M_{cr,FEM}}{M_{cr,ana}}$
0.0	161.3	162.8	0.991	162.7	162.8	1.000
0.2	268.8	270.9	0.992	297.1	298.0	0.997
0.4	375.2	379.1	0.990	430.3	433.1	0.993
0.6	480.7	487.2	0.987	562.2	568.3	0.989
0.8	585.1	595.4	0.983	681.4	690.7	0.986
1.0	678.5	690.7	0.982	713.5	724.5	0.985
1.2	703.8	717.7	0.981	745.3	758.3	0.983
1.4	728.8	744.8	0.979	776.9	792.1	0.981
1.6	753.6	771.8	0.976	808.2	825.9	0.979
1.8	778.2	798.8	0.974	839.2	859.7	0.976
2.0	802.5	825.9	0.972	869.9	893.5	0.974
Torsional Stiffness $\left[\cdot 10^5 \frac{\text{Nm}}{\text{rad}}\right]$	5 purlins			6 purlins		
	$M_{cr,FEM}$ [kNm]	$M_{cr,ana}$ [kNm]	$\frac{M_{cr,FEM}}{M_{cr,ana}}$	$M_{cr,FEM}$ [kNm]	$M_{cr,ana}$ [kNm]	$\frac{M_{cr,FEM}}{M_{cr,ana}}$
0.0	164.1	162.8	1.008	165.5	162.8	1.017
0.2	325.4	325.0	1.001	353.6	352.0	1.005
0.4	485.2	487.2	0.996	540.1	541.3	0.998
0.6	643.6	649.5	0.991	692.3	697.5	0.993
0.8	709.6	717.7	0.989	737.8	744.8	0.991
1.0	748.3	758.3	0.987	782.9	792.1	0.988
1.2	786.6	798.8	0.985	827.7	839.4	0.986
1.4	824.5	839.4	0.982	872.0	886.7	0.983
1.6	862.2	880.0	0.980	915.9	934.0	0.981
1.8	899.4	920.5	0.977	959.4	981.4	0.978
2.0	936.4	961.1	0.974	1002.4	1028.7	0.974

Figure D.2 shows the comparison of the critical buckling moment from the FEM model and the analytical solution from Horne & Ajmani, equations 2.19 and 2.20, for girders with 2 mm thick corrugated web and with 1-6 purlins along its length. The values for this comparison can be seen in Table D.4.

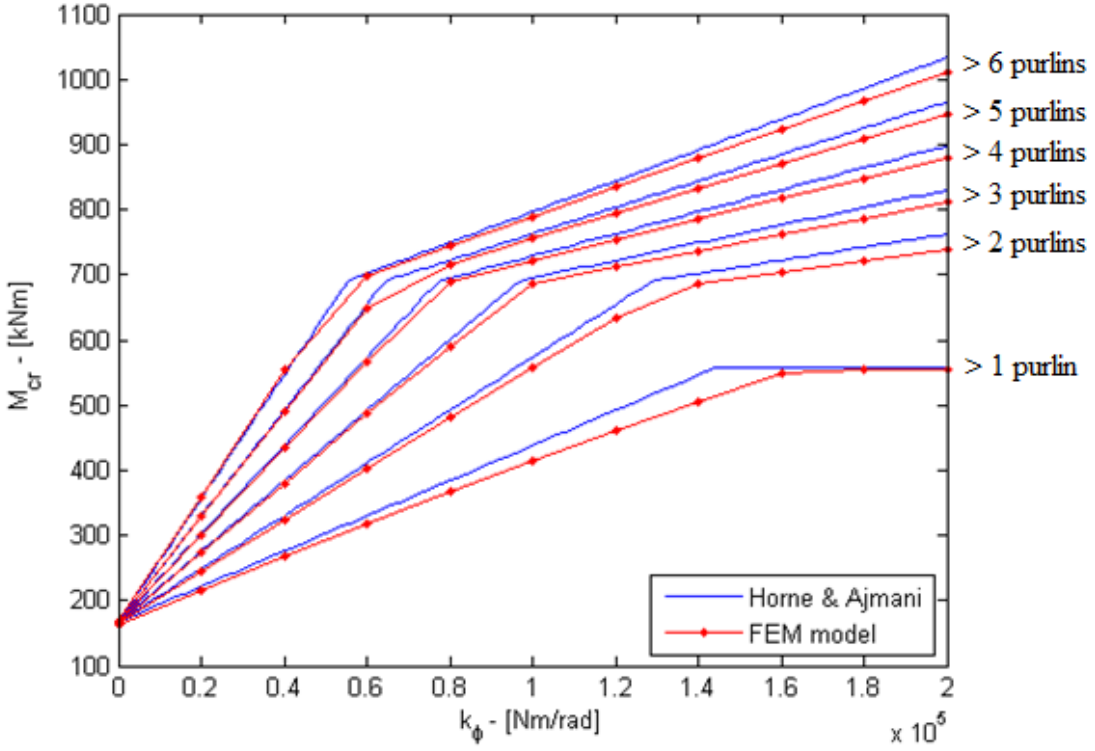

Figure D.2: The critical buckling moment, from the FEM model and the analytical solution, as a function of torsional stiffness provided by each purlin on 6 girders with corrugated web. The girders have 1-6 purlins along its total length.

Appendix D

Table D.4: Comparison of the critical buckling moment from FEM and analytical solution for varying torsional stiffness for girders with corrugated web and number of purlins on the range 1-6.

Torsional Stiffness $\left[\cdot 10^5 \frac{\text{Nm}}{\text{rad}}\right]$	1 purlin			2 purlins		
	$M_{cr,FEM}$ [kNm]	$M_{cr,ana}$ [kNm]	$\frac{M_{cr,FEM}}{M_{cr,ana}}$	$M_{cr,FEM}$ [kNm]	$M_{cr,ana}$ [kNm]	$\frac{M_{cr,FEM}}{M_{cr,ana}}$
0.0	162.2	167.5	0.969	163.8	167.5	0.978
0.2	215.5	221.6	0.973	244.4	248.6	0.983
0.4	267.5	275.6	0.971	324.0	329.7	0.983
0.6	318.3	329.7	0.965	402.9	410.8	0.981
0.8	367.6	383.8	0.958	480.8	491.9	0.977
1.0	415.5	437.9	0.949	557.9	573.0	0.974
1.2	461.7	491.9	0.939	634.1	654.2	0.969
1.4	506.2	546.0	0.927	686.4	701.9	0.978
1.6	548.5	558.7	0.982	704.4	722.1	0.975
1.8	554.4	558.7	0.992	722.0	742.4	0.973
2.0	554.5	558.7	0.992	739.4	762.7	0.969
Torsional Stiffness $\left[\cdot 10^5 \frac{\text{Nm}}{\text{rad}}\right]$	3 purlins			4 purlins		
	$M_{cr,FEM}$ [kNm]	$M_{cr,ana}$ [kNm]	$\frac{M_{cr,FEM}}{M_{cr,ana}}$	$M_{cr,FEM}$ [kNm]	$M_{cr,ana}$ [kNm]	$\frac{M_{cr,FEM}}{M_{cr,ana}}$
0.0	165.7	167.5	0.989	166.3	167.5	0.993
0.2	273.6	275.6	0.992	300.4	302.7	0.993
0.4	380.4	383.8	0.991	433.5	437.9	0.990
0.6	486.3	491.9	0.989	565.3	573.0	0.986
0.8	591.2	600.1	0.985	688.2	695.1	0.990
1.0	685.5	695.1	0.986	720.9	728.9	0.989
1.2	711.5	722.1	0.985	753.0	762.7	0.987
1.4	736.9	749.2	0.984	784.9	796.5	0.985
1.6	762.0	776.2	0.982	816.5	830.3	0.983
1.8	786.8	803.2	0.980	847.8	864.1	0.981
2.0	811.4	830.3	0.977	878.9	897.9	0.979
Torsional Stiffness $\left[\cdot 10^5 \frac{\text{Nm}}{\text{rad}}\right]$	5 purlins			6 purlins		
	$M_{cr,FEM}$ [kNm]	$M_{cr,ana}$ [kNm]	$\frac{M_{cr,FEM}}{M_{cr,ana}}$	$M_{cr,FEM}$ [kNm]	$M_{cr,ana}$ [kNm]	$\frac{M_{cr,FEM}}{M_{cr,ana}}$
0.0	168.2	167.5	1.004	169.6	167.5	1.013
0.2	329.7	329.7	1.000	359.1	356.7	1.007
0.4	489.9	491.9	0.996	555.0	546.0	1.016
0.6	648.7	654.2	0.992	698.0	701.9	0.994
0.8	716.2	722.1	0.992	743.9	749.2	0.993
1.0	755.1	762.7	0.990	789.3	796.5	0.991
1.2	793.7	803.2	0.988	834.4	843.8	0.989
1.4	832.0	843.8	0.986	879.1	891.1	0.986
1.6	870.0	884.4	0.984	923.4	938.4	0.984
1.8	907.7	924.9	0.981	967.5	985.8	0.981
2.0	945.1	965.5	0.979	1011.1	1033.1	0.979

Thickness of the web

Table D.5: Comparison of the critical buckling moment for varying thickness of the web for girders with flat and corrugated web. The torsional stiffness of the restraints are $\mathbf{0.4 \cdot 10^5 NM/rad}$ *and* $\mathbf{1.4 \cdot 10^5 NM/rad}$*, which results in the first and the second mode shape, respectively.*

Web thickness [mm]	Flat web, $k_\phi = 0.4 \cdot 10^5 NM/rad$			Corr web, $k_\phi = 0.4 \cdot 10^5 NM/rad$		
	$M_{cr,FEM}$ [kNm]	$M_{cr,ana}$ [kNm]	$\frac{M_{cr,FEM}}{M_{cr,ana}}$	$M_{cr,FEM}$ [kNm]	$M_{cr,ana}$ [kNm]	$\frac{M_{cr,FEM}}{M_{cr,ana}}$
2				489.9	491.9	0.996
3				491.6	492.9	0.997
4	477.9	483.1	0.989	493.5	494.2	0.999
5	481.6	484.8	0.993	496.0	496.0	1.000
6	485.2	487.2	0.996	499.1	498.5	1.001
7	489.4	490.6	0.998	503.3	501.9	1.003
8	494.6	495.2	0.999	508.6	506.5	1.004
9	500.9	501.0	1.000	515.4	512.3	1.006
10	508.6	508.3	1.000	523.7	519.5	1.008
Web thickness [mm]	Flat web, $k_\phi = 1.4 \cdot 10^5 NM/rad$			Corr web, $k_\phi = 1.4 \cdot 10^5 NM/rad$		
	$M_{cr,FEM}$ [kNm]	$M_{cr,ana}$ [kNm]	$\frac{M_{cr,FEM}}{M_{cr,ana}}$	$M_{cr,FEM}$ [kNm]	$M_{cr,ana}$ [kNm]	$\frac{M_{cr,FEM}}{M_{cr,ana}}$
2				832.0	843.8	0.986
3				834.0	844.8	0.987
4				836.2	846.1	0.988
5				839.1	847.8	0.990
6	824.5	839.4	0.982	842.9	850.4	0.991
7	829.9	843.0	0.984	847.7	853.8	0.993
8	836.0	847.8	0.986	853.8	858.3	0.995
9	843.2	854.0	0.987	861.3	864.1	0.997
10	851.7	861.7	0.988	870.5	871.3	0.999

Appendix D

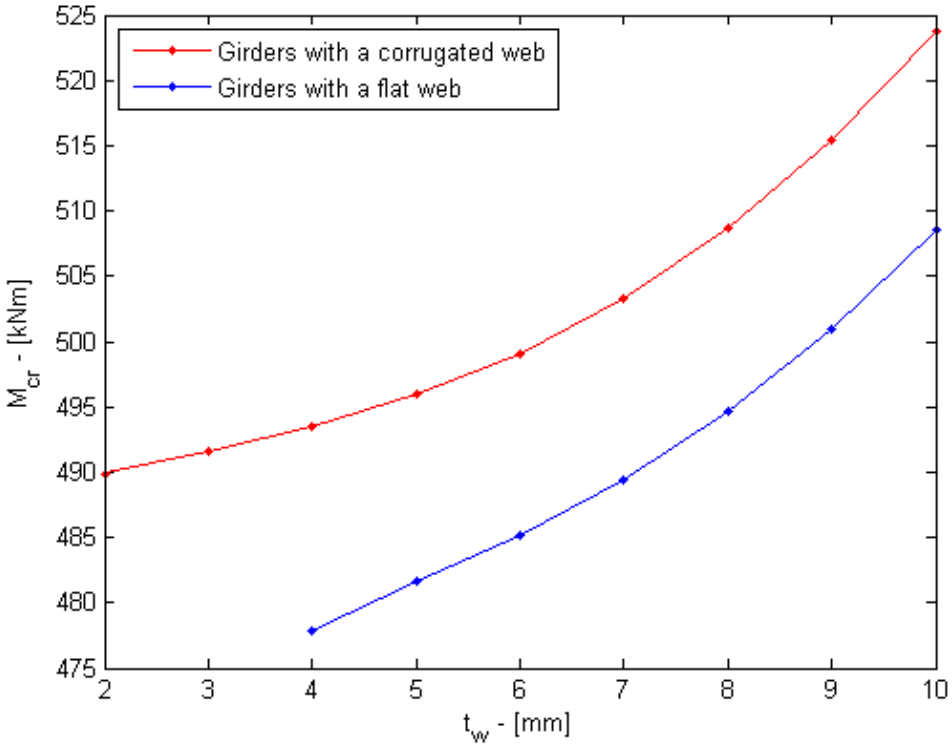

Figure D.3: The critical buckling moment, from the FEM models as a function of torsional stiffness provided by each purlin. The girders have 5 purlins along their total length and torsional stiffness of $\mathbf{0.4 \cdot 10^5 NM/rad}$.

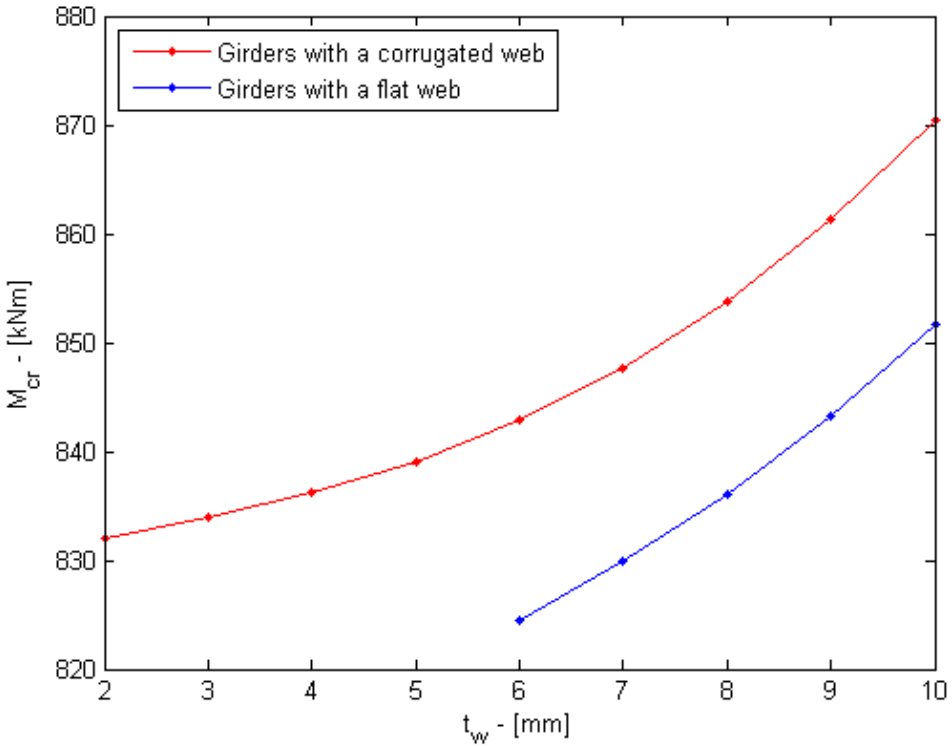

Figure D.4: The critical buckling moment, from the FEM models as a function of torsional stiffness provided by each purlin. The girders have 5 purlins along their total length and torsional stiffness of $\mathbf{1.4 \cdot 10^5 NM/rad}$.

Height of the web

Table D.6: Comparison of the critical buckling moment for varying height of the web for girders with flat and corrugated web. The torsional stiffness of the restraints are $\mathbf{0.3 \cdot 10^5 NM/rad}$ *and* $\mathbf{1.4 \cdot 10^5 NM/rad}$*, which results in the first and the second mode shape, respectively.*

Web height [mm]	Flat web, $k_\phi = 0.3 \cdot 10^5 NM/rad$			Corr web, $k_\phi = 0.3 \cdot 10^5 NM/rad$		
	$M_{cr,FEM}$ [kNm]	$M_{cr,ana}$ [kNm]	$\frac{M_{cr,FEM}}{M_{cr,ana}}$	$M_{cr,FEM}$ [kNm]	$M_{cr,ana}$ [kNm]	$\frac{M_{cr,FEM}}{M_{cr,ana}}$
500	473.1	474.5	0.997	482.0	482.6	0.999
600	430.8	431.7	0.998	438.7	437.9	1.002
700	405.5	406.1	0.998	410.0	410.8	0.998
800	390.9	391.3	0.999	396.1	394.9	1.003
900	383.5	383.8	0.999	387.5	386.5	1.003
1000	381.1	381.5	0.999	383.6	383.3	1.001
Web height [mm]	Flat web, $k_\phi = 1.4 \cdot 10^5 NM/rad$			Corr web, $k_\phi = 1.4 \cdot 10^5 NM/rad$		
	$M_{cr,FEM}$ [kNm]	$M_{cr,ana}$ [kNm]	$\frac{M_{cr,FEM}}{M_{cr,ana}}$	$M_{cr,FEM}$ [kNm]	$M_{cr,ana}$ [kNm]	$\frac{M_{cr,FEM}}{M_{cr,ana}}$
500	799.2	813.3	0.983	808.0	821.2	0.984
600	802.6	816.5	0.983	810.8	822.4	0.986
700	824.5	839.4	0.982	832.0	843.8	0.986
800	857.5	874.8	0.980	868.1	878.0	0.989
900	896.2	918.7	0.976	911.8	920.8	0.990
1000				960.4	969.6	0.990

Appendix D

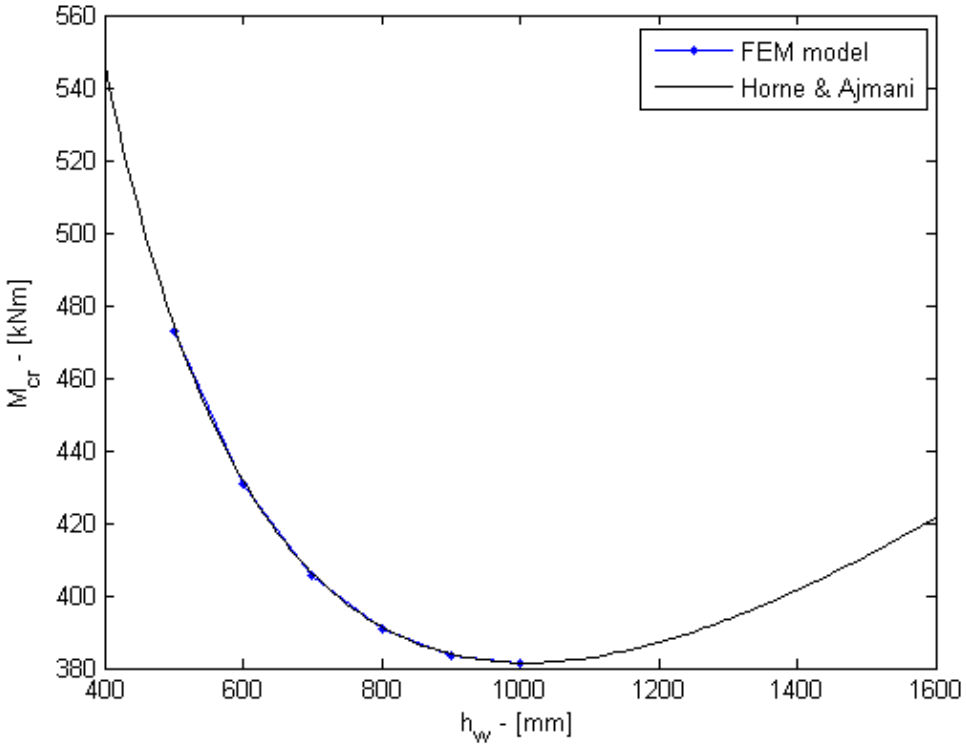

Figure D.5: The critical buckling moment as a function of the height of the web. Comparison between the FEM model and the analytical solution of a girder with a flat web and 5 restraints along its length with torsional stiffness of $\mathbf{0.3 \cdot 10^5 NM/rad}$.

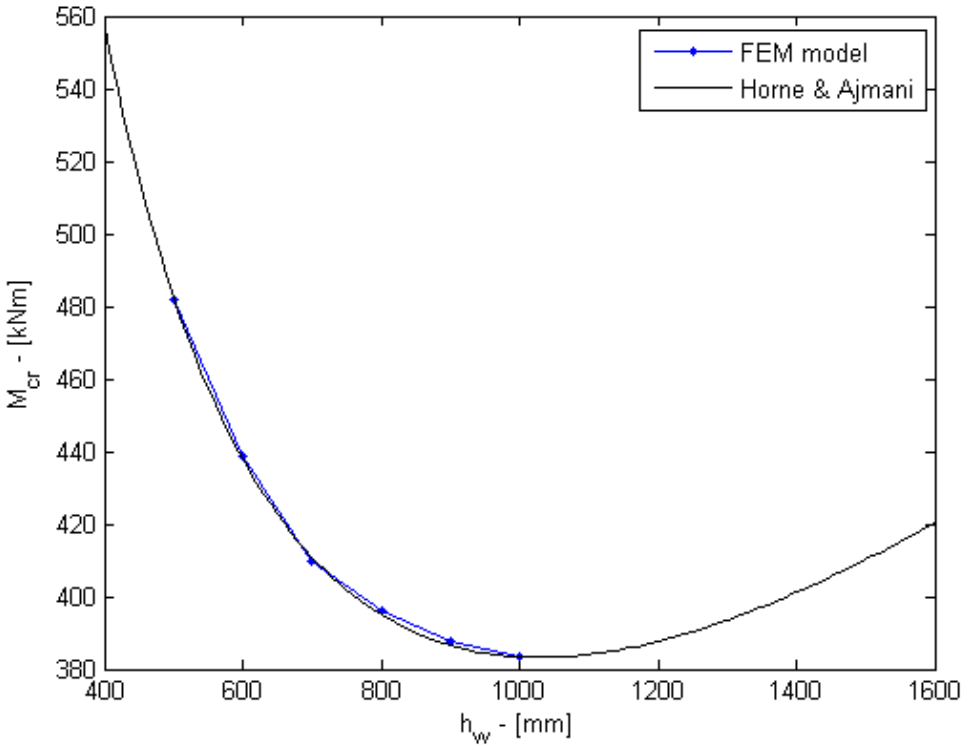

Figure D.6: The critical buckling moment as a function of the height of the web. Comparison between the FEM model and the analytical solution of a girder with a corrugated web and 5 restraints along its length with torsional stiffness of $\mathbf{0.3 \cdot 10^5 NM/rad}$.

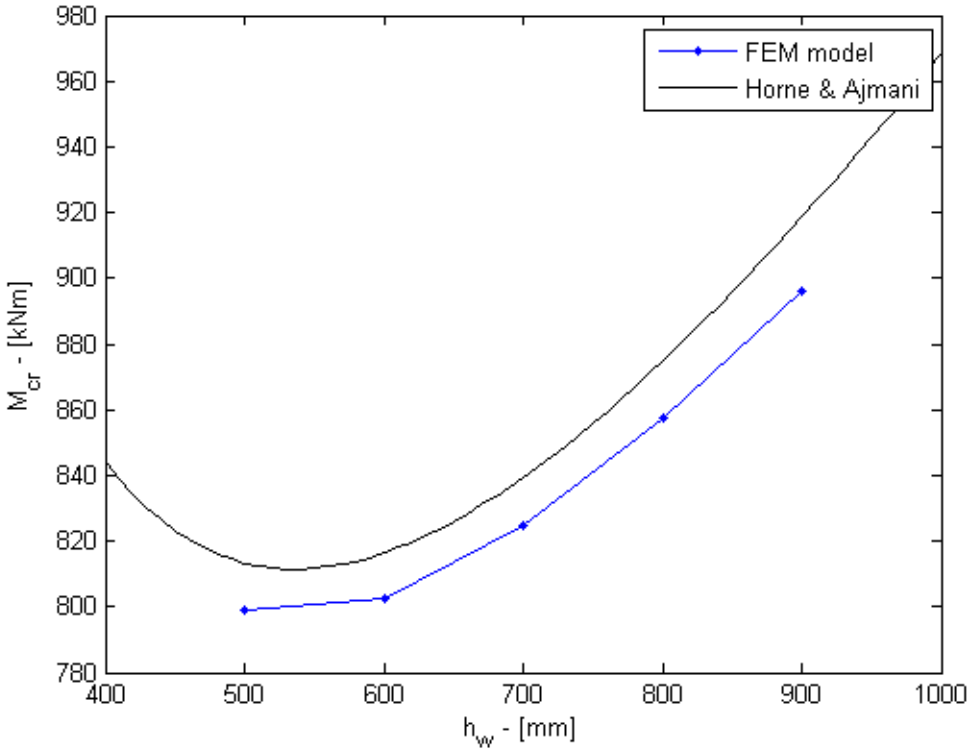

Figure D.7: The critical buckling moment as a function of the height of the web. Comparison between the FEM model and the analytical solution of a girder with a flat web and 5 restraints along its length with torsional stiffness of $\mathbf{1.4 \cdot 10^5 NM/rad}$.

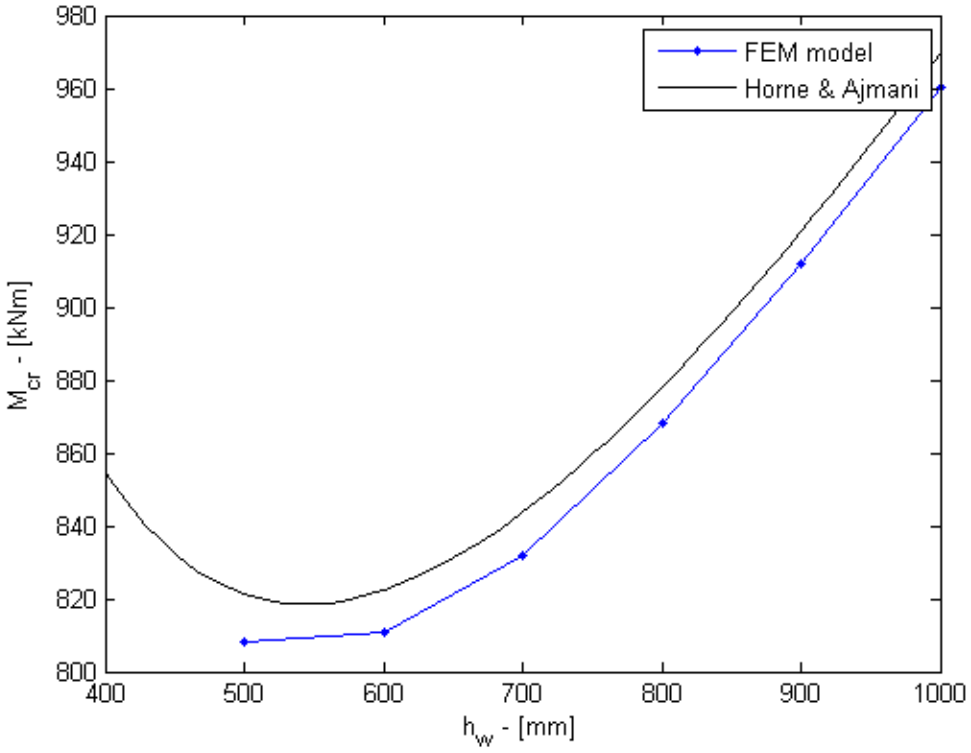

Figure D.8: The critical buckling moment as a function of the height of the web. Comparison between the FEM model and the analytical solution of a girder with a corrugated web and 5 restraints along its length with torsional stiffness of $\mathbf{1.4 \cdot 10^5 NM/rad}$.

Appendix D

Thickness of the Flanges

Table D.7: Comparison of the critical buckling moment for varying thickness of the flanges for girders with flat and corrugated web. The torsional stiffness of the restraints are $\mathbf{0.4 \cdot 10^5 NM/rad}$ *and* $\mathbf{1.4 \cdot 10^5 NM/rad}$*, which results in the first and the second mode shape, respectively.*

Flange thickness [mm]	Flat web, $k_\phi = 0.4 \cdot 10^5 NM/rad$			Corr web, $k_\phi = 0.4 \cdot 10^5 NM/rad$		
	$M_{cr,FEM}$ [kNm]	$M_{cr,ana}$ [kNm]	$\frac{M_{cr,FEM}}{M_{cr,ana}}$	$M_{cr,FEM}$ [kNm]	$M_{cr,ana}$ [kNm]	$\frac{M_{cr,FEM}}{M_{cr,ana}}$
8	425.3	426.6	0.997	423.2	424.4	0.997
9	439.4	440.4	0.998	438.7	439.6	0.998
10	454.1	455.1	0.998	455.0	455.8	0.998
11	469.4	470.6	0.997	472.0	473.2	0.997
12	485.2	487.2	0.996	489.9	491.9	0.996
13	501.7	504.9	0.994	508.7	511.9	0.994
14	518.8	523.8	0.990	528.6	533.3	0.991
15	536.5	543.9	0.986	549.4	556.1	0.988
16	554.9	565.4	0.981	571.3	580.3	0.984
17	573.8	588.4	0.975	594.3	606.1	0.981
Flange thickness [mm]	Flat web, $k_\phi = 1.4 \cdot 10^5 NM/rad$			Corr web, $k_\phi = 1.4 \cdot 10^5 NM/rad$		
	$M_{cr,FEM}$ [kNm]	$M_{cr,ana}$ [kNm]	$\frac{M_{cr,FEM}}{M_{cr,ana}}$	$M_{cr,FEM}$ [kNm]	$M_{cr,ana}$ [kNm]	$\frac{M_{cr,FEM}}{M_{cr,ana}}$
8	632.8	646.3	0.979	634.8	643.8	0.986
9	680.6	693.1	0.982	683.1	691.9	0.987
10	728.2	740.8	0.983	731.9	741.2	0.987
11	776.1	789.6	0.983	781.5	791.9	0.987
12	824.5	839.4	0.982	832.0	843.8	0.986
13	873.5	890.4	0.981	883.4	897.2	0.985
14	923.1	942.8	0.979	935.8	952.0	0.983
15	973.3	996.5	0.977	989.2	1008.3	0.981
16	1024.2	1051.6	0.974	1043.6	1066.2	0.979
17	1075.7	1108.3	0.971	1099.1	1125.6	0.976

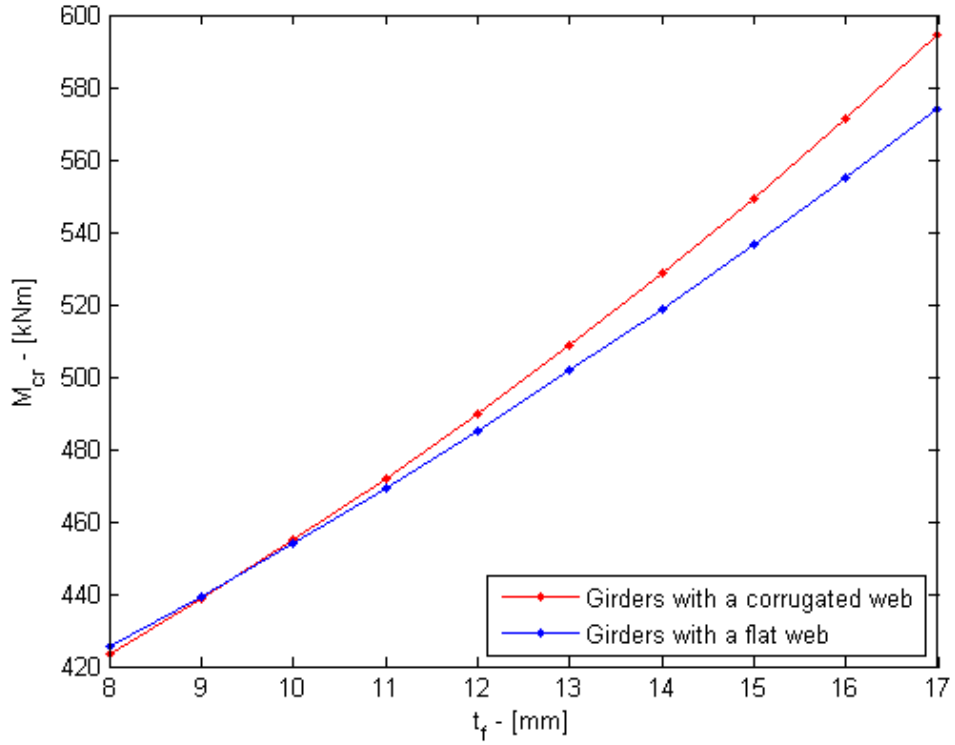

Figure D.9: The critical buckling moment as a function of the thickness of the flanges. Comparison between the results from the FEM models of girders with flat and corrugated web. The girders have 5 restraints along its length with torsional stiffness of $\mathbf{0.4 \cdot 10^5 NM/rad}$.

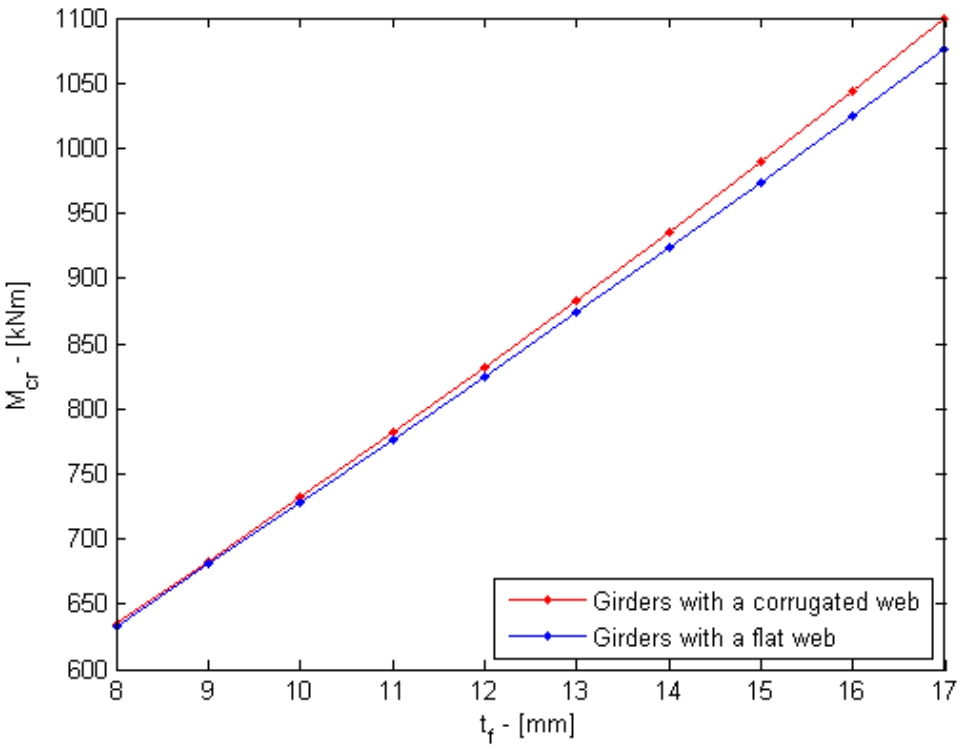

Figure D.10: The critical buckling moment as a function of the thickness of the flanges. Comparison between the results from the FEM models of girders with flat and corrugated web. The girders have 5 restraints along its length with torsional stiffness of $\mathbf{1.4 \cdot 10^5 NM/rad}$.

Appendix D

Width of the Flanges

Table D.8: Comparison of the critical buckling moment for varying width of the flanges for girders with flat and corrugated web. The torsional stiffness of the restraints are $\mathbf{0.2 \cdot 10^5 NM/rad}$ *and* $\mathbf{1.4 \cdot 10^5 NM/rad}$*, which results in the first and the second mode shape, respectively.*

Flange width [mm]	Flat web, $k_\phi = 0.2 \cdot 10^5 Nm/rad$			Corr web $k_\phi = 0.2 \cdot 10^5 Nm/rad$		
	$M_{cr,FEM}$ [kNm]	$M_{cr,ana}$ [kNm]	$\frac{M_{cr,FEM}}{M_{cr,ana}}$	$M_{cr,FEM}$ [kNm]	$M_{cr,ana}$ [kNm]	$\frac{M_{cr,FEM}}{M_{cr,ana}}$
125						
150	242.2	242.8	0.997	244.9	245.2	0.999
175	278.6	278.6	1.000	281.2	282.1	0.997
200	325.4	325.0	1.001	329.7	329.7	1.000
225	384.3	383.7	1.002	389.3	389.5	0.999
250	456.9	456.2	1.001	462.6	463.1	0.999
Flange width [mm]	Flat web $k_\phi = 1.4 \cdot 10^5 Nm/rad$			Corr web $k_\phi = 1.4 \cdot 10^5 Nm/rad$		
	$M_{cr,FEM}$ [kNm]	$M_{cr,ana}$ [kNm]	$\frac{M_{cr,FEM}}{M_{cr,ana}}$	$M_{cr,FEM}$ [kNm]	$M_{cr,ana}$ [kNm]	$\frac{M_{cr,FEM}}{M_{cr,ana}}$
125	406.5	434.1	0.936	411.1	435.0	0.945
150	511.3	530.4	0.964	518.9	532.5	0.974
175	648.1	663.4	0.977	654.6	666.7	0.982
200	842.5	839.4	1.004	832.0	843.8	0.986
225	1047.5	1064.4	0.984	1059.2	1069.9	0.990
250	1321.4	1344.7	0.983	1335.3	1351.2	0.988

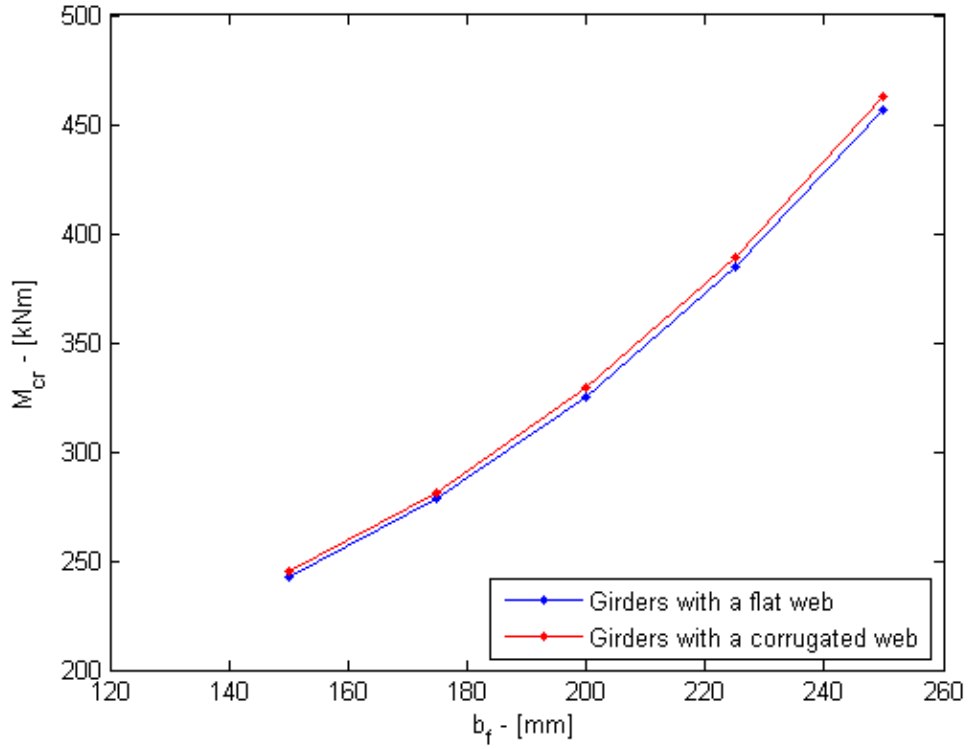

Figure D.11: The critical buckling moment as a function of the width of the flanges. Comparison between the results from the FEM models of girders with flat and corrugated web. The girders have 5 restraints along its length with torsional stiffness of $\mathbf{0.2 \cdot 10^5 NM/rad}$.

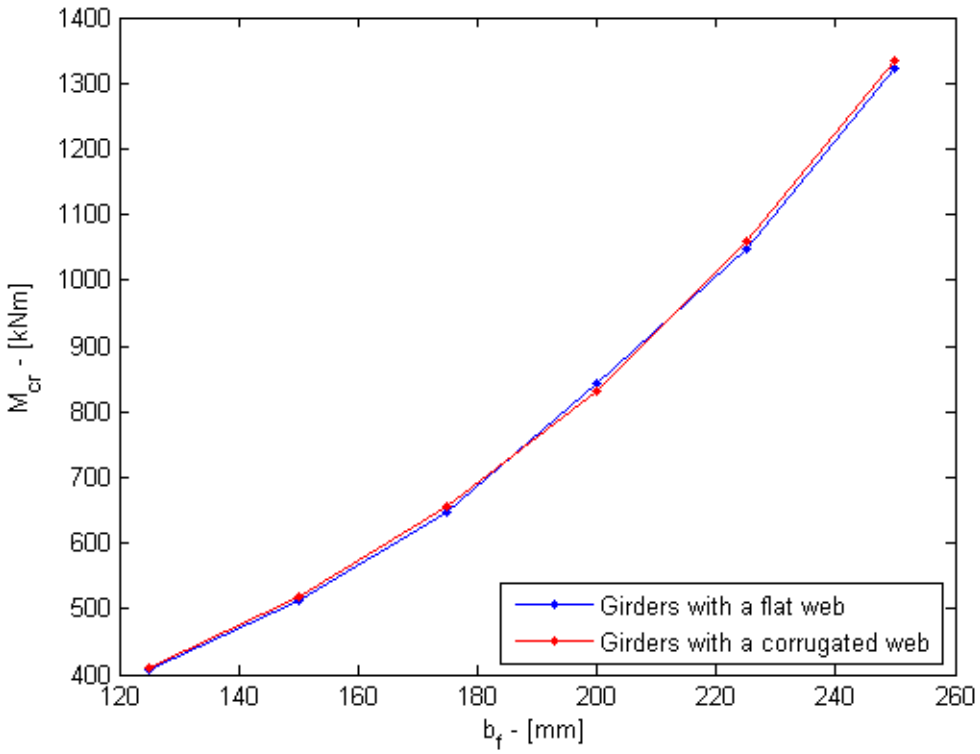

Figure D.12: The critical buckling moment as a function of the width of the flanges. Comparison between the results from the FEM models of girders with flat and corrugated web. The girders have 5 restraints along its length with torsional stiffness of $\mathbf{1.4 \cdot 10^5 NM/rad}$.

Appendix D

Non-linear analyses

Table D.9: Values of the yield stress, yield moment and initial imperfections, for buckling curves d and c, used in the non-linear buckling analyses for the two studied girder types.

	f_y	Wf_y	Curve d	Curve c
	[MPa]	[kNm]	[mm]	[mm]
Flat web	355	727.3	31.67	23.75
Corrugated web	355	596.6	32.67	23.75

Table D.10: Values of the most important variables to create the buckling curves for a girder with flat web. The curves are presented in chapters 5.2.

			curve d		curve c	
k_ϕ	M_{cr}	$\overline{\lambda}_{LT}$	M_u	χ_{LT}	M_u	χ_{LT}
[10^5Nm/rad]	[kNm]		[kNm]		[kNm]	
0	162.8	2.114	160.9	0.221	163.4	0.225
0.5	257.4	1.681	229.8	0.316	235.4	0.324
1	352.0	1.437	296.3	0.407	304.3	0.418
1.5	446.7	1.276	360.2	0.495	371.0	0.510
2	541.3	1.159	421.6	0.580	435.1	0.598
2.5	635.9	1.069	479.9	0.660	496.1	0.682

Table D.11: Values of the most important variables to create the buckling curves for a girder with corrugated web. The curves are presented in chapters 5.2.

			curve d		curve d	
k_ϕ	M_{cr}	$\overline{\lambda}_{LT}$	M_u	χ_{LT}	M_u	χ_{LT}
[10^5Nm/rad]	[kNm]		[kNm]		[kNm]	
0	167.5	1.887	145.8	0.244	150.8	0.253
0.5	262.1	1.509	213.4	0.358	221.5	0.371
1	356.7	1.293	277.1	0.464	289.0	0.484
1.5	451.4	1.150	336.2	0.564	351.0	0.588
2	546.0	1.045	389.7	0.653	406.6	0.682
2.5	640.6	0.965	428.6	0.718	447.6	0.750

E – Matlab code

This appendix contains all Matlab codes used to calculate and plot the results in this project. All graphs are presented in chapter 5 and/or in appendix D

Appendix E

Torsional stiffness & spacing between purlins

Table E.1: Excel file: torsionalstiffness.xlsx; contains the critical buckling moment of the FEM model, used in the following Matlab code.

	Flat web, 6 mm,					
Spring stiffness	1 purlin	2 purlins	3 purlins	4 purlins	5 purlins	6 purlins
0	158.5	159.9	161.3	162.7	164.1	165.5
1	211.7	240.4	268.8	297.1	325.4	353.6
2	263.8	320.0	375.2	430.3	485.2	540.1
3	314.4	398.7	480.7	562.2	643.6	692.3
4	363.7	476.4	585.1	681.4	709.6	737.8
5	411.4	553.3	678.5	713.5	748.3	782.9
6	457.4	629.2	703.8	745.3	786.6	827.7
7	501.7	678.7	728.8	776.9	824.5	872.0
8	544.0	696.4	753.6	808.2	862.2	915.9
9	544.8	713.9	778.2	839.2	899.4	959.4
10	544.8	731.0	802.5	869.9	936.4	1002.4
	Corrugated web, 2 mm					
Spring stiffness	1 purlin	2 purlins	3 purlins	4 purlins	5 purlins	6 purlins
0	162.2	163.8	165.7	166.3	168.2	169.6
1	215.5	244.4	273.6	300.4	329.7	359.1
2	267.5	324.0	380.4	433.5	489.9	555.0
3	318.3	402.9	486.3	565.3	648.7	698.0
4	367.6	480.8	591.2	688.2	716.2	743.9
5	415.5	557.9	685.5	720.9	755.1	789.3
6	461.7	634.1	711.5	753.0	793.7	834.4
7	506.2	686.4	736.9	784.9	832.0	879.1
8	548.5	704.4	762.0	816.5	870.0	923.4
9	554.4	722.0	786.8	847.8	907.7	967.5
10	554.5	739.4	811.4	878.9	945.1	1011.1

```
% Parametric study:
% Torsional stiffness & spacing between purlins
clc, clear all, close all

%% Properties of the girders

% Material properties
E = 210e9;          % [Pa] elastic modulus
v = 0.3;            % Poission ratio
G = E/(2*(1+v));    % [Pa] Shear modulus

% Sectional properties
h_w = 0.700;        % [m] Height of the web
t_w_corr = 0.002;   % [m] Thickness of the corrugated web
t_w_flat = 0.006;   % [m] Thickness of the flat web
b_f = 0.200;        % [m] Width of the flange
t_f = 0.012;        % [m] Thickness of the flange
l = 9.5;            % [m] Length of the girder

h_m = h_w+t_f;      % [m] Distance between centroid of flanges
a = (h_w+t_f)/2;    % [m] Distance from center of cross-section to
restr.

% Second moment of area around the weak axis for girders with flat
and
% corrugated webs
I_y_flat = h_w*t_w_flat^3/12+2*t_f*b_f^3/12;    % [m^4]
I_y_corr = 2*t_f*b_f^3/12;                      % [m^4]

% Shape of the corrugation
a_1 = 0.140;        % [m] length of straight webpanel
a_3 = 0.050;        % [m] length of inclined webpanel
b_t = 0.050;        % [m] eccentricity of the corrugation

u_x = h_m/(2*G*a_1*t_w_corr)+h_m^2*(a_1+a_3)^3/(600*a_1^2*E)*2/...
    (b_f*t_f^3/12);
c_w = b_t^2*h_m^2/(8*u_x*(a_1+a_3));

% Warping and torsion constants for a girder with flat web
I_w_flat = I_y_flat*h_m^2/4;                % [m^6]
I_t_flat = (2*b_f*t_f^3+h_w*t_w_flat^3)/3;  % [m^4]

% Warping and torsion constants for a girder with corrugated
% web using modified Lindner's approach
I_w_corr = I_y_corr*h_m^2/4;                        % [m^6]
I_t_corr = (2*b_f*t_f^3+h_w*t_w_corr^3)/3+c_w/G;    % [m^4]

%% Torsional stiffness & number of purlins:
% spring stiffness ranging from 0-10 MN/m
% number of purlins ranging from 1-6

k_max = 10;         % [MN/m/rad] Maximum spring stiffness
n_max = 6;          % Highest number of restraints

M_flat = zeros(n_max,k_max*10+1);   % M_cr for girders with flat web
M_corr = zeros(n_max,k_max*10+1);   % M_cr for girders with
corrugated web

for n_res = 1:n_max;        % Number of restraints
```

```
    s = l/(n_res+1);        % [m] Spacing between purlins

    % Critical buckling moment from case 2 (eq. 2.19)

    M_bp_flat = pi^2*E*I_y_flat/s^2*sqrt(I_w_flat/I_y_flat+s^2*G*...
        I_t_flat/(pi^2*E*I_y_flat));
    M_bp_corr = pi^2*E*I_y_corr/s^2*sqrt(I_w_corr/I_y_corr+s^2*G*...
        I_t_corr/(pi^2*E*I_y_corr));

    % [Nm] Critical buckling moment from case 1 (eq. 2.18)

    M_t1_flat = zeros; M_t1_corr = zeros;

    % Calculate M_cr as a function of the torsional stiffness
    for k = 0:0.1:k_max   % [MN/m/rad] spring stiffness

        k_phi = k*10^6*b_f^2/2;  % [Nm/rad] torsional stiffness

        M_t_flat = zeros;
        M_t_corr = zeros;

        for n = 1:n_res     % mode shape number

            % M_cr from Horne & Ajmani
            M_t_flat(n) = 1/(2*a)*(pi^2*E*n^2/l^2*...

(I_w_flat+a^2*I_y_flat)+G*I_t_flat+k_phi/s*(l/(pi*n))^2);
            M_t_corr(n) = 1/(2*a)*(pi^2*E*n^2/l^2*...

(I_w_corr+a^2*I_y_corr)+G*I_t_corr+k_phi/s*(l/(pi*n))^2);

        end

        M_t1_flat(round(k*10+1)) = min([M_t_flat,M_bp_flat]);
        M_t1_corr(round(k*10+1)) = min([M_t_corr,M_bp_corr]);
    end

    % M_cr for girders with flat and corrugated web. (n,k) matrix
where n
    % is the number of purlins and k is spring stiffness
    M_corr(n_res,:) = M_t1_corr;    % [Nm]
    M_flat(n_res,:) = M_t1_flat;    % [Nm]

end

A = xlsread('torsionalstiffness.xlsx');

%% Plots of M_cr vs. Spring stiffness, nubmer of purlins on the range
1-6

k1 = 0:0.1:k_max;
k2 = A(:,1);

k1 = k1.*10^6*b_f^2/2;
k2 = k2.*10^6*b_f^2/2;

% Girder with flat web, number of purlins ranging 1-6
```

```
figure
for n = 1:n_max     % Number of purlins

    plot(k1,M_flat(n,:)/1000), hold on
    plot(k2,A(:,n+1),'.-r')
    xlabel('k_{\phi} - [Nm/rad]')
    ylabel('M_c_r - [kNm] ')
    legend('Horne & Ajmani','FEM model','Location','SouthEast')
    xlim([0 2*10^5])
end

% Girder with corrugated web, number of purlins rangin 1-6
figure
for n = 1:n_max       % Number of purlins

    plot(k1,M_corr(n,:)/1000), hold on
    plot(k2,A(:,n+7),'.-r')
    xlabel('k_{\phi} - [Nm/rad]')
    ylabel('M_c_r - [kNm] ')
    legend('Horne & Ajmani','FEM model','Location','SouthEast')
    xlim([0 2*10^5])
end
```

Appendix E

Thickness of the web

Table E.2: Excel file: webthickness.xlsx; contains the critical buckling moment of the FEM model, used in the following Matlab code.

Web thickness				
thickness	$k_\phi = 0.4 \cdot 10^5 \frac{Nm}{rad}$		$k_\phi = 1.4 \cdot 10^5 \frac{Nm}{rad}$	
[mm]	Flat	Corr	Flat	Corr
2		489.91		832.02
3		491.64		833.95
4	477.87	493.54		836.2
5	481.58	495.95		839.08
6	485.21	499.12	824.52	842.86
7	489.43	503.28	829.89	847.7
8	494.61	508.63	836.01	853.8
9	500.92	515.39	843.17	861.34
10	508.59	523.72	851.65	870.51

```
%% Parametric study - web thickness
clc, clear all, close all

% values from the FEM analysis

A = xlsread('parametric study.xlsx');

% 2MN/m for corrugated and flat web

figure
plot(A(1:9,1),A(1:9,3),'.-r'), hold on
plot(A(1:9,1),A(1:9,2),'.-b')
xlabel('t_w - [mm]')
ylabel('M_c_r - [kNm]')
legend('Girders with a corrugated web','Girders with a flat web',...
    'Location','NorthWest')

% 7MN/m for corrugated and flat web

figure
plot(A(1:9,1),A(1:9,5),'.-r'), hold on
plot(A(1:9,1),A(1:9,4),'.-b')
xlabel('t_w - [mm]')
ylabel('M_c_r - [kNm]')
legend('Girders with a corrugated web','Girders with a flat web',...
    'Location','NorthWest')
```

Height of the web

Table E.3: Excel file: webheight.xlsx; contains the critical buckling moment of the FEM model, used in the following Matlab code.

Web height				
height [mm]	$k_\phi = 0.3 \cdot 10^5 \frac{Nm}{rad}$		$k_\phi = 1.4 \cdot 10^5 \frac{Nm}{rad}$	
	Flat	Corr	Flat	Corr
500	473.1	482.0	799.2	808.0
600	430.8	438.7	802.6	810.8
700	405.5	410.0	824.5	832.0
800	390.9	396.1	857.5	868.1
900	383.5	387.5	896.2	911.8
1000	381.1	383.6		960.4

```
% Parametric study - web height
% Plots the critical buckling moment as a fucntion of the web height
clc, clear all, close all

% material properties
E = 210e9;          % [Pa] elastic modulus
v = 0.3;            % Poission ratio
G = E/(2*(1+v));    % [Pa] shear modulus

% values from the FEM analysis

A = xlsread('webheight.xlsx');

% web height

t_w_corr = 0.002;   % [m] Thickness of the corrugated web
t_w_flat = 0.006;   % [m] Thickness of the flat web
b_f = 0.200;        % [m] Width of the flanges
t_f = 0.012;        % [m] Thickness of the flanges
l = 9.5;            % [m] Length of the girder

% Sectional properties

M_f1 = zeros;
M_c1 = zeros;

M_f2 = zeros;
M_c2 = zeros;

for h = 500:10:1000

    x = round(h/10-49);
    h_w = h/1000;       % [m] height of the web


    h_m = h_w+t_f;      % [m] distance between centroid of flanges
    a = (h_w+t_f)/2;    % [m] dist. from centre of cross-section to
restr.

    % [m^4] second moment of area of the weak axis for girders with
flat
```

Appendix E

```
    % and corrugated web

    I_y_flat = h_w*t_w_flat^3/12+2*t_f*b_f^3/12;
    I_y_corr = 2*t_f*b_f^3/12;

    % shape of the corrugation
    a_1 = 0.140;        % [m] length of straight webpanel
    a_3 = 0.050;        % [m] length of inclined webpanel
    b_t = 0.050;        % [m] eccentricity of the corrugation

    u_x =
h_m/(2*G*a_1*t_w_corr)+h_m^2*(a_1+a_3)^3/(600*a_1^2*E)*2/...
        (b_f*t_f^3/12);
    c_w = b_t^2*h_m^2/(8*u_x*(a_1+a_3));

    % warping [m^6] and torsional [m^4] constants for girders with
flat web
    I_w_flat = I_y_flat*h_m^2/4;
    I_t_flat = (2*b_f*t_f^3+h_w*t_w_flat^3)/3;

    % warping [m^6] and torsional [m^4] constants for girders with
    % corrugated web using modified Lindner's approach
    I_w_corr = I_y_corr*h_m^2/4;
    I_t_corr = (2*b_f*t_f^3+h_w*t_w_corr^3)/3+c_w/G;

    n_b = 5;        % Number of restraints
    s = l/(n_b+1);  % Spacing between purlins

    % Torsional stiffness of 7 MN/m

    n = 2;                      % Mode shape number
    k_s = 7;                    % [MN/m] spring stiffness
    k_phi = k_s*10^6*b_f^2/2;   % [Nm/rad] torsional stiffness

    % The critical buckling moment

    M_f1(x) = (1/(2*a)*(pi^2*E*n^2/l^2*(I_w_flat+a^2*I_y_flat)+...
        G*I_t_flat+k_phi/s*(l/(pi*n))^2))/1000;
    M_c1(x) = (1/(2*a)*(pi^2*E*n^2/l^2*(I_w_corr+a^2*I_y_corr)+...
        G*I_t_corr+k_phi/s*(l/(pi*n))^2))/1000;

    % Torsional stiffness of 2 MN/m

    n = 1;                      % Mode shape number
    k_s = 1.5;                  % [MN/m] spring stiffness
    k_phi = k_s*10^6*b_f^2/2;   % [Nm/rad] torsional stiffness

    % The critical buckling moment

    M_f2(x) = (1/(2*a)*(pi^2*E*n^2/l^2*(I_w_flat+a^2*I_y_flat)+...
        G*I_t_flat+k_phi/s*(l/(pi*n))^2))/1000;
    M_c2(x) = (1/(2*a)*(pi^2*E*n^2/l^2*(I_w_corr+a^2*I_y_corr)+...
        G*I_t_corr+k_phi/s*(l/(pi*n))^2))/1000;

end

h = 500:10:1000;
```

```
% 1.5 MN/m for corrugated 2mm and flat web 6 mm

% Flat web vs. Horne & Ajmani
figure
plot(A(:,1),A(:,2),'.-b'), hold on
plot(h,M_f2,'k')
xlabel('h_w - [mm]')
ylabel('M_c_r - [kNm]')
legend('FEM model','Horne & Ajmani')

% Corrugated web vs. Horne & Ajmani
figure
plot(A(:,1),A(:,3),'.-b'), hold on
plot(h,M_c2,'k')
xlabel('h_w - [mm]')
ylabel('M_c_r - [kNm]')
legend('FEM model','Horne & Ajmani')

% 7MN/m for corrugated 2mm and flat web 6 mm

% Flat web vs. Horne & Ajmani
figure
plot(A(:,1),A(:,4),'.-b'), hold on
plot(h,M_f1,'k')
xlabel('h_w - [mm]')
ylabel('M_c_r - [kNm]')
legend('FEM model','Horne & Ajmani')

% Corrugated web vs. Horne & Ajmani
figure
plot(A(:,1),A(:,5),'.-b'), hold on
plot(h,M_c1,'k')
xlabel('h_w - [mm]')
ylabel('M_c_r - [kNm]')
legend('FEM model','Horne & Ajmani')
```

Appendix E

Thickness of the flanges

Table E.4: Excel file: flangethickness.xlsx; contains the critical buckling moment of the FEM model, used in the following Matlab code.

Flange thickness				
thickness [mm]	$k_\phi = 0.4 \cdot 10^5 \frac{Nm}{rad}$		$k_\phi = 1.4 \cdot 10^5 \frac{Nm}{rad}$	
	Flat	Corr	Flat	Corr
8	425.33	423.21	632.79	634.79
9	439.43	438.74	680.61	683.11
10	454.11	454.97	728.17	731.94
11	469.36	471.99	776.1	781.54
12	485.21	489.91	824.52	832.02
13	501.68	508.74	873.51	883.41
14	518.79	528.58	923.11	935.77
15	536.51	549.4	973.33	989.16
16	554.85	571.3	1024.2	1043.6
17	573.76	594.27	1075.7	1099.1

```
% Parametric study - flange thickness
clc, clear all, close all

A = xlsread('flangethickness.xlsx');

% torsionals stiffness 2 MN/m

figure
plot(A(:,1),A(:,3),'.-r'), hold on
plot(A(:,1),A(:,2),'.-b')
xlabel('t_f - [mm]')
ylabel('M_c_r - [kNm]')
legend('Girders with a corrugated web','Girders with a flat web',...
    'Location','SouthEast')

% torsionals stiffness 7 MN/m

figure
plot(A(:,1),A(:,5),'.-r'), hold on
plot(A(:,1),A(:,4),'.-b')
xlabel('t_f - [mm]')
ylabel('M_c_r - [kNm]')
legend('Girders with a corrugated web','Girders with a flat web',...
    'Location','SouthEast')
```

Width of the flanges

Table E.5: Excel file: flangewidth.xlsx; contains the critical buckling moment of the FEM model, used in the following Matlab code.

Flange width				
	$k_\phi = 0.2 \cdot 10^5 \frac{Nm}{rad}$		$k_\phi = 1.4 \cdot 10^5 \frac{Nm}{rad}$	
width [mm]	Flat	Corr	Flat	Corr
125			406.5	411.125
150	242.18	244.9	511.275	518.850
175	278.60	281.2	648.1125	654.588
200	325.37	329.7	842.5	832.000
225	384.3	389.25	1047.488	1059.188
250	456.875	462.625	1321.375	1335.250

```
% Parametric study - flange width
% Plots the critical buckling moment as a fucntion of the flange
thickness
clc, clear all, close all

A = xlsread('flangewidth.xlsx');

% 0.2 Nm/rad corrugated web 2 mm and flat web 6 mm

figure
plot(A(:,1),A(:,2),'.-b'), hold on
plot(A(:,1),A(:,3),'.-r')
xlabel('b_f - [mm]')
ylabel('M_c_r - [kNm]')
legend('Girders with a flat web','Girders with a corrugated web',...
    'Location','SouthEast')

% 1.4 Nm/rad corrugated web 2 mm and flat web 6 mm

figure
plot(A(:,1),A(:,4),'.-b'), hold on
plot(A(:,1),A(:,5),'.-r')
xlabel('b_f - [mm]')
ylabel('M_c_r - [kNm]')
legend('Girders with a flat web','Girders with a corrugated web',...
    'Location','SouthEast')
```

Appendix E

Bucling curves

Table E.6: Excel file: buckling curve.xlsx; contains the ultimate moment from the non-linear buckling analysi, used in the following Matlab code.

k_ϕ $[10^5\ Nm/rad]$	Corrugated web		Flat web	
	Curve c	Curve d	Curve c	Curve d
0.0	150.8	145.8	163.4	160.9
0.1	221.5	213.4	235.4	229.8
0.2	289.0	277.1	304.3	296.3
0.3	351.0	336.2	371.0	360.2
0.4	406.6	389.7	435.1	421.6
0.5	447.6	428.6	496.1	479.9

```
% Buckling curve
% Non linear analysis
clc, clear all, close all

% material properties
E = 210e9;          % [Pa] elastic modulus
v = 0.3;            % Poission ratio
G = E/(2*(1+v));    % [Pa] shear modulus
f_y = 355e6;        % [N/m^2] yield stress

% Dimensional properties of the girder

b_f =  0.200;       % [m] width of the flange
t_f = 0.012;        % [m] thickness of the flange
h_w = 0.700;        % [m] height of the web
t_w_corr = 0.002;   % [m] thickness of the web
t_w_flat = 0.006;
l = 9.5;            % [m] length of the beam

h_tot = h_w+t_f*2;  % [m] total depth of the beam
h_m = h_w+t_f;      % [m] dist. between centroid of flanges

a = (h_w+t_f)/2;    % [m] dist. from centre of cross-section to
restr.

% sectional modulus

I = (b_f*h_tot^3/12-b_f*h_w^3/12);  % [m^4] around the strong axis
y = h_tot/2;                        % [m]
W_corr = I/y;                       % [m^3] sectional modulus

I = (b_f*h_tot^3/12-b_f*h_w^3/12)...% [m^4] around the strong axis
    +t_w_flat*h_w^3/12;
y = h_tot/2;                        % [m]
W_flat= I/y;                        % [m^3] sectional modulus

I_y_corr = 2*t_f*b_f^3/12;                    % [m^4] around the weak
axis
I_y_flat = 2*t_f*b_f^3/12+h_w*t_w_flat^3/12;  % [m^4] around the weak
axis

% shape of the corrugation
a_1 = 0.140;        % [m] length of straight webpanel
a_3 = 0.050;        % [m] length of inclined webpanel
```

```
b_t = 0.050;        % [m] eccentricity of the corrugation

u_x = h_m/(2*G*a_1*t_w_corr)+h_m^2*(a_1+a_3)^3/...
    (600*a_1^2*E)*2/(b_f*t_f^3/12);
c_w = b_t^2*h_m^2/(8*u_x*(a_1+a_3));

% warping- and torsion constants

I_w_corr = I_y_corr*h_m^2/4;
I_t_corr = (2*b_f*t_f^3+h_w*t_w_corr^3)/3+c_w/G;

I_w_flat = I_y_flat*h_m^2/4;
I_t_flat = (2*b_f*t_f^3+h_w*t_w_flat^3)/3;

% Yield moment

M_y_corr = W_corr*f_y/1000;
M_y_flat = W_flat*f_y/1000;

% Critical buckling moment

n = 1;          % Mode shape number
n_b = 6;        % number of restraints
s = l/(n_b+1);  % spacing between purlins

X_ec_corr = zeros(5,6);
X_ec_flat = zeros(5,6);

X_ec_corr2 = zeros(5,6);
X_ec_flat2 = zeros(5,6);

X_corr = zeros;
X_flat = zeros;

U_corr = zeros(5,6);
U_flat = zeros(5,6);

lam_corr = zeros;
lam_flat = zeros;

X_Euler_flat = zeros;
X_Euler_corr = zeros;

A = xlsread('buckling curve.xlsx');

for k = 1:length(A(:,1))

    % critical moment M_cr
    k_phi = A(k,1)*10^5;
    M_c_corr = (1/(2*a)*(pi^2*E*n^2/l^2*(I_w_corr+a^2*I_y_corr)+...
        G*I_t_corr+k_phi/s*(l/(pi*n))^2))/1000;
    M_c_flat = (1/(2*a)*(pi^2*E*n^2/l^2*(I_w_flat+a^2*I_y_flat)+...
        G*I_t_flat+k_phi/s*(l/(pi*n))^2))/1000;

    % Lambda_LT
    lam_corr(k) = sqrt(M_y_corr/M_c_corr);
    lam_flat(k) = sqrt(M_y_flat/M_c_flat);
```

Appendix E

```
    for i = 1:2

        X_corr(i,k) = A(k,i+1)/M_y_corr;
        X_flat(i,k) = A(k,i+3)/M_y_flat;

        % X_LT from EC: General case
        alpha = [0.49 0.76];    % imperfection factor for curves c
and d

        P_corr = 0.5*(1+alpha(i)*(lam_corr(k)-0.2)+lam_corr(k)^2);
        P_flat = 0.5*(1+alpha(i)*(lam_flat(k)-0.2)+lam_flat(k)^2);

        X_ec_corr(i,k) = 1/(P_corr+sqrt(P_corr^2-lam_corr(k)^2));
        X_ec_flat(i,k) = 1/(P_flat+sqrt(P_flat^2-lam_flat(k)^2));

        % X_LT from EC: welded sections
        beta = 0.75;

        P_corr2 = 0.5*(1+alpha(i)*(lam_corr(k)-
0.4)+beta*lam_corr(k)^2);
        P_flat2 = 0.5*(1+alpha(i)*(lam_flat(k)-
0.4)+beta*lam_flat(k)^2);

        X_ec_corr2(i,k) = 1/(P_corr2+sqrt(P_corr2^2-
beta*lam_corr(k)^2));
        X_ec_flat2(i,k) = 1/(P_flat2+sqrt(P_flat2^2-
beta*lam_flat(k)^2));

        % Euler
        X_Euler_flat(i,k) = 1/lam_flat(k)^2;
        X_Euler_corr(i,k) = 1/lam_corr(k)^2;

    end
end


for i = 1:2
    figure
    plot(lam_flat,X_flat(i,:),'.-k'), hold on
    plot(lam_corr,X_corr(i,:),'+-k')
    grid on
    xlabel('$\bar{\lambda}_{LT}$','Interpreter','latex')
    ylabel('{\chi}_{LT}')
    legend('Girder with flat web','Girder with corrugated web')
end

for i = 1:2
    figure
    plot(lam_corr,X_Euler_corr(i,:),'k'), hold on
    plot(lam_corr,X_corr(i,:),'*k')
    plot(lam_corr,X_ec_corr2(i,:),'.-k')
    plot(lam_corr,X_ec_corr(i,:),'x-k')
    grid on
    axis([0.9 2.2 0.1 1.1])
    xlabel('$\bar{\lambda}_{LT}$','Interpreter','latex')
    ylabel('{\chi}_{LT}')
    legend('Euler buckling curve','FEM model','EC3: Welded
sections',...
        'EC3: General case')
```

```
end

for i = 1:2
    figure
    plot(lam_flat,X_Euler_flat(i,:),'k'), hold on
    plot(lam_flat,X_flat(i,:),'*k')
    plot(lam_flat,X_ec_flat2(i,:),'.-k')
    plot(lam_flat,X_ec_flat(i,:),'x-k')
    grid on
    axis([0.9 2.2 0.1 1.1])
    xlabel('$\bar{\lambda}_{LT}$','Interpreter','latex')
    ylabel('{\chi}_{LT}')
    legend('Euler buckling curve','FEM model','EC3: Welded
sections',...
        'EC3: General case')
end
```